SYNTHESIS AND CRYSTAL STRUCTURE OF (*E*)-3-(4-BUTOXYPHENYL)-1-(NAPHTHALEN-1-YL)-PROP-2-EN-1-ONE

Sanjay Kumar,[a] A. Jayashree,[b] B. Narayana,[b] B. K. Sarojini,[c] László Kótai,[d] Sumati Anthal[a] and Rajni Kant[a]*

Keywords: Chalcone; butoxyphenyl; crystallography; direct methods; enone; intramolecular interactions.

Chalcone derivative (*E*)-3-(4-butoxyphenyl)-1-(naphthalen-1-yl)prop-2-en-1-one (C23H22O2) crystallizes in monoclinic system with space group 'P2$_1$/c ' and unit cell parameters: a = 15.1595(14) Å, b = 7.6644(7) Å, c = 15.8634(15) Å, β = 96.942(7)°. The crystal structure was solved using direct methods and refined by full matrix least squares procédures to a final R-factor of 0.0911 for 1591 observed reflections. The enone moiety adopts *E* conformation with respect to C12=C13 bond.The molecules in the unit cell are linked by weak C–H···O and π-π interactions. The molecule contains two C–H···O intramolecular interactions which stabilizes the crystal structure

*Corresponding Authors
Fax: +911912432051
E-Mail: rkant.ju@gmail.com
[a] X-ray Crystallography Laboratory, Department of Physics, University of Jammu, Jammu-Tawi, 180006.
[b] Department of Chemistry, Mangalore University, Mangalagangothri-574199, D.K., Mangalore, India.
[c] Department of Industrial Chemistry, Manglore Univrsity, Mangalagangothri- 574199, D.K.,Mangalore, India.
[d] Institute of Materials and Environmental Chemistry, Research Centre for Natural Sciences, Hungarian Academy of Sciences

Introduction

Chalcones are main precursors in the biosynthesis of flavonoids and isoflavanoids that are abundant in edible plants.[1] These are valuable intermediates in the synthesis of pyridines,[2] benzodiazepines,[3] pyrazolines,[4] cyclohexene derivatives[5] etc. Chalcones display tremendous pharmacological activities like anticancer,[6] antimalarial,[7] anti-inflammatory,[8] antitubercular,[9] larvicidal,[10] anticonvulsant,[11] cytotoxic,[12] antidepresent,[13] antimicrobial,[14] antiHIV.[15] Chalcone and their derivatives demonstrate wide range of biological activities such as anti-diabetic, anti-neoplastic, anti-hypertensive, anti-retroviral, anti-inflammatory, anti-parasitic, anti-histaminic, anti-malarial, anti-oxidant, anti-fungal, anti-obesity, anti-platelet, anti-tubercular, immunosuppressant, anti-arrhythmic, hypnotic, anti-gout, anxiolytic, anti-spasmodic, anti-nociceptive, hypolipidemic, anti-filarial, anti-angiogenic, anti-protozoal, anti-bacterial, anti-steroidal, cardioprotective, etc.[16-19] Besides this, the chalcone derivative shows non-linear optical (NLO) properties with excellent blue light transmittance and good crystallizability.[20-24]

In view of the extensive biological activities as exhibited by a large variety of chalcone derivatives, we report synthesis and crystal structure of (*E*)-3-(4-butoxyphenyl)-1-(naphthalen-1-yl)prop-2-en-1-one.

Experimental

Synthesis

Sodium hydroxide (0.4 g, 0.01mol) was dissolved in 20 ml of methanol and stirred at room temperature. 1-Acetylnaphthalene (1.7 g, 0.01mol) was dissolved in 20 ml of methanol and added drop wise to the sodium hydroxide solution with constant stirring. 4-Butoxybenzaldehyde (1.78 g, 0.01mol) dissolved in 20 ml methanol and added drop wise to the previous solution and continued stirring for 24 hours. The precipitated product was diluted with cold water and kept aside for 15 minutes. The product was then filtered, washed with distilled water and dried. The pure product was obtained by recrystallization from ethanol. Single crystal of the purified product developed from DMF by slow evaporation method (M.P.: 333-335 K). The complete reaction procedure is given in Figure 1.

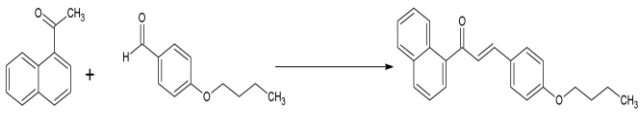

Figure 1. Reaction for the preparation of (*E*)-3-(4-Butoxyphenyl)-1-(naphthalen-1-yl)prop-2-en-1-one

Crystal structure determination

X-ray intensity data of the crystal of dimensions 0.30 x 0.20 x 0.20 mm^3 were collected on *X'calibur* CCD area-detector diffractometer equipped with graphite monochromated MoK$_\alpha$ radiation (λ = 0.71073 Å). X-ray intensity data of 6252 reflections were collected at 293(2) K and out of these reflections 3194 were found unique. The intensities were measured by ω scan mode for θ ranges 3.71° to 24.99°. 1591 reflections with I>2σ(I) were treated as observed.

Data were corrected for Lorentz-polarization and absorption factors. The structure was solved by direct methods using SHELXS97[25] and was refined using SHELXL97.[25] All non-hydrogen atoms of the molecule were located from the map. All the hydrogen atoms were geometrically fixed and allowed to ride on the corresponding carbon with C-H= 0.93-0.97Å and best U_{iso}= 1.2 $U_{eq}(C)$, except for the methyl groups where $U_{iso}(H)$ = 1.5 U_{eq}(C). The final refinement cycles converged to an R-factor of 0.0911 [$wR(F^2)$ = 0.2477] for 1591 observed reflections. Residual electron densities ranges from -0.289 to 0.562 eÅ^{-3}. Geometrical calculations of the molecule was done using the WinGX,[26] PARST[27] and PLATON[28] softwares.

Crystallographic information has been deposited to Cambridge Crystallographic Data Centre with CCDC number 1507484. This data can be accessed free of charge at Cambridge Crystallographic Data Centre via www.ccdc.cam.ac.uk/data_request/cif . Details of crystallographic and X-ray diffraction data are given in Table 1, bond distances and bond angles in Table 2 and torsion angles in Table 3.

Table 1. Crystallographic characteristics, X-ray data collection and structure refinement parameters of $C_{23}H_{22}O_2$.

CCDC No.	1507484
System,	Monoclinic,
Space group,	P 2_1/c
Z	4
a, Å	15.1595(14)
b, Å	7.6644(7)
c, Å	15.8634(15)
β, °	96.942(7)
V, Å^3	1829.63(16)
D_x g.cm^{-3}	1.20
Radiation, λ, Å	0.71073
μ, mm^{-1}	0.075
T, K	293(2)
Sample size, mm^3	0.30*0.20*0.20
Diffractometer	X' calibur Sapphire 3 CCD area-detector
Scan mode	ω scan
Absorption correction,	multi-scan
T_{min}	0.76841,
T_{max}	1.00000
θ range	3.71→24.99
h, *k*, *l* ranges	*h*=-11→18
	k= -8 →9
	l=-17→18
Number of reflections:	
measured/unique (N_1),	1591/3194
R_{int}/with $I > 2\sigma(I)$ (N_2)	0.0430/6252
R_{int}	0.0430
R_{sigma}	0.0790
F(000)	704
R	0.0911
*wR*2	0.2477
$(\Delta/\sigma)_{max}$	0.00
Number of refined parameters	228
S	1.094
$\Delta\rho_{max}/\Delta\rho_{min}$, e/Å^3	0.562/-0.289
Programs	SHELXS97,[25] SHELXL97,[25] PARST,[27] PLATON,[28] ORTEP[29]

Results and discussion

The molecular structure with atomic labeling is shown in Figure 2 (ORTEP).[29] The molecule consists of two aromatic rings (naphthalene and phenyl) bridged by prop-2-en-1-one group. The structural parameters, including bond distances and bond angles show a normal geometry.[30]

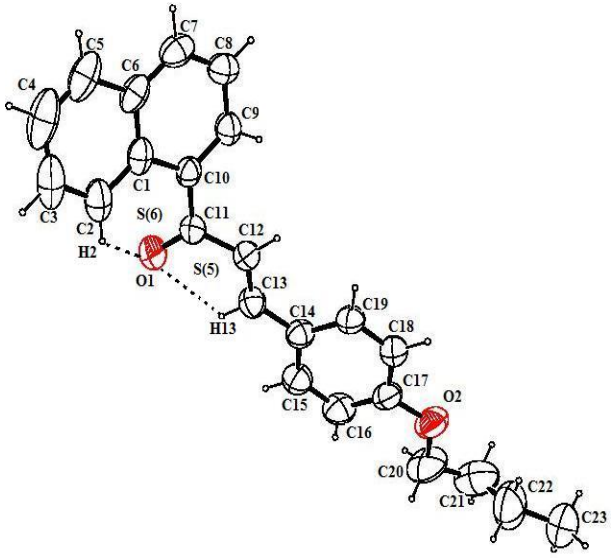

Figure 2. ORTEP view of the molecule at 40% displacement ellipsoid probability level along with atomic labeling scheme. Hydrogen atoms are drawn at arbitrary radii and are not labeled for clarity. The dashed line shows intra-molecular hydrogen bonds.

Table 2. Selected bond distances and bond angles (Å, °)

Bond Distances		Bond Angles	
C1–C2	1.413(5)	C2–C1–C10	122.9(4)
C10–C11	1.482(5)	C13–C14–C15	119.8(3)
C11– C12	1.475(5)	C9–C10–C11	119.3(3)
C20–O2	1.447(6)	C13–C14–C19	122.9(4)
C12–C13	1.317(5)	C1–C10–C11	121.9(3)
C15–C16	1.362(6)	C16–C17–O2	124.7(4)
C11–O1	1.223(4)	O1–C11–C12	121.0(4)
C17–O2	1.364(5)	O2–C17–C18	115.3(4)
C21– H21A	0.9700	O1–C11–C10	120.6(3)
C20– C21	1.484(7)	O2–C20–O21	111.3(5)
C22–H22A	0.9700	C17–O2–C20	117.7(4)
C23– H23A	0.9600	C21–C22–C23	114.0(7)

Table 3. Selected torsion angles (°)

Torsion angles	
C2–C1–C10–C11	-13.6(5)
C8–C9–C10–C11	-169.6(4)
C9–C10–C11–O1	140.8(4)
C1–C10–C11–O1	-32.4(6)
C1–C10–C11–C12	148.6(4)
C12–C13–C14–C19	-1.2(7)
C12–C13–C14–C15	178.1(4)
C20–O2–C17–C16	-3.1(7)
O2–C20–C21–C22	-66.4(8)
C20–O2–C17–C18	175.8(4)

Table 4. Hydrogen bonding geometry (e.s.d.'s in parentheses)

D–H...A	D–H(Å)	H...A(Å)	D...A(Å)	D-H...A(o)
C2–H2...O1	0.93	2.40	2.921(5)	116
C13–H13...O1	0.93	2.44	2.790(4)	102
C18–H18...O1i	0.93	2.56	3.291(5)	136

Symmetry code: (i) *x*, 1/2 - *y*,-1/2 + *z*

Table 5. Geometry of π-π interactions*

CgI…CgJ	CgI…CgJ(Å)	CgI…P(Å)	α(º)	β(º)	Δ(Å)
Cg2…Cg2^i	3.7179(2)	3.629	0.03	12.56	0.81

Symmetry code: (i) 1- *x*, -*y*, 1-*z*

The bond lengths within the conjugated linear fragment suggests the large degree of localization: the bond length C11–C12 =1.475(5)Å, C12=C13 =1.317(5)Å and C11=O1 =1.223(4)Å, and it agrees well with the corresponding distances in some analogous structures.[31] The naphthalene and phenyl rings are approximately planar and are inclined at a dihedral angle 44.54(1)° with respect to each other. The prop-2-en-1-one group is inclined with the naphthalene ring with a torsion angle (C1-C10-C11-C12) of 148.6(4)°. The prop-2-en-1-one group is approximately linear with phenyl ring having torsion angle (C12-C13-C14-C15) of 178.1(4)°.

The atoms of naphthalene and phenyl rings are almost planar with maximum deviation of 0.0629(5)Å observed for C3 atom and 0.0072(4)Å corresponding to C19 atom for respective rings. The naphthalene ring is significantly folded, even though both the individual rings are almost planar, the dihedral angles between their planes is as high as 3.68(1)°. The butoxy part is tilted with phenyl ring at a dihedral angle of 17.58(2)°. The atoms C21 and C22 are significantly deviated by 0.3024(7)Å and -0.3779(8)Å, respectively, from the mean molecular axis.

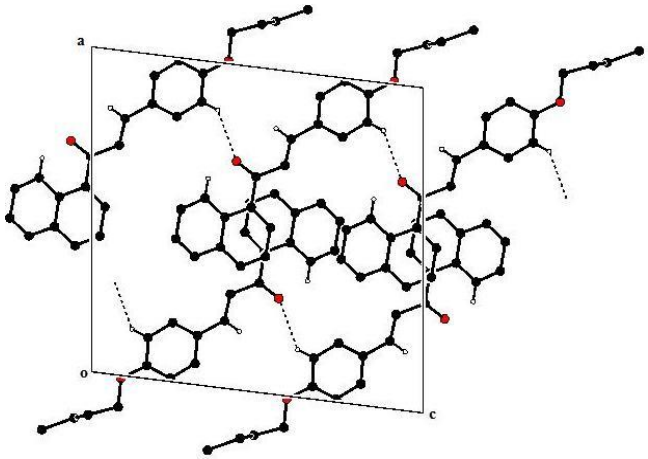

Figure 3. Packing of the molecule along *b-axis*. Intermolecular C–H···O contacts are also shown.

In the crystal structure, presence of C2-H2…O1 and C13-H13…O1 intra-molecular hydrogen bonds respectively results in the formation of S(6) and S(5) graph-set motifs (Figure 2). In the crystal structure, there is only one intermolecular hydrogen bond C18-H18…O1 that links molecule into infinite chains along *y*-direction, and a weak π-π interaction, which stabilize the packing, otherwise determined by the van der Waals interactions and close packing requirements (Figure 3).

Details of intra/inter-molecular hydrogen bonds are given in Table 4 and that of π-π bonding are given in Table 5.

Acknowledgements

Rajni Kant is thankful to the Indian Council of Medical Research and the Department of Science and Technology, New Delhi for funding under sponsored research project (No. BIC/12(14)/2012 and EMR/2014/000467). BN thanks the UGC for financial assistance through BSR one time grant for the purchase of chemicals. JA thanks University Grants Commission, New Delhi, for providing financial support for the research work through Junior Research Fellowship.

References

[1]Neelu, S. and Yogesh, C. J., *Int. J. Pharm. Pharm. Sci.*, **2012**, *4(4)*, 436-439.

[2]Samshuddin, S., Narayana, B., Divya, N. S. and Ramappa, R., *Der Pharma Chem*., **2011**, *3(3)*, 232-240.

[3]Baktir, Z., Akkurt, M., Samshuddin, S., Narayana, B. and Yathirajan, H. S., *Acta Cryst. E*, **2011**, *67(5)*, o1262-o1263.

[4]Samshuddin, S., Narayana, B., Sarojini, B. K., Khan, M. T. H., Yathirajan, H. S., Raj, C. G. D. and Ramappa, R., *Med. Chem. Res*., **2012,** *21(8)*, 2012–2022.

[5]Ashalatha, B. V., Narayana, B. And Vijaya Raj, K. K., *Phosphorus, Sulfur, Silicon Rel. Elem*., **2009**, *184(7)*, 1904–1919.

[6]Anto, R. J., Sukumaran, K., Kuttan, G., Rao, M. N. A., Subbaraju, V. and Kuttan, R., *Cancer Lett*., **1995**, *97(1)*, 33-37.

[7]José, N. D., Caritza, L., Juan, R., Neira, G. D., Jiri, G. and Philip J. R., *J. Med. Chem*., **2005**, *48(10)*, 3654–3658.

[8]Ballesteros, J. F., Sanz, M. J., Ubeda, A., Miranda, M. A., Iborra, S., Paya, M. and Alcaraz, M. J., *J. Med. Chem*., **1995**, *38(14)*, 2794–2797.

[9]Lin, Y. M., Zhou, Y., Flavin, M. T., Zhou, L. M., Nie, W. and Chen, F. C., *Bioorg. Med. Chem*., **2002**, *10(8)*, 2795-2802.

[10]Begum, N. A., Roy, N., Laskar, R. A. and Roy K., *Med. Chem. Res*., **2011**, *20(2)*, 184-191.

[11]Kaushik, S., Kumar, N. and Drabu, S., *The Pharma Res*., **2010**, *3(1)*, 257-262.

[12]Bhat, B. A., Dhar, K. L., Puri, S. C., Saxena, A. K., Shanmugavel, and Qazi, G. N., *Bioorg. Med. Chem., Lett.*, **2005**, *15(12)*, 3177-3180.

[13]Prasad, Y. R., Kumar, P. R. and Ramesh, B., *Int. J. Chem., Sci*., **2007**, *5(2)*, 542-548.

[14]Samshuddin, S., Narayana, B., Sarojini, B. K., Yathirajan, H. S. and Ramappa, R., *Der Pharma Chem.*, **2012**, *4(4)*, 1445-1457.

[15]Ansari, F. L., Umbreen, S., Hussain, L., Makhmoor, T., Sarfraz, A., Nawaz, S. A. and Lodhi, M. A., *Chem. Biodiver*., **2005**, *2(4)*, 487- 496.

[16]Mahapatra, D. K., Asati, V. and Bharti, S. K., *Eur. J. Med. Chem*., **2015**, *92*, 839-865.

[17]Mahapatra, D. K., Asati, V. and Bharti, S. K., *Eur. J. Med. Chem*., **2015**, *98*, 69-114.

[18]Mahapatra, D. K., Asati, V. and Bharti, S. K., *Eur. J. Med. Chem*., **2015**, *101*, 496-524.

[19]Mahapatra, D. K., Asati, V. and Bharti, S. K., *Life Sci*., **2016**, *148*, 154-172.

[20]Jasinski, J. P., Guild, C. J., Samshuddin, S., Narayana, B. and Yathirajan, H. S., *Acta Cryst*., *E*, **2010**, *66(8)*, 2018.

[21]Sreevidya, T. V., Narayana, B. and Yathirajan, H. S., *Central Eur. J. Chem.*, **2010**, *8(1)*, 174–181.

[22]Harrison, W. T. A., Yathirajan, H. S., Sarojini, B. K., Narayana, B. and Raj, K. K. V., *Acta Cryst. E*, **2006**, *62(4)*, o1578–o1579.

[23]Yathirajan, H. S., Mayekar, A. N., Narayana, B., Sarojini, B. K. and Bolte, M., *Acta Cryst. E*, **2007**, *63(2)*, o540-o541.

[24]Butcher, R. J., Yathirajan, H. S., Anilkumar, H. G., Narayana, B. and Sarojini, B. K., *Acta Cryst. E*, **2006**, *62(4)*, o1659-o1661.

[25]Sheldrick, G. M., University of Gottingen, Germany, **1997**.

[26]Farrugia, L. J., *J. Appl. Cryst*., **1999**, *32(4)*, 837-838.

[27]Nardelli, M., *J. Appl. Cryst*., **1995**, *28(5)*, 659.

[28]Spek, A. L., *Acta Cryst. D*, **2009**, *65(2)*, 148-155.

[29]Farrugia, L. J., *J. Appl. Cryst.*, **1997**, *30(5)*, 565.

[30]Allen. F. H., Kennard. O., Watson. D. G., Brammer. L., Orpen. A. G. and Taylor, R., *J. Chem. Soc., Perkin Trans*., **1987**, *2*, S1-S19.

[31]Dutkiewicz, G., Samshuddin, S., Narayana, B., Yathirajan, H. S. and Kubicki, M., *Acta Cryst. E*, **2009**, *65*, o3255–o3256.

Received:
Accepted:

ALCEA: TRADITIONAL MEDICINE, CURRENT RESEARCH AND FUTURE OPPORTUNITIES

Abdullatif Azab[a]

Keywords: *Alcea*, traditional medicine, A*lcea rosea*, polysaccharides, polyphenols, anthocyanins.

The genus *Alcea* consists more than 40 subspecies. Most of them were partly studied but some of them were not. In this review we will introduce the traditional medicinal knowledge and uses of this genus, summarize and discuss the modern research reports of the medicinal/biological activities of the various subspecies. Special attention will be paid to *A. rosea*, the most investigated subspecies of this genus. Clear emphasis will be laid upon some reported natural products isolated from subspecies of *Alcea*. Future possible studies will be suggested.

* Corresponding Authors
Fax: +972-4-986-1173
Phone : +972-4-986-1171
E-Mail: abedazab@gal-soc.org
[a] Institute of Applied Research, The Galilee Society Box 437, Shefa Amr 20200, Israel.

Introduction

Subspecies of the genus *Alcea* are among the most spectacular flowering plants, they bloom with relatively large, very colorful flowers. According to the Barcode of Life Data (BOLD) Systems, the genus is native to Asia and Europe.[1,2] The number of subspecies that consist this genus is not definite, and it varies from 21 according to the "U.S. National Plant Germplasm System",[3] to 40 subspecies,[4] and even higher in some reports.

Most of the subspecies can be found in Asia, especially in Iran (34 ssp.) and Turkey (18 ssp.).[5,6] Humans have taken this genus with them, mainly *Alcea rosea*, while migrating to the "New World", and with the plants, the traditional medicine uses of them were aslo adopted.[7]

Traditional uses of *Alcea* subspecies

Peoples of Euroasia used the various subspecies of this plant genus since very ancient times. The extinct Neandarthal humans used *A. rosea* about 60000 years ago for medicinal and ritual purposes.[8]

In table 1, a summary of the traditional uses of *Alcea* subspecies is presented.

Biological and medicinal activities of *Alcea* subspecies (excluding *A. rosea*)

The reported biological/medicinal activities of the *Alcea* subspecies are of a wide variety, which includes most of the typical medicinal activities of plants, such as antioxidant, antimicrobial, antiviral, hepatoprotective and others. Along with that, it is interesting to notice some reports of last few years that present modern uses, such as nanomaterials synthesis (section 4). But it is also notable that these activities do not include psychoactive or mind-altering activities of the plants, their extracts or of natural products isolated from them. This might be understood on the basis of the low content of alkaloids (and closely active compounds) in the subspecies of *Alcea*, which have no reported toxic effects on humans and other mammals. In table 2, a summary of the biological/medicinal activities of *Alcea* subspecies is listed, as well as reported active natural products and chemical composition, if reported.

Biological and medicinal activities of *Alcea rosea*

Alcea rosea is the most investigated subspecies of *Alcea*. Most of the biological/medicinal activities that were mentioned in table 2 related to all other studied subspecies of *Alcea*, can also be found in publications related to *A. rosea*. The chemical composition was extensively studied, and despite the fact that it is not completely known yet, some of its constituents were widely tested for medicinal/biological activities. Moreover, in addition to its traditional medicinal uses, *A. rosea* was used for tarditional dye industry, and recent years in nanochemistry. Summary of research articles of *A. rosea* properties are shown in table 3.

Discussion and Future Opportunities

Antioxidant acticity was reported for some subspecies of *Alcea*: *acaulis*,[41] *apterocarpa*, *pallida*,[43] *hyrcana*,[49] *kurdica*,[51,52] *setosa*,[72] *rosea*.[92,93,95] All these studies indicate two important facts. One, the major compound family responsible for the antioxidant activity is polyphenols. Two, various extracts of differents parts of these plants vary in their antioxidant capacity, but all of them have strong capacities. When these polyphenols (aqueous extract of *A. rosea*) were force fed to rats, these animals, swam longer time than the control group.[94] This result suggests the need for more studies of the application of this activity in sports and food industry.

Table 1. Region-wise traditional use of Alcea sub-species

Subspecies	Country/Region	Part Used /Objective /Mode of Use
A. acaulis	Jordan	NS[b] .[9]
	Lebanon	Whole plant, flower/ cough, catarrh, respiratory infections, constipation/ infusion.[10]
A. angulata	Iran	Flower/ antitussive, febrifuge, treatment of pimples, laxative, depurative, treatment of gum swelling, mouth wounds, bone fracture/ NS.[11]
A. apterocarpa	Turkey	Root, shoots, herb/ vulnerary, anti-inflammatory, skin disorders, urinary system disorders, kidney stones, pulmonary disorders, intestinal disorders, stomach ailments, cough/ decoction, infusion.[12]
A. arbelensis	Iran	Flower/ constipation, coughs, sores/ infusion, decoction, crude.[13]
	Iran	Flowers/ constipation/ NS.[14]
A. aucheri	Iran	Flower/ antitussive, febrifuge, treatment of pimples, laxative, depurative, treatment of gum swelling, mouth wounds, bone fracture/ NS.[11]
	Iran	Leaf, flower/ colds, influenza, sore throat/ decoction.[15]
A. biennis	Turkey	Flowers/ bronchitis/ infusion, maceration.[16]
A. calvertii	Turkey	Root, herb/ vulnerary, anti- inflammatory, skin disorders, kidney stones, urinary system disorders, pulmonary disorders, stomach disorders/ decoction, infusion.[12] Flower/ respiratory system, coughs, infection, asthma/ maceration.[13]
	Iran	Flower/ asthma, coughs, infections, respiratory disorders/ extraction, infusion,
	Iran	maceration.[17]
A. damascena	Lebanon	Whole plant, flower/ cough, catarrh, respiratory infections, constipation/ infusion.[10] Flowers/ herbal tea/ infusion.[18]
	Syria	
A. dissecta	Turkey	Leaf/ injuries, asthma/ pounding, poultice.[12]
	Turkey	Leaves/ expectorant/ decoction.[19]
A. excubita	Turkey	Leaf, Flower/ vulnerary, expectorant, cold/ pounding , poultice.[12]
	Turkey	Leaves, flowers/ joint injuries/ decoction.[19]
A. fasciculiflora	Turkey	Root/ kidney stones, abscess, scabies/ decoction, poultice.[12]
A. flavovirens	Turkey	Root/ kidney stones, abscess, scabies/ decoction, poultice.[12]
	Iran	Flower/ stomachache.[13]
	Azarbaijan	Flower/ NS/ NS.[20]
A. koelzii	Iran	Flower/ infection, respiratory system/ decoction.[13]
A. kurdica	Iran	Flower/ Carminative in veterinary, coughs/ infusion.[13,17]
	Iraq	Flowers/ tonsillitis, gastric ulcers, duodenal ulcers, pneumonia, urinary tract infections, expectorant, alopecia/ infusion.[21]
A. lavateriflora	Iran	Flower/antitussive, febrifuge, treatment of pimples, laxative, depurative, treatment of gum swelling, mouth wounds, bone fracture/ NS.[11]
A. pallida	Turkey	Leaf/ demulcent, expectorant, diuretic, anthilitic, emollient/ herbal medicine commercial product.[22]
A. rechingeri	Iran	Flower/ , respiratory system/ decoction.[13]
A. rhyticarpa	Iran	Flower/ antitussive, febrifuge, treatment of pimples, laxative, depurative, treatment of gum swelling, mouth wounds, bone fracture/ NS.[11]
A. rosea	Iran	Flower/ antitussive, febrifuge, treatment of pimples, laxative, depurative, treatment of gum swelling, mouth wounds, bone fracture/ NS.[11]
	Ecuador	Whole plant/ kidney problems, used as tonic/ pounded .[23]
	Saudi Arabia	Leaves, branches, fruits/ carminative, deworming/ mixed with food of livestock.[24]
	India	Flowers, roots, whole plant/ cough, asthma, throat infection, urinary irritation. Kidney pain, aunndice, urinary irritation, bladder, dandruff, dermatitis, easy delivery, goitre, gynecological disorders, inflammation, emollient.[25]
	Italy	Leaf/ cough, cold, bronchitis/ boiled with wine, decoction .[26]
	India	Whole plant/ bleeding gums/ NS.[27]
A. rufescens	Jordan	NS/ NS/ NS.[28,29]
A. rugosa	Azerbaijan	NS/ respiratory system illnesses/ NS.[30]
A. setosa	Jordan	NS/ NS/ NS.[9,28,29]
	Turkey	Leaf/ expectorant, diuretic, emollient/ infusion.[12]
	Turkey	Leaf/ demulcent, expectorant, diuretic, anthilitic, emollient/ herbal medicine commercial product.[22]
	Palestine	Whole plant/ stomach and intestine pain, inflammation, asthma/ decoction.[31,32]
	Arab countries	Flower, leaf, root/ cough, cold, stomach pain, urinary system pain, female sex stimulant, anti-inflammatory, wound relief, skin laxative.[33]

		NS/ Inflammation/ NS.[34]
	Greco-Arab	Leaf/ hair care, cleaning the house against dust/ NS.[35]
	Turkey	Flower/ cough, / decoction.[36]
	Turkey	Flower/ cough, chest pain/ infusion .[37]
	Jordan	Leaves, roots/ wounds, vegetable, gastritis, marshmallows, ornamental, saline tolerant/
	Jordan	infution, dried powder.[38]
A. striata	Turkey	Leaf, flowers/anti-inflammatory, anemia, cough/ decoction, infusion.[12]
	Turkey	Leaf/ anemia/ decoction.[39]
A. tarica	Iran	Flower/ throat, joint pains, fever, respiratory system/ infusion, decoction, extraction.[13]
	Iran	Flower/ joint pains, coughs, fever, infections, respiratory system disorders/ decoction, infusion.[17]
NS	Iran	Flower/ wound, burn/ decoction, ointment.[40]

Table 2. Biological/medicinal activities of *Alcea* subspecies and active constituent

Alcea Subspecies	Biological-medicinal activities/ major active material(s)
A. acaulis	Antioxidant/ aqueous and methanolic extracts.[41]
A. angulata	Anti-hyperlipidemia/ alcoholic extract .[42]
A. apterocarpa	Antioxidant, anticholineesterase, antimicrobial/ acetone extract, detailed composition of essential oil is listed, fatty acid content is provided and phenolic content is detailed.[43]
A. aucheri	Heavy metal hyperaccumulator.[44]
A. digitata	NAR[c]/ phytochemical screening for biologically active compound families.[45]
	Relief of radiotherapy symptoms (mainly xerostomia)/ plant powder.[46]
A. flavovirens	NAR/ polysaccharide identified that contains: ribose, rhamnose, glucose, glucuronic acid, galacturonic acid (3:6:3:7:2).[47]
A. hyrcana	NAR/ polysaccharides isolated and analysed (%): uronic acids (32.3-45.7), glucose and galactose (24.5-38.7), arabinose (9.6-9.9), xylose (4.9-6.3), rhamnose (12.9-14.8).[48]
	Antioxidant (various methods)/ total phenolic content was determined.[49]
A. koelzii	NAR/ mineral content was determined (K, Ca, Mg, P, Fe, Mn, Cu, Zn).[50]
A. kurdica	Antioxidant/ total phenolic and total flavanoidic contents.[51]
	Antioxidant, antimicrobial, but not cytotoxic/ total phenolic content measured.[52]
	Acetylcholinesterase (ACE) inhibition/ methanolic extract.[53]
A. kusariensis	NAR/ Polysaccharides isolated from roots and stems, analysed with average values of uronic acids (39%), and the rest is composed of galactose, rhamnose with traces of glucose.[54]
A. longipedicellata	Anticariogenic against oral bacteria/ malvidin-3,5-diglucoside (from ethanolic extract).[55]
	Anticancer (gastric cancer cell line, AGS)/ malvidin-3,5-diglucoside with/without cisplatin.[56]
A. nudiflora	NAR/ Astraglin.[57]
	NAR/ Polysaccharides isolated and analysed with uronic acids (42%), and the rest is composed of glucose, galactose, arabinose, rhamnose with traces of xylose and mannose.[58]
	NAR/ polyprenols and triterpenoids were isolated and identified.[59]
	NAR/ Aliphatic contents was analyzed of two extracts of the aerial parts: EtOH, MTBE.[60]
	Immunomodulatory action/ polyprenols.[61]
A. pallida	Antioxidant, anticholineesterase, antimicrobial/ acetone extract, detailed composition of essential oil is listed, fatty acid content is provided and phenolic content is detailed.[43]
	Antistress/ infusion, no specific compound(s).[62]
	Resistance to allelophathy of some aromatic plants/ no specific compound was indicated to be resposible for this activity.[63]
	Accumulator of heavy metals, especially in leaves, where Pb had highest concentration/ Pb, Zn, Cu, Cd.[64]
	Liquid biofuels production by catalytic (zinc chloride on alumina) pyrolysis of stems/ bio-char, bio-oil, bio-gas.[65]
A. rhyticarpa	NAR/ investigation of semiemprical formula of dihydroxylignin content.[66]
	NAR/ investigation of the content and structures of dioxan lignins.[67]
	Antiviral activity/ no extract or sprcific compound is presented, but the article reviews research studies.[68]
A. rugosa	NAR/ four polysaccharides were isolated and analyzed. The average composition (%) is: rhamnose, 25.5; glucose, 17.1; galactose, 21.1; arabinose, 10.9; uronic acids, 25.4.[69]
	Diuretic and natriuretic/ kaempferol and its glycosides.[70]
	Sensitive to stagonolide, a phytotoxin isolated from *Stagonospora cirsii*.[71]
A. setosa	Antioxidant/ total phenolics and flavanoids were determined.[72]
A. sulphurea	Anti-inflammatory in mucociliary system of chicken trachea / aqueous and ethanolic extracts.[73]

Table 3. Summary of research articles on *A. rosea*

Properties	Active Materials / Mode of Action
Fatty acids changes	Changes in the composition of fatty acids during plant life/ the general change is formation of
Coloring, pigmentation	Althaein, the blue pigment, 11% of all pigmentation.[75]
	Anthocyanins/ red dyes for food coloring.[76]
	Structure elucidation of the 12 compounds that give *A. rosea* (var. nigra) its color.[77]
Nanochemistry uses	Ethanolic extract as natural, low cost sensitizer for the synthesis of strontium-titanate nanoparticles.[78]
	Silver nanoparticles (AgNP's) were prepared and used as antimicrobial agents. AgNP's were prepared by reduction of $AgNO_3$ by aqueous extract of the plant.[79]
Chemical composition	Acidic polysaccharides were isolated and identified (compared with *Malva sylvestris*).[80]
	Acidic polysaccharide, rhamnoglucouronan, was isolated from the stems of the plant and analyzed.[81]
	Phenolic acids (ferulic, vanillic, syringic, *p*-coumaric, *p*-hydroxybenzoic, *p*-hydroxyphenylacetic and caffeic) were identified and determined quantatively.[82]
	Partial chemical composition: some metals, amino acids and monosaccharides were identified and quantified.[83]
	Mercury accummulation in roots introduced compared with other plants in Poland.[84]
	Pictinic polymers (water and alcohol insoluble) from the flowers were isolated and analyzed to result mainly rhamnoglucogalacturonan, that consists rhamnose, glucorunic and galactorunic acids.[85]
	Two new compounds from ethanolic extract.[86]
	Isolation and identification of 17 known compounds.[87]
	Sono-assisted extraction of alcohol-insoluble compounds that yielded mainly high molecular weight polymers like peptides and polysaccharides (acidic).[88]
Antibacterial/Antimicribial/ Antifungal	Antimicrobial and cytotoxicity evaluation of *n*-hexane, ethanol, methanol, ethyl acetate and water extracts, against ten bacterial species and the fungus *Candida albicans*.[89]
	Ethanolic extract activity against nine bacteria species.[90]
	Water-ethanol (50%) extract found active against *Streptococcus pneumoniae* and *Klebsiella pneumonia*.[91]
Antioxidant	Antioxidant activity of methanolic extract (DPPH) with chemical analysis of phenolic compounds and saccharides.[92]
	Antioxidant activities of water, ethanol, butanol and chloroform extracts of the seeds were measured by three different methods and phenolic content was identified and quantified.[93]
	Aqueous mixture of polyphenols was force fed to rats and the animals were forced to swim to exhaustion. These animals showed longer swimming time compared to control. This was confirmed by tests of various metabolites.[94]
	Kaempferol and its 3-glucoside (astragalin) contained in ethanolic extract have strong antioxidant activity.[95]
Anticancer	Kaempferol and its 3-glucoside (astragalin) contained in ethanolic extract have strong anticancer activity.[95]
	Antiproliferative activity of methanolic extract against rat brain tumor and human cervix carcinoma cell lines compared with 5-florouracil and cisplatin (control).[96]
	Ethyl acetate seed extract inhibits the growth of stem cell driven colon cancer cells *in vitro* and antagonize the growth of tumor xenografts *in vivo*.[97]
Antiviral	80% Aqueous methanolic extract with anti-HIV activity.[98]
	Aqueous and ethanol extracts were tested for acyclovir-resistant Hsv type-1 in cell culture.[99]
Immunomodulatory	Aqueous extract is B-lymphocyte polyclonal activator.[100]
Urolithiasis preventive	70% Ethnaol/water extract prevented or reduced the formation of urinary tract stones.[101]
Cardiovacular protective*	Ethanolic extract of the flowers showed important preventive and curative effects of cariovasular disorders.[102] * See remark to this property after this reference.
Hepatoprotective	70% Methanol/water extract of the plant found active against acetaminophen-induced hepatotoxicity in mice. The systematic work included three control groups.[103]
Hypoglycemic	Ethanolic extract showed hypoglycemic activity and three new compound were isolated and characterized.[104]
Latex allergy prevention	Hospital staff were treated with 8% aqueous extract where the test group washed their hands with it before and after use of latex gloves.[105]
Tyrosinase inhibition	80% Aqueous ethanol inhibits the enzyme tyrosinase that is responsible for hyperpemintation of foods.[106]

The antimicrobial activity was also observed for few subspecies of *Alcea*. these reports are consistent. Ertas *et al*. reoprted in 2016 weak to moderate activity against different types of bacteia,[43] while Benli *et al*. stated that this subspecies had no antibacterial activity at all.[107] Despite the fact that this might seem contradicting, it is not: Ertas[43] used acetone while Benli[107] used methanol extract. When Ertas used methanol, no activity was observed. This may indicate that the active compound(s) that has the antimicrobial activity that was reported by Ertas, can not be extracted by methanol, possibly due to its high polarity of this solvent. So, further studies are needed, using not only both the solvents, but also other solvents like n-butanol, since using either very polar (water, Ertas) or non-polar (petroleum ether, Ertas) extracts showed no activity. Qader and Awad tested the antimicrobial activity of the aqueous extract of *A. kurdica* and found it to be moderate.[52] This strengthens the need for extensive tests of antimicrobial activities for all *Alcea* subspecies, with as many solvents as possible. Strong antibacterial activity was reported by Esmaeelian *et al*..[55] They isolated the active compound from ethanolic extract and found it to be malvidin-3,5-diglucoside (Figure 1).

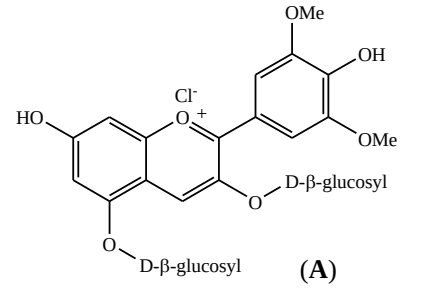

(**A**)

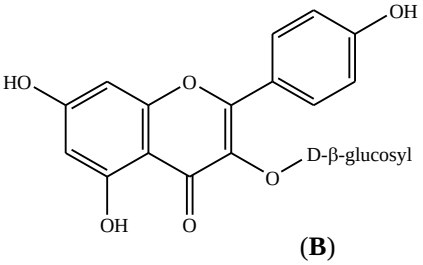

(**B**)

Figure 1. (**A**) malvidin-3,5-diglucoside (**B**) astragalin

These results were confirmed by later studies that investigated the antimicrobial activity of this compound present in other plants such as *Syzygium cumini*.[108] It is also consistent with the fact that malvidin-3,5-diglucoside is the dimethyl ether derivative of delphinin-3,5-diglucoside, an anthocyanin with strong antimicrobial activity.[109] The structures difference can also explain the higher activity of the free anthocyanin compared with the methylated form. The same active natural product was also tested for anticancer activity and showed positive results, separately or with cisplatin.[56] An interesting glucosylated polyphenol was isolated from *A. Nudiflora* is astragalin (Figure 1),[56] and its antimicrobial was discovered in later studies.[110] Relying on these and other findings, it is important to expand the search of such compounds in *Alcea* subspecies for antimicrobial testing.

In addition to malvidin-3,5-diglucoside and *A. nudiflora*, anticancer activity was reported only for *A. rosea*.[95,96,97] All the reported results indicate significant activities compared with well known anticancer agents such as cisplatin and 5-fluorouracil, where the anticancer activity of the plant material was higher than the later agent. These findings support the need for expansion of anticancer activity studies of other *Alcea* subspecies like *A. setosa*, which is very common on east Mediterranean region.

The antibacterial activity of *A. rosea* was reported by several groups. Mert *et al*.[89] studied the antimicrobial, cytotoxic and antifungal (*Candida albicans*) of four extracts of this plant. In this work, the ethanolic extract proved to be most effective. This extract was reported to have significant antibacterial activity against nine bacteria species, and only *Escherichia coli* was resistant.[90] This result is similar to the findings in the previous study. *Streptococcus pneumoniae* and *Klebsiella pneumonia* are also antibiotic resistant bacteria, but hydro-alcoholic exract of *A. rosea* seeds was effective against them.[91]

Unlike the antibacterial/antimicrobial activities of *Alcea* subspecies that have been reported in several publications, the antiviral activities of these plants have been studied rather poorly. Popov *et al*. do not specify whether an extract or a single compound that is responsible for the antiviral activity that they reported.[68] This makes their report hardly useful. Asres *et al*. found that the hydromethanolic extract has the potenial as an anti-HIV agent.[98] Despite the fact that aqueous and ethanolic extracts showed weak antiviral activity against acyclovir-resistant Hsv type-1 in cell culture,[99] this opens a window for further research in this area.

The bioremediation of heavy metal contaminated soils is an issue with growing concern, especially in the context of hi-tech massive use of these metals for different purposes, and specifically metals that are used in batteries production. *A. aucheri* was found as a promising plant for this task.[44] Two other *Alcea* subspecies were reported as heavy metal accumulators are *A. pallida* [64] and *A. rosea*,[83,84] and both were found to be less effective in accumulating heavy metals as compared to that by *A. aucheri*.

One of the notable indicators of the need of further investigations of the genus *Alcea* is the fact that the subspecies *A. digitata* was analysed only for families of some compound like phenolics, alkaloids and saponines.[45] Even though the same publication indicated the traditional uses of *A. digitata* (anti-inflammatory, mild cathartic), and a modern study indicates that its "compound" gave releif to cancer patients treated with radiotherpay, this "compound" is actually the plant powder.[46] At for the time of writing this article, the chemical coposition of *A. digitata* is completely unknown, and its potential therapeutic potential needs further studies.

Polysaccharide content of *Alcea* ssp. was among the first chemical analyses of these plants. Looking into the reports that cited here,[47,48,54,58,69,80,81,85] it is clear that acidic

polysaccharides are the dominant type. That is to say that uronic acids, mainly glucuronic and galactorunic acids are present in high concentrations. These natural produts have been reported to have various biological activities such as anticomplementary, hypoglycemic, antitumorial, diuretic and antidiarrheic.[111] Further studies of these polysaccharides are needed in connection with *Alcea* subspecies research.

In recent years there is a growing number of publications concerning acetylcholinesterase (AChE) inhibition activity, due to its importance in Alzheimer disease treatment. Synthetic drugs are being developed but notable efforts are being invested in the discovery of natural products that can be used for this objective.[112] Until the time of writing this article, two research article about this activity of *Alcea* genus as acetylcholinesterase inhibitorss were published. A significant activity was found for *A. kurdica*,[53] but activity was reported by Ertas *et al*. was very weak (butyrylcholineesterase).[43] Although it is clear that this genus has low content of alkaloids, which is the major known compound family responsible for AChE inhibition so far,[112] it is also known that other compounds can inhibit AChE, and more important, this inhibition can occur from synergism of natural products.[113] So, it is a clear need to study this activity of *Alcea* plants in depth, and possibly, in combinations with other plants.

Several authors,[59,60,61] have thoroughly investigated the polyprenol and other aliphatic content of *A. nudiflora*. It is interesting to see that different extracting solvents yielded different compounds and that the polyprenols are of the type shown in Figure 2.

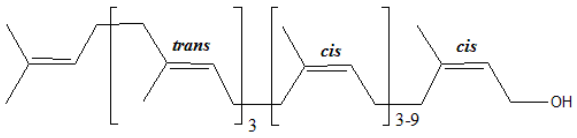

Figure 2. Polyprenols occurring in *A. nudiflora*

Interestingly, this general structure contains both geometries of the carbon-carbon double bond bond, cis and trans, unlike most naturally occurring polyprenols that contain one of these geometries.[114,115] These differences occur not only between species of different families, but within the same genus. A good and detailed example was published by Ertas *et al*.,[43] and details can be viewed there. But for interested readers, we bring here in table 4, the major compounds (in percentage terms) in the essential oils of *A. apterocarpa* and *A. pallida*. The phenolic compounds (ascorbic acid, caffeic acid, salicylic acid, p-hydroxybenzoic acid and quercetin) content was almost identical in both subspecies.

Azirak and Karaman[63] reported that among seven plants that they tested their resistance towards the allelopathy of essential oils extracted from ten different very common aromatic plants, only *A. pallida* showed full resistance. This research was cited by many later studies but this activity was never reported for other *Alcea* subspecies, and it might be interesting to test this. The test must include strong allelopathic plants like walnut (*Juglans* ssp.).

Table 4. Major constituents in the essential oils of the given species

Compound	% in oil of *A. pallida*	% in oil of *A. apterocarpa*
α-Selinene	8.0	6.5
2,5-Ditertoctyl-p-benzoquinone	5.2	6.6
Arachidic acid	34.2	1.2
Hexadecanoic acid	6.6	1.0
Heptacosane	7.0	1.1
Nonacosane	6.3	1.1
Hexatriacontane	0.0	25.3
Tetratetracontane	7.0	15.4

In Table 3, medicinal/biological and other uses of *A. rosea*, a plant that thoroughly studied, are listed. In our opinion, other *Alcea* subspecies can be investigated in similar manner, especially the common ones such as *A. setosa*. One of the subjects that can be studied is the coloring and pigmentation of *Alcea* subspecies. As for *A. rosea*, it was sufficiently studied as can be seen in table 3.[75,76,77,78] These compounds are shown in figure 3.

It is interesting to notice some ambiguity in literature concerning the material named althaein.[75] While some publications consider it a mixture of glucosides,[116] others consider it the 3-glucoside of myrtillidin or petunidine.[117] Modern methods are being applied to identify and quantify antocyanins in plant matter.[118] The major advantage of these spectroscopic techniques is that they rely of fast sampling without needing long processing that can damage these relatively unstable compounds.

The isolation and characterization of two new and very interesting compounds shown in figure 4 below,[86] rises up the very basic fact that a complete chemical composition was never reported for any one of *Alcea* subspecies, especially *A. rosea*. The researchers named them "Rosea A" and "Rosea B" and the IUPAC names are given in the article.

Most efforts are still being targeted for studying the chemical composition of *A. rosea*, such as the recent work of Rakhmatova *et al*.,[87] who isolated seventeen known compounds viz., phytol, octanal, tetrahydrogeranylacetone, geranylacetate, farnesylacetone, menthone, acetylacetone, octacosane, stearyl alcohol, 2,5-dimethylfuran, isopulegol, α-tocopherol, α-tocopherylquinone, α-amyrin, β-amyrin, sitosterol, stigmasterol. In the same year, a report was published of new, very interesting compounds that were also isolated from *A. rosea* (Figure 5).[104] Therefore, further research work is required in this field since even partial chemical compositions of many *Alcea* subspecies is unkown.

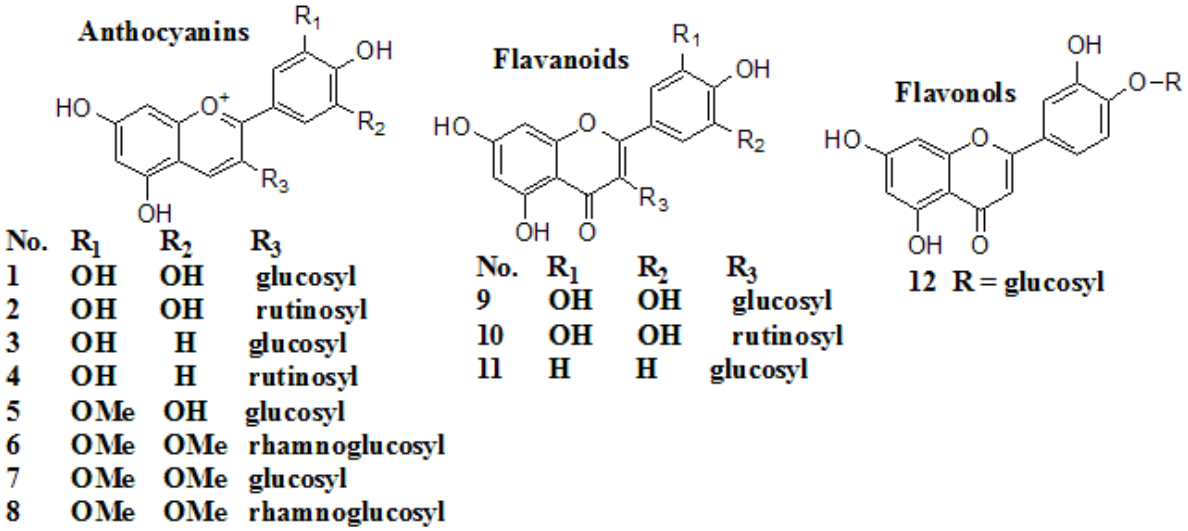

No.	R_1	R_2	R_3
1	OH	OH	glucosyl
2	OH	OH	rutinosyl
3	OH	H	glucosyl
4	OH	H	rutinosyl
5	OMe	OH	glucosyl
6	OMe	OMe	rhamnoglucosyl
7	OMe	OMe	glucosyl
8	OMe	OMe	rhamnoglucosyl

No.	R_1	R_2	R_3
9	OH	OH	glucosyl
10	OH	OH	rutinosyl
11	H	H	glucosyl

Figure 3. Coloured compounds present in *A. rosea*

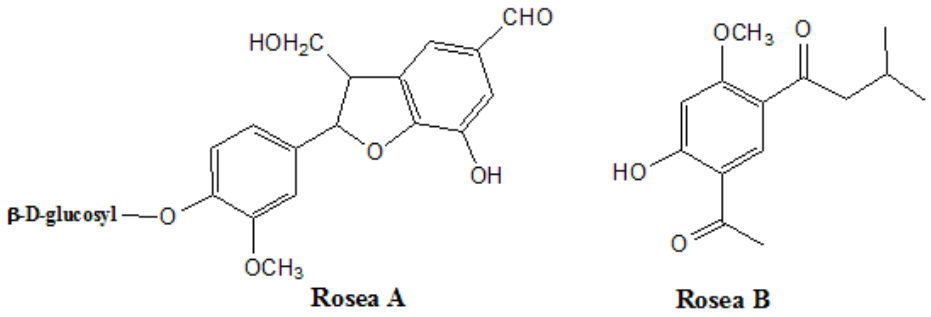

Figure 4. Compounds isolated from *A. rosea*

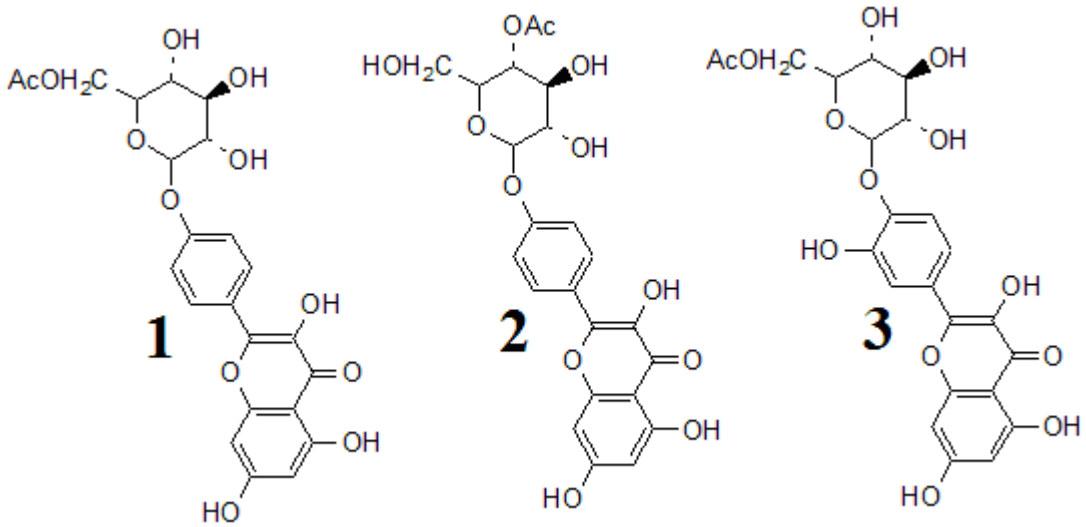

Figure 5. New compounds isolated from *A. rosea*

 DOI: 10.17628/ecb.2016.5.505-514

Immunomodulatory activities related to *Alcea* were reported only twice until today.[61,100] In both these reports there are encouraging results but there was no followup research so far. And again, it is interesting why very common subspecies like *A. setosa* were not studied for this activity.

The last item in table 3, that reports the tyrosinase inhibition activity of hydroalcoholic extract of *A. rosea*,[106] is interesting because this article includes the same activity of three other plants, *Physalis alkekengi* L., *Bunium persicum* B. Fedtsch. and *Marrubium vulgare* L. Among these, *P. alkekengi* was the most active inhibitor of this enzyme that causes hyperpegmintaion, such as human skin and food browning, through catalysis of oxidative processes.[119] Efficient inhibition of this enzyme can be done by strong antioxidants. *P. alkekengi* and *A. rosea* contain considerable amounts of polyphenols, but *P. alkekengi* contains notable amounts of another antioxidant group of compound, steroids, which some of them were reported in the last decade.[120]

Finally, all activities reported in references 101 to 106 need extensive investigations for more *Alcea* subspecies.

Conclusions

Reviewing the scientific literature related to the genus *Alcea* that was published over almost five decades, it is concluded that

(a) The traditional uses of *Alcea* plants are well documented.

(b) The biological, medicinal and other activities of *Alcea* extend over a wide range, from direct use of the plant or its parts to nanochemistry.

(c) Only *A. rosea* has been well studied, but its complete chemical composition is still unknown and additional research is needed to explore its biological activities.

(d) For all other subspecies of *Alcea*, the chemical compositions are unknown and their biological activities were partially or very narrowly investigated.

(e) Few subspecies of *Alcea* were never studied for biological and other activities.

(f) The research of this genus is very far from completion.

References

[1]The Barcode of Life Data (BOLD) Systems, the genus *Alcea*: http://www.boldsystems.org/index.php/Taxbrowser_Taxonpage?taxid=561083

[2]The previous website is considered as a reliable reference: Ratnasingham, S., Hebert, D. N., *Mol. Ecol. Notes*, **2007**, *7*, 355.

[3]The U.S. National Plant Germplasm System: https://npgsweb.ars-grin.gov/gringlobal/taxon/taxonomysimple.aspx

[4]Joharchi, M. R., Amiri, M. S., *Avicenna J. Phytomed*., **2012**, *2*, 105.

[5]Badrkhani, N. Rahmani, F., Larti, M., *Botan. Sci*., **2014**, *92*, 433.

[6]Uzunhisarcikli, M. E., Vural, M. *Turk. J. Bot*., **2012**, *36*, 603.

[7]See Cornell University website, Growing Guide, "Special Considerations":http://www.gardening.cornell.edu/homegarde-ning/scene3280.html

[8]Cowan, M.M., *Clin. Microbiol. Rev*., **1999**, *12*, 564.

[9]Oran, S. A., Al-Eisawi, D. M., *Int. J. Biodivers. Conserv*., **2014**, *6*, 436.

[10]Baydoun, S., Chalak, L., Dalleh, H., Arnold, N., *J. Ethnopharmacol*., **2015**, *173*, 139.

[11]Amiri, M. S., Joharchi, M. R., *Avicenna J. Phytomed*., **2013**, *3*, 254.

[12]Altundag, E., Ozturk, M., *Procedia Soc. Behav. Sci*., **2011**, *19*, 756.

[13]Mosaddegh, M., Esmaeili, S, Hassanpour, A., Malekmohammadi, M, Naghibi, F., *Iranian Res. J. Pharmacogn*., **2016**, *3*, 7.

[14]Parsaei, P., Bahmani, M., Naghdi, N., Asadi-Samani, M., Rafieian-Kopaei, M., *Der Pharmacia Lettre*. **2016**, *8*,188.

[15]Zali, S. H., Tahmasb, R., *J. Adv.Health Med. Sci*., **2016**, *2*, 18.

[16]Sargin, S. A., Akcicek, E., Selvi, S., *J. Ethnopharmacol*., **2013**, *150*, 860.

[17]Naghibi, F., Esmaeli, S., Melekmohammadi, M., Hassanpour, A., Mosaddegh, M., *Res. J. Pharmacogn.*, **2014**, *1*, 7.

[18]Carmona, M. D., Llorach, R., Obon, C., Rivera, D., *J. Ethnopharmacol*., **2005**, *102*, 344.

[19]Tuzlaci, E., Dogan, A., *Marmara Pharm. J.*, **2010**, *14*, 136.

[20]Toupchi, Zh., *J. Rangeland Sci.*, **2011**, *1*, 103.

[21]Mati, E., de Boer, H., *J. Ethnopharmacol*., **2011**, *133*, 490.

[22]Aslan, M., *KSU J. Nat. Sci*., **2013**, 16, 28. http://dergi.ksu.edu.tr/article/view/1017000230/5000014625

[23]Tene, V., Malagon, O., Finzi, P. V., Vidari, G., Armijos, C., Zaragoza, T., *J. Ethnopharmacol*., **2007**, *111*, 63.

[24]Alyemeni, M. N., Sher, H., Wijaya, L., *J. Med. Plants Res*., **2010**, *4*, 2298.

[25]Gairola, S., Sharma, J., Bedi, Y.S., *J. Ethnopharmacol*., **2014**, *155*, 925.

[26]Menale, B., DeCastro, O., Cascone, C., Muoio, R., *J. Ethnopharmacol*., **2016**, *192*, 320.

[27]Sharma, S. D., Sahu, K., Chandrol, G. K., Jain, P. K., Sharma, V., *Int. J. Adv. Res. Biol. Sci*., **2016**, *3*, 104.

[28]Oran, S. A., *J. Agric. Sci. Technol. A.* **2014**, *4*, 461.

[29]Oran, S. A., *Int. J. Biodivers. Conserv*., **2015**, *7*, 308.

[30]Agayeva, E. Z., Ibadullayeva, S. J., Asgerov, A. A., Isayeva G. A., *Am. J. Res.Commun.*, **2013**, *1*, 51.

[31]Said, O., Khalil, K., Fulder, S., Azaizeh, H., *J. Ethnopharmacol*., **2002**, *83*, 251.

[32]Azaizeh, H., Saad, B., Khalil, K., Said, O., *eCAM*, **2006**, *3*, 229.

[33]Khalifa, A. B., *Herbs: Nature's Pharmacy*, V1, 1st ed., Casablanca, Arab Cultural Center, Morocco, **2004**, pp. 300-302. (Arabic)

[34]Saad, B., Said, O., *Greco-Arab and Islamic Herbal Medicine*, Hoboken, New-Jersy, John Wiley & Sons, Inc., **2011**, pp. 305.

[35]Kizilarslan, C., Ozhatay, N., *Marmara Pharm. J.*, **2012**, *16*, 194.

[36]Kizilarslan, C., Ozhatay, N., *Turk. J. Pharm. Sci*., **2012**, *9*, 199.

[37]Oran, S. A., Al-Eisawi, D.M., *J. Biol. Env. Sci*., **2015**, *6*, 381.

[38]Qasem, J. R., *Pak. J. Bot*., **2015**, *47*, 551.

[39]Erbay, M. S., Anil, S., Melikoglu, G., *Marmara Pharm. J.*, **2016**, *20*, 164.

[40]Tahvilian, R., Shahriari, S., Faramarzi, A., Komasi, A., *Iranian J. Pharm. Res.*, **2014**, *13*, 1029.

[41]Alali, F. Q., Tawaha, K., El-Elimat, T., Syouf, M., El-Fayad, M., Abulaila, K., Nielsen, S. J., Wheaton, W. D., Falkinham III, J. O., Oberlies, N. H., *Nat. Prod. Res*., **2011**, *21*, 1121.

[42]Fahimi, Z., Cheraghi, J., Pilehvarian, A. A., K Sayehmiri, K., Khosravi, A., *Sci. J. Ilam Univ. Med. Sci.,* **2012**, *2*, 23.

[43]Ertas, A., Boga, M., Gazioglu, I., Yesil, Y., Hasimi, N., Ozaslan, C., Yilmaz, H., Kaplan, M., *Chiang Mai J. Sci*., **2016**, *43*, 1143.

[44]Ravanbakhsh, M., Ronaghi, A., Taghavi, S. M., Jousset, A., *J. Environ. Chem. Eng.*, **2016**, *4*, 2350.

[45]Mojab, F., Kamalinejad, M., Ghaderi, N., Vahidipour, H. R., *Iranian J. Pharm. Res.*, **2003**, *2*, 77.

[46]Ameri, A., Heydarirad, G., Rezaeizadeh, H., Choopani, R., Ghobadi, A., Gachkar, L., *Evid. Based Complement. Altern. Med*., **2016**, *21*, 30.

[47]Zaitseva, N. E., Kozhina, I. S., *Khim. Prirod. Soedin.*, **1980**, *16*, 29.

[48]Kozhina, I. S., Mamatov, G. Z., *Khim. Prirod. Soedin.*, **1970**, *6*, 397.

[49]Zakizadeh, M., Nabvi, S. F., Nabvi, S. M., Ebrahimzadeh, M. A., *Eur. Rev. Med. Pharmacol. Sci*., **2011**, *15*, 406.

[50]Boostani, H., Mahmoodi, A., Farrokhnejad, E., *J. Chem. Health Risks*, **2016**, *6*, 105.

[51]Bouayed, J., Piri, K., Rammal, H., Dicko, A., Desor, F., Younos, C., Soulimani, R., *Food Chem*., **2007**, *104*, 364.

[52]Qader, S. W., Awad, H. M., *Jordan J. Biol. Sci.*, **2014**, *7*, 205.

[53]Mohammadi, R., Zarei, M. A., Ghobadi, S., *J. Med. Plants*, **2016**, *2*, 54.

[54]Imanova, A. A., Fokina, N. E., Trukhaleva, N. A., Kozhina, I. S., Ismailov, N. M., *Rastitel'nye Resursy*, **1979**, *15*, 389.

[55]Esmaeelian, B., Karmani, Y. Y., Amoozegar, M. A., Rahmani, S., Rahimi, M., Amanlou, M., *Int. J. Pharm*., **2007**, *3*, 468.

[56]Kamrani, Y. Y., Esmaeelian, B., Jabbari, M., Tabaraei, B., Yazdanyar, A., Ebrahimi, S. N., *Planta Med*., **2008**, *74*, 174. (DOI: 10.1055/s-0028-1084172)

[57]Pakudina, Z. P., Sadykov, A. S., Zuparov, A., *Khim. Prirod. Soedin.*, **1970**, *5*, 628.

[58]Zaitseva, N. E., Kozhina, I. S., *Khim. Prirod. Soedin.*, **1980**, *16*, 145.

[59]Khidyrova, N. K., Rakhmatova, M. Z., Shakhidoyatov, R. K., Shakhidoyatov, K. M., *Chem. Nat. Compd*., **2012**, *48*, 180.

[60]Kukina, T. P., Salnikova, O. I., Khidyrova, N. K., Rakhmatova, M. D., Pankrushina, N. A., Grazhdannikov, A. E., *Chem. Nat. Compd*., **2016**, *52*, 285.

[61]Syrov, V. N., Vais, E. V., Khidyrova, N. K., Rakhmatova, M. D., Shakhidoyatov, R. K., Khushbaktov, Z. A., *Pharm. Chem. J*., **2016**, *50*, 29.

[62]Aydin, S., Oztiirk, Y., Bapr, K. H. C., Kmmer, N., Kurtar-Oztiirk, N., *Phytother. Res*., **1992**, *6*, 219.

[63]Azirak, S., Karaman, S., *Acta Agric. Scand. Sect. B*. **2008**, *58*, 88.

[64]Yener, S. H., Yarci, C., *Fresen. Environ. Bull*., **2010**, *19*, 1024.

[65]Aysu, T., *Bioresour. Technol*., **2015**, *191*, 253.

[66]Geronikaki, A. A., Abduazimov, K. A., *Khim. Prirod. Soedin.*, **1975**, *10*, 242.

[67]Geronlkaki, A. A., Abduazimov, K. A., *Khim. Prirod. Soedin.*, **1976**, *11*, 93.

[68]Popov, P. L., *J. Stress Physiol. Biochem*., **2008**, *4*, 17.

[69]Kozhina, I. S., Mamatov, G. Z., *Khim. Prirod. Soedin.*, **1970**, *9*, 146.

[70]Movsumov, I. S., Garayev, E. A., *Chem. Plant Raw Mater*., **2010**, *3*, 5.

[71]Yuzikhin, O., Mitina, G., Berestetskiy, A., *J. Agric. Food Chem.*, **2007,** *55*, 7707.

[72]Jamous, R. M., Abu Zaitoun, S. Y., Husein, A. I., Iman B. Y. Qasem, I. B. Y., Ali-Shtayeh, M. S., *Eur. J. Med. Plants*, **2015**, *9*, 1.

[73]Moogahi. S. M. H. N., Khanehzad, M., Sadr, M., Roholahi, S. H., Kameli, S. M., *J. Med. Plants*, **2013**, *4*, 54.

[74]Gopalakrishnan, N., Kaimal, T. N. B., Lakshminarayana, G., *Phytochemistry*, **1982**, *21*, 2205.

[75]Huntress, E. H., *J. Chem. Educ*., **1928**, *5*, 1615.

[76]Kasumov, M. A., *Dokl. Akad. Nauk Azerb.*, **1984**, *40*, 76.

[77]Hosaka, H., Mizuno, T., Iwashina, T., *Bull. Natl. Mus. Nat. Sci., Ser. B*. **2012**, *38*, 69.

[78]Gholamrezaei, S., Salavati-Niasari, M., *J. Mater. Sci: Mater. Electron*., **2016**, *27*, 2467.

[79]Ebrahiminezhad, A., Barzegar, Y., Ghasemi, Y., Berenjian, A., *Chem. Ind. Chem. Eng. Quart.*, **2016**, *1*. DOI:10.2298/ciceq150824002e.

[80]Classen, B,, Blaschek, W., *Planta Med*., **1998**, *64*, 640.

[81]Atkhamova, S. K., Rakhmanberdyeva, R. K., Rakhimov, D. A, Levkovich, M. G., Abdullaev, N. D, Ismailov, A. I., Dalimov, D. N., *Chem. Nat. Compd*., **2001**, *37*, 203.

[82]Dudek, M., Matlawska, I., Szkudlarek, M., *Acta Pol. Pharm*., **2006**, *63*, 207.

[83]Azizov, U. M., Mirakilova, D. B., Umarova, N. T., Salikhov, S. A., Rakhimov, D. A., Mezhlumyan, L. G., *Chem. Nat. Compd*., **2007**, *43*, 508.

[84]Ordak, M., Wesolowski, M., Radecka, I., Muszynska, E., Bujalska-Zazdrozny, M., *Biol. Trace Elem. Res*., **2016**, *173*, 514.

[85]Rakhimov, D. A., Atkhamova, S. K., Khvan, A. M., *Chem. Nat. Compd*., **2007**, *43*, 685.

[86]Cheng, W., Cheng, X., Liu, Z., Zeng, Y., *Asian J. Chem.*, **2013**, *25*, 2243.

[87]Rakhmatova, M. Z., Kiyamova, S. E., Khidyrova, N. K., Shakhidoyatov, K. M., *Chem. Nat. Compd*., **2015**, *51*, 769.

[88]Eskandari, M., Samavati, V., *Int. J. Biol. Macromol.*, **2015**, *72*, 347.

[89]Mert, T., Fafal, T., Kivcak, B., Ozturk, H. T., *Hacettepe Univ. J. Fac. Pharm.*, **2010**, *30*, 17.

[90]Seyyednejad, S. M., Koochak, H., Darabpour, E., Motamedi, H., *Asian Pac. J. Trop. Med*., **2010**, *3*, 351.

[91]Ghasemi, M., Atakishiyeva, Y., *Infect. Epidemiol. Med.*, **2016**, *2*, 12.

[92]Ammar, N. M., El-Kashoury, E. A., El-Kassem, L. T., Abd El-Hakeem, R. E., *J. Arab Soc. Med. Res.*,**2013**, *8*, 48.

[93]Liu, F., Du, W., Bai, X., Tian, S., *J. Chem. Pharm. Res*., **2014**, *6*, 1466.

[94]Swamy, M. S., Sivanna, N., Anand Tamatam, A., Khanum, F., *Functional Foods Health Disease*, **2011**, *1*, 482.

[95]Abd El-Salam, N. M., Radwan, M. M., Wanas, A. S., Shenouda, M. L., Sallam, S. M., Piacente, S., ElSohly, M. A., Ghazy, N. A., *Planta Med*., **2016**, *82*, 83.

[96]Yaglioglu, A. S., Eser, F., Tekin, S., Onal, A., *Front. Life Sci*., **2016**, *9*, 69.

[97]Ahmed, I., Roy, B. C., Subramaniam, D., Ganie, S. A., Kwatra, D., Dixon, D., Anant, S., Zargar, M. A., Umar, S., *Carcinogenesis*. **2016**, *37*, 385.

[98]Asres, K., Bucar, F., Kartnig, T., Witvrouw, M., PannecouquE, C., De Clercq, E., *Phytother. Res.*, **2001**, *15*, 62.

[99]Shoeib, A.R.S., Zarouk, A.W., El-Esnawy, N.A., *Aust. J. Basic Appl. Sci.*, **2011**, *5*, 75.

[100]El Ghaoui, W., Bou Ghanem, E., Abou Chedid, L., Abdelnoor, A. M., *Phytother. Res.*, **2008**, *22*, 1599.

[101]Ahmadi,M., Rad, A. K., Rajaei, Z., Hadjzadeh, M., Mohammadian, N., Tabasi, N. S., *Indian J. Pharmacol.*, **2012**, *44*, 304.

[102]Al-Snafi, A. E., *Int. J. Pharm. Techn. Res.*, **2013**, *5*, 1378. This review aricle cites a Chinese research article by W. Dongfeng *et al*. for cardiovascular activity of ethanolic extract of *Alcea rosea* flowers. This article was published in Chinese in 1988. We tried several times to reach this article but we failed. The link to it is: http://en.cnki.com.cn/Article_en/CJFDTOTAL-SYYD198804008.htm

[103]Hussain, L., Akash, M. S. H., Tahir, M., Rehman, K., Ahmed, K. Z., *Bangladesh J. Pharmacol*., **2014**, *9*, 322.

[104]Zhang, Y., Jin, L., Chen, Q., Wu, Z., Dong, Y., Han, L., Wang, T., *Fitoterapia*. **2015**, *102*, 7.

[105]Manesh, H. J., Alibazi, A., Sohrabi, R., Skandari, Z., Ranjbaran, M.,Mirnezami, M., *Complementary Med. J. Fac. Nursing Midwifery*. **2015**, *4*, 954.

[106]Namjoyan, F., Jahangiri, A., Azemi, M. E., Arkian, E., Mousavi, H., *Jundishapur J. Nat. Pharm. Prod.*, **2015**, *10*, e23356, https://www.ncbi.nlm.nih.gov/pubmed/25866725

[107]Benli, M., Guney, K., Bingol, U., Geven, F., Yigit, N., *Afr. J. Biotechnol*., **2007**, 6, 1774.

[108]Priya, S. S. L., Devi, P. R., Eganathan, P., Kingsley, J., *Afr. J. Pharm. Pharmacol*., **2013**, *7*,1719.

[109]Genskowsky, E., Puente, L. A., Perez-Alvarez, J. A., Fernandez-Lopez, J., Munoz, L. A., Viuda-Martos, M., *J. Sci. Food Agric*., **2016**, *96*, 4235.

[110]Saito, S., Silva, G., Santos, R. X., Gosmann, G., Pungartnik, C., Brendel, M., *Int. J. Mol. Sci.*, **2012**, *13*, 2846.

[111]Ohtani, K., Okai, K., Yamashita, U., Yuasa, I., Misaki, A., *Biosci. Biotech. Biochem*., **1995**, *59*, 378.

[112]Murray, A. P., Faraoni, M. B., Castro, M. J., Alza, N. P., Cavallaro,V., *Curr. Neuropharmacol*., **2013**, *11*, 388.

[113]Mak, S., Luk, W. W. K., Cui, W., Hu, S., Tsim, K. W. K.., Han, Y., *J. Mol. Neurosci*., **2014**, *53*, 511.

[114]Vencislav, V., Hertel, J., Skoczylas, E., Swiezewska, E., Chojnacki, T., *Acta Biochem. Pol*., **1996**, *43*, 707.

[115]Bamba, T., Fukusaki, E., Kajiyama, S., Ute, K., Kitayama, T., Kobayashi, A., Eucommiaulmoides, O., *Lipids*, **2001**, *36*, 727.

[116]Speath, F.C., Rosenblatt, D. H., *Anal. Chem.*, **1950**, *22*, 1321.

[117]Wurdack, J. H., *J. Pharm. Sci.*, **1924**, *13*, 399.

[118]Zaffino, C., Bruni, S., Russo, B., Pilu, R., Chiara Lago, C., Colonna, G. M., *J. Raman Spectr.*, **2016**, *47*, 269.

[119]Chang, T-S., *Int. J. Mol. Sci.*, **2009**, *10*, 2440.

[120]Qiu, L., Zhao, F., Jiang, Z-H., Chen, L-X., Zhao, Q., Liu, H-X., Yao, X-S., Qiu, F., *J. Nat. Prod*., **2008**, *71*, 642.

Received : 26.12.2016.

Accepted : 31.01.2017

REMOVAL OF POLYPHOSPHATES FROM WASTEWATER BY MAGNETIC COMPOSITE MINERAL SORBENTS

Oksana Makarchuk[a] and Tetiana Dontsova[a]*

Keywords: Composite magnetic sorbent, natural clay, magnetite, adsorption, magnetic separation.

Magnetic composite mineral sorbents based on saponite, spondyle, palygorskite clays and magnetite were created. The ability of magnetic sorbents to remove tripolyphosphate and hexametaphosphate from aqueous solutions has been studied for different adsorbate concentrations by varying the amount of adsorbent, temperature and shaking time. The kinetics of adsorption process data was examined using the pseudo-first-order, pseudo-second-order kinetics and the Boyd-Adamson internal diffusion kinetic models. The adsorption kinetics is best described by the pseudo second-order model with good correlation ($R^2 \approx 1.00$). The experimental isotherm data were analyzed using the Langmuir, Freundlich, Temkin and Dubinin–Radushkevich equations. The experimental data well fitted to Langmuir isotherm model. It was found that calculated adsorption capacities of magnetic composites relatively tripolyphosphate (550-620 mg g^{-1}) and hexametaphosphate (670-730 mg g^{-1}) were good agreed with experimentally obtained values. The thermodynamic parameters, such as ΔG^0, ΔH^0 and ΔS^0 were also determined. It was indicated that the adsorption of polyphosphates was feasible, spontaneous and exothermic in nature and the physical nature of the process was confirmed. Thus, cheap magnetic sorbents based on natural clays and magnetite, which not only quickly separated from the solution by magnetic separation, but effectively removed polyphosphates were obtained.

* Corresponding Authors
E-Mail: xtfhn9207@ukr.net, dontsova@xtf.kpi.ua
[a] Chemical Technology Department, National Technical University of Ukraine "Igor Sikorsky Kyiv Polytechnic Institute", Victory Avenue, 37, Kyiv-03056, Ukraine

Introduction

Currently one of the major problems in wastewater treatment is the removal the biogenic elements, such as nitrogen and phosphorus, that cause eutrophication of water bodies.[1] Soluble phosphorus is the main limiting element that mostly affects the growth of vegetation of aquatic bodies. It is known that eutrophication of water is not observed at concentrations of phosphorus less than 0.2 mg L^{-1}.[2]

The main source of biogenic polluting substances of water bodies is municipal wastewater. Functioning of most urban wastewater treatment plants is based on traditional biotechnology, which provides a low degree of phosphates removal (20-30 %).[3] Especially polyphosphates, intensively used in the composition of household detergents and washing powders, are difficult to remove.[4]

Adsorption is the most promising method of disposal of contaminated wastewater. Recently, sorption materials of natural origin, such as clays acquired great popularity. Compared with traditional sorbents, clay minerals have a higher sorption capacity, greater mechanical and chemical resistance and lower cost. In particular, the clay materials were tested for the removal of phosphates. Clays has a sufficiently high sorption activity with respect to phosphate.[5]

The high sorption activity of clay sorbents was due to their colloidal dispersibility. In this regard, the problem of removing of spent sorbent particles from the aquatic environment arose. Also, it creates the risk of secondary water pollution.

To overcome this difficulty, the creation of the magnetic composites based on clays materials and magnetite (Fe_3O_4) is proposed. The waste magnetic materials can be easily removed from the water after completion of the sorption process by magnetic separation. In addition, creation of composite sorbents based on clay minerals and magnetic iron oxide provides[6] aggregative stability of nanosized Fe_3O_4, due to its stabilization in the structure of clay matrix and high efficiency of composite sorbent based on cheap mineral raw materials.

Therefore, in this article the creation of magnetic composite mineral sorbents (MC) based clay minerals (saponite, spondyle clay, palygorskite) and magnetite Fe_3O_4 is reported. The sorption, kinetic and thermodynamic laws of tripolyphosphate (TPP) and hexametaphosphate (HMP) removal from aqueous solutions by clay minerals, magnetite and composite sorbents based on them have been investigated.

Experimental

Synthesis of MC samples

Synthesis of MC by impregnation method was based on the process of physical adsorption of magnetic Fe_3O_4 particles in the pores and on the surface of clay.[7] Magnetite in the form of magnetic fluid is produced by chemical deposition from a solution according to the Elmore method.[8] Saponite, spondyle clay, palygorskite (particle size less than 230 meshes (63 μm)) and magnetic fluid was stirred for 30 min. The resultant suspension was separated by the magnetic filter and dried at a temperature of 60-80 °C for 24 h. Thus, samples of magnetic sorbents based on saponite (MCSp-2, MCSp-4, MCSp-7, MCSp-10), spondyle clay (MCSd-2, MCSd-4, MCSd-7, MCSd-10) and palygorskite (MCP-2, MCP-4, MCP-7, MCP-10) containing 2 %wt., 4 %wt., 7 %wt. and 10 %wt. of magnetite, respectively were obtained.

Adsorption kinetic

In kinetic studies, 1 g of each adsorbent was added into a flask with 100 mL of 200 mg L^{-1} TPP solution or 400 mg L^{-1} HMP solution. The sealed flasks were put in a shaker bath at 20±2 °C and shaken at 35 rpm for15, 30, 60, 120 and 180 min. After the expiry of the specified time suspension was centrifuged at 3000 rpm for 5 min and residual (equilibrium) concentration of polyphosphates were determined by photometric method using a UV-5800PC Spectrophotometer.

Adsorption procedure

Batch adsorption experiments were carried out by adding a fixed amount of sorbent (1 g) into a number of 250 mL stoppered glasses containing a 100 mL of different initial concentrations (50–10000 mg L^{-1}) solution of tripolyphosphate or hexametaphosphate. The flasks were placed in a thermostatic water bath shaker (20±2 °C) and agitation was provided at 350 rpm for 60 min to ensure equilibrium was reached. After setting of adsorption equilibrium the suspension was separated in a field of centrifugal forces during 5 min at 3000 rpm. After adsorption experiments, the concentrations of phosphate in the solutions were determined by photometric method using a UV-5800PC Spectrophotometer.

The amount of adsorption at equilibrium, $Q_{t(e)}$ (mg g^{-1}), was calculated by eqn. (1),

$$Q_{t(e)} = \frac{(C_0 - C_e)\cdot V}{m}, \quad (1)$$

where

C_0 and C_e (mg L^{-1}) are liquid-phase concentrations of TPP or HMP at initial and equilibrium, respectively,

V (L) is the volume of solution and

m (g) is the mass of sorbent used.

Adsorption kinetic parameters

In the process of surfactants removal from aqueous solutions sorption kinetics is important to select the optimal conditions of water purification. It provides important information about the ways and mechanisms of sorption. As is well known, sorption process is complicated and multistage, therefore, traditional kinetic models are not always suitable to describe complex adsorption process. To describe the sorption kinetics in modern scientific literature the kinetic model of the pseudo-first order, pseudo-second order and diffusion Boyd-Adamson models are used, which reveal the influence of the chemical stage.[9]

The pseudo-first order model of the rate is the earliest sorption kinetics model (eqn. 2),[10] where $Q_{t(e)}$ and Q_t is sorption capacity of surfactant, in mg g^{-1}, at equilibrium and at time t and k_1 is pseudo-first order model rate constant in min^{-1}.

$$\frac{dQ_t}{dt} = k_1 \cdot \left(Q_{t(e)} - Q_t\right), \quad (2)$$

Eqn. (2) in the integration of boundary conditions of $t = 0$ to $t = t$ and $Q_t = 0$ from to $Q_e = Q_t$ takes the form of Eqn.(3).

$$\ln\left(Q_{t(e)} - Q_t\right) = \ln(Q_{t(e)}) - \frac{k_1}{2{,}303}\cdot t, \quad (3)$$

where $Q_{t(e)}$ and Q_t are calculated as follows,

$$Q = \frac{(C_t - C_0)\cdot V}{m}\cdot 1000, \quad (4)$$

where

C_0 and C_t are the initial surfactant concentration and concentration of surfactant in solution at time t, respectively in mg L^{-1},

V is model solution volume in L and

m is the mass of sorbent sample in g.

For description of sorption process in aqueous solution the following pseudo-second order model of the rate is also used,[11] where k_2 is pseudo-second order rate constant, (g mg^{-1} min^{-1}).

$$\frac{dQ_t}{dt} = k_2 \cdot \left(Q_{t(e)} - Q_t\right)^2, \quad (5)$$

The integrated form of the classical rate equation of pseudo-second order model is given by Eqn. (6).

$$Q_t = \frac{t}{\frac{1}{k_2 \cdot Q_{t(e)}^2} + \frac{t}{Q_{t(e)}}} \quad (6)$$

The analysis of primary kinetic curves was conducted using the equation for Boyd-Adamson internal diffusion kinetic model (Eqn. 7),[12]

$$F = \frac{\theta_t}{\theta_\infty} = 1 - \frac{6}{\pi}\sum_{n=1}^{\infty}\frac{1}{n^2}\exp\left(-\frac{D\cdot\pi^2\cdot n^2\cdot t}{r^2}\right), \quad (7)$$

where

θ_t and θ_∞ is the degree of sorbent saturation after t seconds and infinite time, respectively,

F is the degree of equilibrium achievement,

D is diffusion coefficient (cm^2 s^{-1}),

r is sorbent particle radius (mm) and

n is number of integers 1, 2, 3, 4, 5.

Criterion of Fourier is given by Eqn. (8), where B, the rate constant of diffusion is given by Eqn. (9).

 DOI: 10.17628/ecb.2016.5.515-523

$$\frac{D \cdot \pi^2 \cdot t}{r^2} = Bt, \quad (8)$$

$$B = \frac{D \cdot \pi^2}{r^2}. \quad (9)$$

By substituting the Eqn. (8) into the Eqn. (9) we get Eqn. (10),

$$F = 1 - \frac{6}{\pi} \sum_{n=1}^{\infty} \frac{1}{n^2} \exp\left(-Btn^2\right), \quad (10)$$

where

Bt is the dimensionless parameter, which is the solution of task of diffusion in the solid part.

For experimentally obtained values of *F* the appropriate value of *Bt* is determined.[13] To confirm the diffusion limiting sorption process the construction of *Bt* versus *t* and *-ln(1-F)* versus *t* are used. The linear dependence *Bt* on *t* evidences in favor of limiting internal diffusion. Linearity depending *-ln (1-F)* on *t* can point to external diffusion mechanism or adsorption kinetics.

If dependence $Bt = f(t)$ is linear the limiting stage of adsorption treatment is diffusion in sorbent phase. Slope of this line is equal to *B*, and then the average diffusion coefficient in the sorbent particle is, $cm^2\ s^{-1}$.

$$D = \frac{B \cdot r^2}{\pi^2}. \quad (11)$$

Adsorption isotherms models

The adsorption isotherms express the specific relation between the concentration of adsorbate and its degree of accumulation onto adsorbent surface at constant temperature. Several isotherm models have been used to fit to the experimental data and evaluate the isotherm performance for polyphosphate adsorption. Langmuir, Freundlich, Temkin and Dubinin-Radushkevycha isotherms models have been employed in the present study.[14]

Langmuir adsorption isotherm quantitatively describes the formation of adsorbate monolayer on the external adsorbent pores surface. The model assumes equal adsorption energy on the surface of the sorbent. Based on these assumptions, the Langmuir model in the linear form is represented by the eqn. (12),[15] where $C_{t(e)}$ is equilibrium concentration of surfactant ($mg\ L^{-1}$) and K_L is constant of Langmuir equation ($L\ mg^{-1}$).

$$\frac{1}{Q_{t(e)}} = \frac{1}{Q_t} + \frac{1}{Q_t \cdot K_L \cdot C_{t(e)}}, \quad (12)$$

Freundlich adsorption isotherm is used to describe adsorption on heterogeneous surfaces. According to this model, adsorption centers have different energies of interaction. Since active centers with maximum energy are saturated primarily. The linear form of Freundlich model is described by Eqn. (13),[15]

$$\log Q_{t(e)} = \log K_f + \frac{1}{n} \cdot \log C_{t(e)}, \quad (13)$$

where

K_f is Freundlich equilibrium constant ($mg\ g^{-1}$) and

n^{-1} is parameter that indicates the intensity of interaction between adsorbent and adsorbate.

Temkin model takes into account the interaction between adsorbent and adsorbate. The model assumes that the heat of molecules adsorption in the layer will decrease linearly, not logarithmic with increasing degree of filling surface. The linear form of Temkin model is given in Eqns. (14) and (15),[15]

$$Q_{t(e)} = B \cdot \ln A_T + B \cdot \ln C_{t(e)}, \quad (14)$$

$$B = \frac{RT}{b_T}, \quad (15)$$

where

A_T is Temkin equilibrium constant ($L\ g^{-1}$),

b_T is Temkin equations constant ($L\ g^{-1}$) and

B is constant of adsorption heat ($J\ mol^{-1}$).

Dubinin–Radushkevich isotherm is generally applied to express the adsorption mechanism with a Gaussian energy distribution onto a heterogeneous surface.[9] The model has often successfully fitted high solute activities and the intermediate range of concentrations data.

$$\ln Q_{t(e)} = -\beta \cdot \varepsilon^2 + \ln Q_{t(e)}, \quad (16)$$

Here β is Dubinin–Radushkevich equilibrium constant ($mol^2\ K^{-1}\ J^{-2}$) and ε is the Polanyi potential.

This approach was usually applied to distinguish the physical and chemical adsorption of organic pollutants. Its mean free energy per molecule of adsorbate (for removing a molecule from its location in the sorption space to the infinity) can be computed by Eqn. (17), where β is denoted as the isotherm constant.

$$E = \frac{1}{\sqrt{2\beta}}, \quad (17)$$

Meanwhile, the parameter ε can be calculated as:

$$\varepsilon = RT \cdot \ln(1+\frac{1}{C_{t(e)}}). \quad (18)$$

The impact of temperature is one of the most important factors that determine the effectiveness of sorption wastewater treatment. Adsorption removal of polyphosphates from aqueous solutions was determined at three temperatures (290, 323, 343 K). Fundamental thermodynamic parameters, like heat of sorption ΔH^0, entropy ΔS^0, and free energy of activation ΔG^0, play an important role in predicting the adsorption behavior because these are strongly dependent on temperature. ΔG^0 was calculated according to the following equation,[12]

$$\Delta G^0 = -RT \cdot \ln K_D, \quad (19)$$

where

R is the gas constant and

K_D is equilibrium constant at the temperature T.

The numerical values of the equilibrium constant were calculated from:

$$K_D = \frac{C_{Be}}{C_{Ae}}, \quad (20)$$

where C_{Be} and C_{Ae} are the equilibrium concentrations of polyphosphates on adsorbent solid phase and in solution liquid phase, respectively, mg L^{-1}.

ΔH^0 and ΔS^0 were evaluated using Van't Hoff equation as follows

$$lnK_D = \frac{\Delta S^0}{R} - \frac{\Delta H^0}{RT} \quad (23)$$

where,

R is the gas constant (8.314 J $mol^{-1}K^{-1}$),

T is solution temperature (K) and

K_D is the distribution coefficient of the surfactant between the adsorbed layer and the solution.

The slope and intercept of the linear plot of $ln\ K_D$ versus T^{-1} were used to determine the values of ΔH^0 and ΔS^0.

Results

Adsorption kinetic

Kinetic dependences of polyphosphates adsorption by minerals (saponite, spondyle clay, palygorskite), magnetite and composites on their base are presented on Figure 1.

Isotherm data

Adsorption isotherms of tripolyphosphate (a, c, e) and hexametaphosphate (b, d, f) on clay minerals, magnetite and composites based on them are shown in Figure 2.

Model fitting and kinetic parameters

In order to investigate rate-controlling steps that include mass transport and adsorption processes, kinetic models were used to test the experimental data. Table 1 presents the results of fitting of experimental data with pseudo-first-order, pseudo-second-order and Boyd-Adamson internal diffusion kinetics models using values of k_1, k_2, D and correlation coefficient (R^2).

Model fitting and adsorption isotherm parameters

To establish the mechanism of interaction between adsorbate and adsorbent the adsorption isotherms models were applied to obtained experimental data. The parameters of Langmuir, Freundlich, Temkin and Dubinin-Radushkevych adsorption isotherms are summarized in table 2.

Termodynamic parameters of adsorption

For determination of nature of polyphosphates sorption removal (physisorption or chemisorption) the thermodynamic patterns were analyzed. Values of thermodynamic parameters (ΔH^0, ΔS^0, and ΔG^0) obtained at different temperatures during polyphosphate adsorption are given in table 3.

Discussion

Adsorption kinetic

According to the kinetic dependencies of polyphosphates removal from aqueous solutions (Figure 1) the equilibrium time was reached in 30 minutes for the magnetic composites MCSp-7 and MCSp-10. The purification of water model solutions of TPP and HMP by using the rest of composite sorbents and clay minerals was lasted for 60 min. Moreover, the percentages of polyphosphates adsorption for magnetic composites were in 1.5-2.0 times higher compared with native natural clays. If using nanosized magnetite as a sorbent the removal of TPP (40 min) was occurred faster compared with HMP (60 min).

Isotherm data

The maximum sorption capacity of MCSp, MCSd and MCP in the disposal of polyphosphates was in the range of 490-570 mg TPP g^{-1} and 610-810 mg HMP g^{-1}, 500-550 mg TPP g^{-1} and 660-820 mg HMP g^{-1}, 490-540 mg TPP g^{-1} and 650-790 mg HMP g^{-1} respectively (Figure 2). The efficiency of removal of polyphosphates is directly proportional to the magnetite content in the composition of the composites.

The sorption capacities of native saponite, spondyle clay and palygorskite towards polyphosphates, as obtained from the sorption isotherms, are 2-3 times lower as compared with composites on their base.

High sorption capacity relative to TPP (770 $mg \cdot g^{-1}$) and HMP (1200 $mg \cdot g^{-1}$) was inherent for nanosized magnetite received in the form of magnetic fluid. A significant magnetite sorption activity is guaranteed within one hour after the synthesis of magnetic fluid. Fe_3O_4 is nonporous sorbent and the adsorption of pollutants takes place on the surface of its particles. Nanosized magnetite is prone to aggregation and is not stable over time. In forming micro particles due to aggregation the Fe_3O_4 sorption capacity is reduced by an order. Thus, the nanosized magnetite stabilization on the surface of pores of clay minerals will provide the creation of composite sorbents with high sorption activity.

As can be seen from the figure 2, the highest sorption capacity towards TPP and HMP was achieved using magnetic composites MCSp-7, MCSd-7 and MCP-7, which contain magnetite in an amount of 7 wt. %.

Adsorption kinetic models

In order to determine and interpret the mechanisms of polyphosphates adsorption processes onto MCSp-7, MCSd-7 and MCP-7 and major parameters governing sorption kinetics were fitted to the pseudo-first-order, pseudo-second-order and Boyd-Adamson internal diffusion kinetics models. The correlation coefficients for pseudo-second-orderand kinetic model obtained for all the studied sorbents were relatively high. The R^2 values for the plots of integrated form of rate equations were in the range 0.9874 – 0.9999 (Table 1).

It is clear from the accuracy of the model that the adsorption kinetic of the TPP and HMP onto magnetic composites is described by a pseudo second-order and that this interaction is significant in the rate-controlling step. Based on the rate constants of pseudo-second order model, k_2, the choice of magnetic composites mineral base was suggested. As follows, the TPP and HMP removal occurred most intense with application of composites based on saponite.

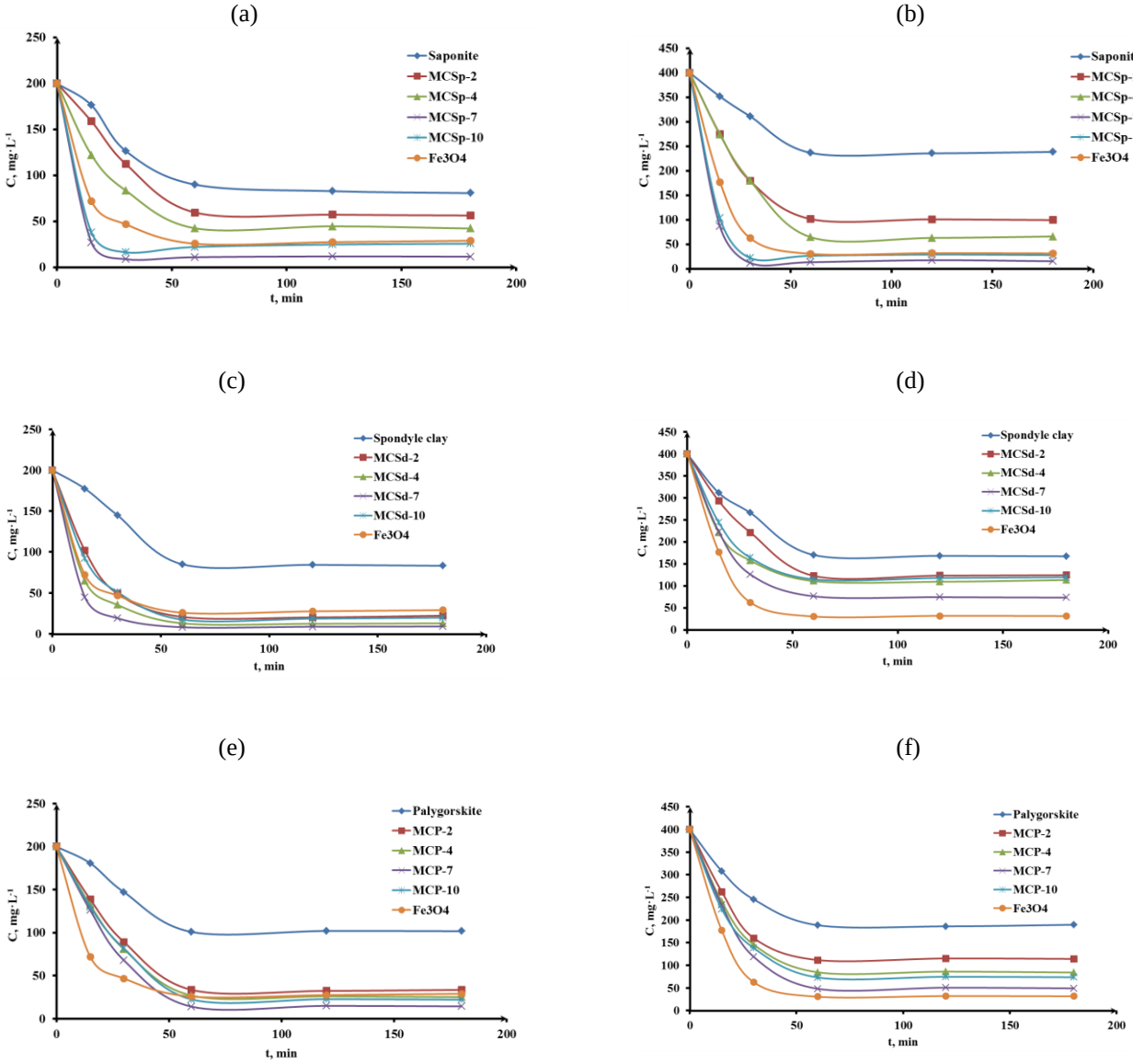

Figure 1. Dependences of the residual concentration of TPP (a, c, e) and HMP (b, d, f) of the duration of sorbents contact with water model solutions

Table 1. Kinetic parameters and correlation coefficients of pseudo-first order, pseudo-second order and diffusion model of TPP and HMP adsorption by magnetic mineral sorbents

Kinetic model	Pseudo-first order model		Pseudo-second order model		Diffusion model		
	k_1	R^2	k_2	R^2	R^2	$D \cdot 10^6$, $cm^2 \cdot s^{-1}$	R^2
Sample of polyphosphates				**TPP**			
MCSp-7	0.0205	0.4245	0.1266	0.9999	0.4245	1.517	0.5345
MCSd-7	0.0532	0.8217	0.0219	0.9997	0.5217	1.270	0.7754
MCP-7	0.1200	0.6312	0.0025	0.9874	0.6312	3.300	0.7199
Sample of polyphosphates				**HMP**			
MCSp-7	0.0299	0.3053	0.0175	0.9996	0.3053	1.198	0.5343
MCSd-7	0.1092	0.8725	0.0031	0.9969	0.5725	2.890	0.7153
MCP-7	0.0815	0.9733	0.0029	0.9965	0.7733	1.970	0.8906

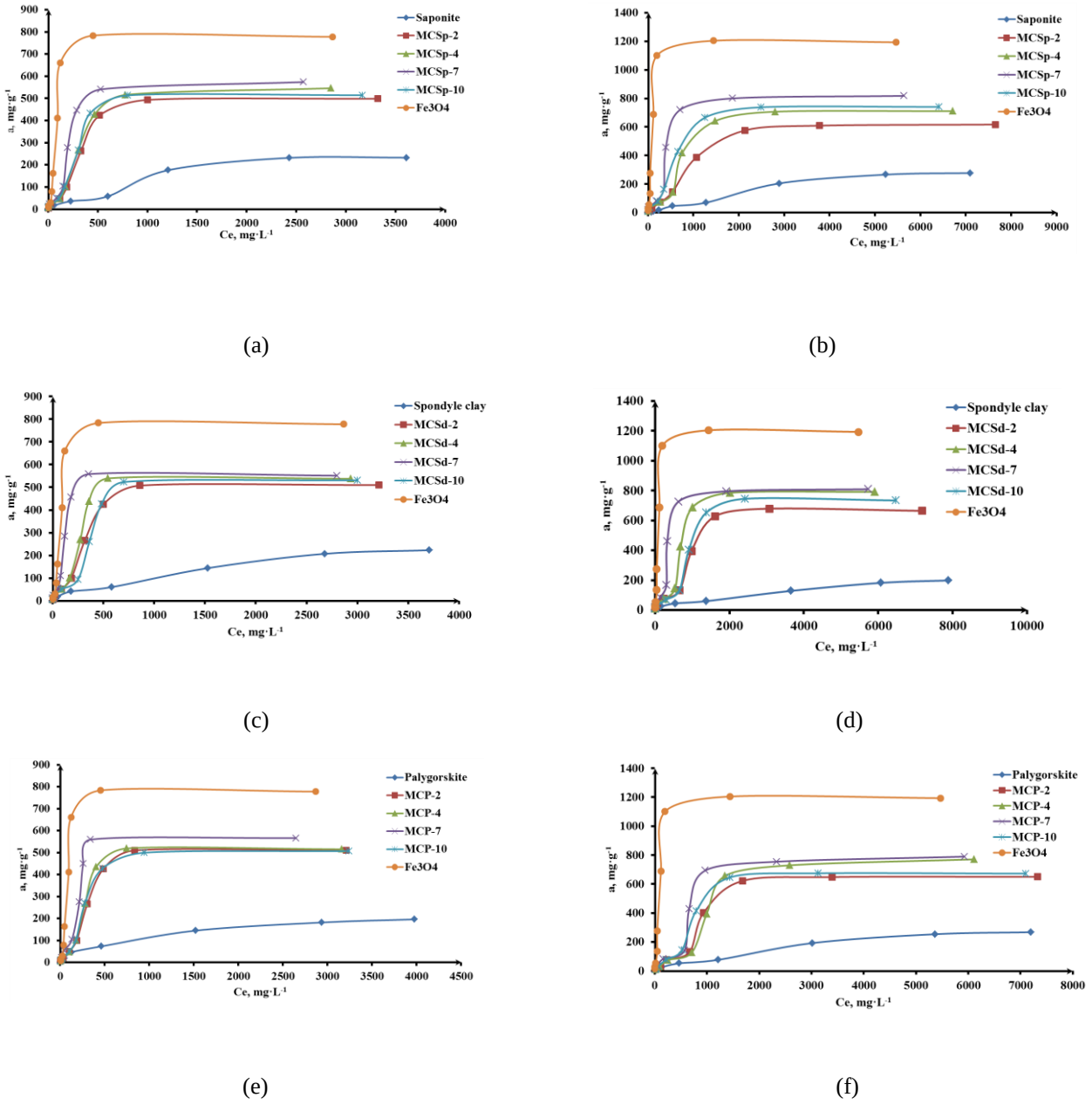

Figure 2. Adsorption isotherm of TPP (a, c, e) and HMP (b, d, f) on sorbents samples

The kinetic data of polyphosphates sorption were analyzed by Boyd-Adamson diffusion kinetics model. As noted in table 1 correlation coefficient of dependence *-ln(1-F)=f(t)* were significantly lower compared to R^2 of *Bt=f(t)*. Thereby, the assumption about the possibility of limiting sorption process of purification in the internal diffusion field was not confirmed. The values of diffusion coefficient are found to be on the order of 10^{-6} cm^2 s^{-1} for all the investigated sorbent samples, so the pore diffusion in this study was not significant.

Adsorption isotherms models

The adsorption isotherms express the specific relation between the concentration of adsorbate and its degree of accumulation onto adsorbent surface at constant temperature.

Several isotherm models as Langmuir, Freundlich, Temkin and Dubnin–Radushkevich adsorption isotherm model have been used to fit to the experimental data and evaluate the isotherm performance for polyphosphate adsorption onto MCSp-7, MCSd-7 and MCP-7.

The conformity of adsorption data (Table 2) to the Langmuir isotherm ($R^2 \approx 1.00$) could be interpreted as a homogeny adsorption process, leading to monolayer binding. So, the relatively uniform energy distribution of active adsorption sites on the pores surface of composites was achieved. The theoretical maximum adsorption capacities of magnetic composites containing magnetite in an amount of 7 wt. % were calculated by Langmuir equation. It was found that calculated adsorption capacities were good agreed with experimentally obtained values.

Table 2. Adsorption isotherm parameters and correlation coefficient of TPP and HMP adsorption by MC sorbents

Sample	**TPP**					
Sorbent	**Langmuir isotherm**			**Freundlich isotherm**		
	R^2	K_L, L·mg^{-1}	$Q_{t(e)}$, mg·g^{-1}	R^2	K_f, mg·g^{-1}	n
MCSp-7	0.9959	0.0070	625.0000	0.9211	2.0674	1.5163
MCSd-7	0.9986	0.0179	555.5556	0.8995	3.1925	1.9212
MCP-7	0.9935	0.0085	588.2352	0.9204	1.8360	1.3763
Sorbent	**Temkin isotherm**			**Dubinin-Radushkevych isotherm**		
	R^2	A_T, L·g^{-1}	B, J·mol^{-1}	R^2	E, kJ·mol^{-1}	$Q_{t(e)}$, mg·g^{-1}
MCSp-7	0.7072	0.2528	78.6020	0.3693	0.7906	127.8043
MCSd-7	0.6648	1.2674	60.9900	0.5208	1.5811	156.1004
MCP-7	0.7366	0.1871	88.7370	0.3835	0.5000	131.0659
Sample	**HMP**					
Sorbent	**Langmuir isotherm**			**Freundlich isotherm**		
	R^2	K_L, L·mg^{-1}	$Q_{t(e)}$, mg·g^{-1}	R^2	K_f, mg·g^{-1}	n
MCSp-7	0.9981	0.0049	733.3333	0.9273	2.4051	1.6906
MCSd-7	0.9989	0.0063	814.3011	0.9277	2.2235	1.6000
MCP-7	0.9938	0.0025	678.1200	0.9444	1.5300	1.4100
Sorbent	**Temkin isotherm**			**Dubinin-Radushkevych isotherm**		
	R^2	A_T, L·g^{-1}	B, J·mol^{-1}	R^2	E, kJ·mol^{-1}	$Q_{t(e)}$, mg·g^{-1}
MCSp-7	0.7337	0.1707	108.96	0.4796	0.4082	228.3546
MCSd-7	0.7576	0.1362	116.24	0.3851	0.4082	205.5933
MCP-7	0.7604	0.0547	126.17	0.4502	0.1581	209.1391

The result shows that the value of Freundlich adsorption isotherm parameter n is greater than unity for all analyzed sorbents indicating that the polyphosphates is favorably adsorbed on MC samples. The magnitude of Freundlich constant indicates easy uptake of TPP and HMP from aqueous solution.

Adsorption thermodynamics parameters

The values of thermodynamic parameters, i.e. ΔG^0, ΔH^0 and ΔS^0, are used to determine the spontaneous nature of the processes and provide essential information evaluating adsorbent practicability.

Table 3. Thermodynamic parameters for TPP and HMP adsorption by magnetic mineral sorbents

Sorbent	*T*, K	ΔG^0, J·mol^{-1}	ΔH^0, J·mol^{-1}	ΔS^0, J·mol^{-1}·K^{-1}
Sample			**TPP**	
MCSp-7	293	-4787.0	-32110.7	-93.3
	323	-1989.4		
	343	-124.3		
MCSd-7	293	-6575.4	-32021.8	-86.8
	323	-3969.9		
	343	-2233.0		
MCP-7	293	-5176.3	-34740.0	-100.9
	323	-2149.3		
	343	-131.3		
Sample			**HMP**	
MCSp-7	293	-3889.7	-38247.6	-117.3
	323	-371.9		
	343	1973.4		
MCSd-7	293	-4301.9	-27713.0	-79.9
	323	-1904.8		
	343	-306.8		
MCP-7	293	-7241.7	-38492.8	-106.7
	323	-4041.9		
	343	-1908.8		

The values of ΔG^0 obtained at all temperatures were negative, indicating that the adsorption of polyphosphates onto MCSp-7, MCSd-7 and MCP-7 is a spontaneous and favorable process in nature.

The calculated activation energy of anionic SAs sorption by magnetic composites was approximately 5 kJ·mol^{-1}, which confirmed the physical nature of the process. Furthermore, activation energy values lower than 40 kJ·mol^{-1} indicated diffusion control processes.[16]

The negative value of ΔH^0 was confirmed the exothermic nature of TPP and HMP adsorption. The increasing ΔG^0 values with increasing temperature testified that the adsorption of SAs becomes unfavorable at higher temperature because the process does not require energy to take place. The negative value of ΔS^0 corresponds to decreasing of degree of freedom in the system as a result of adsorption of the TPP and HMP molecules.

It can be concluded that the adsorption mechanism is dominated by physic sorption, in keeping with the finding that the adsorption is rapid and more spontaneous at the temperature corresponding to the normal conditions of the experiment.

Conclusions

Effective magnetic composite sorbents MCSp, MCSd and MCP with a content of magnetite from 2 to 10 % wt. based on cheap mineral raw material have been prepared. The sorption capacities of the resultant magnetic composites containing magnetite 4-7 %wt. towards TPP and HMP were 1.5-2.0 times higher compared with native natural clays. In our opinion, this effect is caused by changes in the porous structure of natural clay minerals and stabilization of magnetite nanoparticles on pores surface.

The adsorption kinetics of polyphosphates removal by magnetic composites can be predicted by pseudo-second-order kinetic model. The values of diffusion coefficient are found to be on the order of 10^{-6} cm^2 s^{-1} for all the investigated sorbent samples, so the pore diffusion in this study was not significant. Sorption isotherms were best adjusted to the Langmuir model. This means that magnetic composite sorbents have a homogeneous surface. Thermodynamic studies showed that polyphosphates adsorption was spontaneous and endothermic nature. Estimated thermodynamic parameters (ΔG^0, ΔH^0 i ΔS^0) of TPP and HMP sorption by magnetic mineral sorbents indicated that the sorption process was physical.

As a result, cheap magnetic sorbents based on natural clays and magnetite for polyphosphates removal from wastewater were obtained. Magnetic composite sorbents were successfully precipitated from purified water by magnetic separation that guaranteed the elimination of risk of secondary water pollution. The results of the present investigation indicated that effective and low-cost magnetic composite could be employed as an alternative to commercial adsorbents for the removal of polyphosphates from water bodies.

Acknowledgements

The authors wish to express their acknowledgements to Professor Astrelin, I. M. for the consultation. This paper has been presented at the 4th International Conference "Nanotechnologies", October 24 – 27, 2016, Tbilisi, Georgia (Nano – 2016).

References

[1]Gan, F., Luo, Y., Hang, X., *J. Env. Manag*., **2016**, *166*, 23-30.

[2]Chen, J., Yan, L., Yu, H., *Chem. Eng. J.*, **2016**, *287*, 162-172.

[3]Yao, Y., Gao, B., Inyang M., *J. Hazard. Mater*., **2011**, *190*, 501-507.

[4]Nawar, N., Ahmad, M., Said, W., *Am. J. Chem. Appl*., **2015**, *2(6)*, 79-85.

[5]Chmielewska, E., Hodossyova, R., Bujdos, M., *Polish J. Env. Stud.*, **2013**, *22(5)*, 1307-1316

[6]Makarchuk, O. V., Dontsova, T. A., Astrelin, I. M., *Nanoscale Res. Lett.*, **2016**, *11*, No. 161 p. 7.

[7]Makarchuk, O. V., Dontsova, T. A., Astrelin, I. M., *Res. Bull. Natl. Techn. Univ. Ukr., "Kyiv Polytechnic Institute*", **2015**, *6*, 109–114.

[8]Thach, C. V., Hai, N. H., Chau, N., *J. Korean Phys. Soc*., **2008**, *5(52)*, 1332–1335.

[9]Elmoubarki, R., Mahijoubi, F. Z., Tounsadi, S., Moustadraf, J., *Water Res. Ind.*, **2015**, *9*, 16–29

[10]Gunay, A.; Ersoy, B.; Dikmen, S.; Evcin, A., *Adsorption*, **2013**, *19(2-4*), 757–768

[11]Hernandez, K., Solache, M., Diaz-Nava, C., *Water Air Soil Pollut*., **2013**, **224(5)**, 1–11.

[12]Makarchuk, O. V., Dontsova, T. A., *J. Water Secur*., **2016**, *2*, 1–9.

[13]olyansky, N. G.; Gorbunov, G. V.; Polyanskaya, N. L., *Research methods of ion exchangers*, Chemistry, Moscow, **1976**, 207 p.

[14]Hameed, B. H., *J. Hazard. Mater*., **2009**, *162*, 939-944.

[15]Dada, A. O, Olalekan, A. P., Olatunya, A. M., *J. Appl. Chem*., **2012**, *3*, 38–45.

[16]Eren, E., *J. Hazard. Mater*., **2009**, *166(1)*, 88–93.

Received: 22.01.2016.
Accepted: 01.02.2017.

PHASE COMPOSITION, THERMAL BEHAVIOR AND MAGNETIC PROPERTIES OF ZINC- AND NICKEL-BEARING POWDERS FORMED ON THE STEEL SURFACE IN AN OPEN-AIR SYSTEM

O. Lavrynenko,[a]* N. Dudchenko,[b] O. Pavlenko[a] and A. Brik[b]

Keywords: Steel surface, nanoparticles, spinel ferrites, thermal transformation, superparamagnetics.

The nanosized powders formed on the steel surface in contact with aqueous solutions of zinc and nickel inorganic salts have been studied using an X-ray diffraction method, thermal analytical measurements (TG / DTG, DTA), scanning electron microscopy and magnetometry. It has been shown that a single mineral phase of a non-stoichiometric spinel ferrite is formed when zinc and nickel nitrate solutions were used as the dispersion medium, but in the presence of chloride-containing salts three mineral phases (spinel ferrite, lepidocrocite, and goethite) are formed in the phase composition of the surface powders. When sulfate solutions were chosen as the dispersion medium the mixed hydroxysulfate layered double hydroxides (LDHs) simultaneously appeared among other components of the powders. Due to cation exchange between Fe^{2+} and Zn^{2+} or Ni^{2+} the mixed LDH structures achieved stability against further oxidation and thermal transformation. Hence, the presence of mixed LDHs in the phase composition of the powders significantly complicates the obtaining of homogenous superparamagnetic 3*d*-metal doped spinel ferrite and iron oxide powders.

* Corresponding Author:
E-Mail: alena-lavry@yandex.ru
[a] Frantsevich Institute for Problems of Material Science of NAS of Ukraine, Kyiv, Ukraine
[b] M.P. Semenenko Institute of Geochemistry, Mineralogy and Ore Formation of NAS of Ukraine, Kiev, Ukraine

Introduction

Nowadays magnetic iron oxides – hematite, maghemite, and spinel ferrite (magnetite) have been recognized as a perspective material for biomedical applications.[1] So, gamma ferric oxide – maghemite, as a bio-comparable nanophase, is used for cell-separation, vector drug delivery, magnetic-induced hyperthermia, immune magnetic separation as well as it plays a role of a contrasting agent for the obtaining of the images applying magnetic resonance.[2-4] In addition, maghemite has unique magneto-optical[5] and catalytical[6] properties. Alpha ferric oxide – hematite possesses weak magnetic properties at Morin temperature (260 K)[7] and it is specified by complex ferromagnetic properties together with antiferromagnetic properties at *T* below 950 K.[8] Typically, hematite particles are used as a catalyst,[9] magnetic material,[10] pigment, inhibiting agent and reactant for soils remediation.[11]

Currently, the obtaining of 3*d*-metal doped iron oxide nanoparticles is carried out by various chemical and physical methods that include either gradual growth of primary precursor species (molecules or clusters) or dispergation of a bulk mineral phase or its microaggregates.[12] The small amount of transition 3*d*-metals in the structure of iron oxides may cardinally change their physical chemical properties and biological activity.[13] Hence, thermal homogenization of ferro- and ferrimagnetic disperse materials, varying magnetic properties of heated nanopowders and the presence or the absence of doped transition 3*d*-metal cations in a crystal lattice of iron oxides, in general, are widely discussed in the science sources.

The aim of the present work is to study the composition, thermal behaviour and magnetic properties of nickel- and zinc-bearing nanopowders formed on the steel surface in an open-air system.

Experimental

The rotating disk electrode made of steel 3 (St3), which has the composition (%): C 0.14-0.22, Si 0.05-0.15, Mn 0.4-0.5, Cr 0.3, Ni 0.3, P 0.04, S 0.05 and N 0.01, was chosen for obtaining of the raw iron-oxygen powders. The phase formation process was carried out in an open-air system under galvanostatic conditions via the rotation-corrosion dispergation route.[14] During the experiment, the electrode surface was alternately contacting with dispersion medium and air. Before every experiment the steel surface was exposed to mechanical treatment to remove an oxidized layer. Sulfuric acid was used for activating procedure. The activated steel electrode was repeatedly rinsed in water and onwards it was placed into the cell filled with distilled water or the 3*d*-metal water salt solution. Zinc and nickel chlorides, nitrates and sulfates were chosen to prepare the aqueous salt solution with the concentrations of cations as 100 mg dm^{-3} and pH of the solutions was set 6.5. The phase formation process was carried out in thermostat TS-1 /80-SPU and it lasted 24 h at 20 and 50 °C, afterwards the disk electrode was dried in air. The prepared powders were annealed in the induction furnace SNOL 6.7/1300 for 1 h at 440 and 740 °C.

The phase composition of iron-oxygen powders was determined by X-ray diffraction (XRD) method, thermal analytical measurements (TG / DTG, DTA) and scanning

electron microscopy (SEM). The phase composition of the nanopowders was conducted using computer-aided X-ray diffractometer (DRON – UM1) equipped with two Soller's slits and filtered radiation of cobalt anode CoK_α. The rate of the recording was set 1°·min^{-1} and the interfacial Woolf-Bragg's angle was made up to 80 degrees. The primary particle size was calculated according to the standard Debye-Scherrer's formula. Thermogravimetric and differential thermal analysis (TG-DTA) of the powders was performed in the static air atmosphere by derivatograph Q-1500D (Hungary). The record was made using computer data registration. The parameters of the pattern recording were the following: the samples of 150 mg were heated at the rate 10 °C min^{-1} from 20 to 1000 °C, the sensitivity was 20 mg, TG – 500, DTG – 500 and DTA – 250. The samples were placed into a corundum crucible and covered by quartz beaker to create an equal temperature field. A scanning electron microscopy (SEM) using JOEL-6700 microscope equipped with an energy-dispersive and cathode-luminescence attachment to obtain EDS-spectra permitted to estimate the morphology of the surface structures. The weight ratio of iron to the second 3*d*-metal (nickel or zinc) in the samples was evaluated using an X-ray fluorescence spectroscopy (XRFS) carried out in the automatic spectrometer (ElvaX) equipped with a titanium anode. The magnetic properties of the raw and annealed powders were estimated via magnetometry performed with the help of a magnetometer equipped by Hall sensor.

Results

Preparation of the raw powders

The colloid-chemical mechanisms of the formation of magnetite (spinel ferrite) particles in the natural systems are determined by red-ox conditions in the system and depend on the quantity of dissolved ferrous aquahydroxo forms in the dispersion medium. Our kinetic study[15] of the phase formation processes on the steel electrode surface in contact with water dispersion medium and air showed the development of hydroxycarbonate Green Rust layer within 1-3 h and its oxidation into lepidocrocite γ-FeOOH within 3-5 h. At that, to compare the phase composition of the iron-oxygen structures formed on the refined and oxidized steel surface we proposed the following procedure: at first the prepared and activated disk electrode was placed in distilled water at T = 20 °C for 1, 3, and 5 h or at T = 50 °C for 1 h, afterwards the dispersion medium was replaced with zinc or nickel salt solutions. For the comparison we chosen the samples formed under initial contact of the steel surface with corresponding salt solutions.

Phase composition of the raw powders

The X-ray diffraction data of the nickel- and zinc-iron-oxygen-containing structures formed on the steel surface in contact with corresponding chloride solutions within 24 h at 20 and 50 °C are presented in figure 1. Also, when the zinc chloride and nickel chloride solutions were in contact with activated surface of the steel electrode at T = 20 °C, the obtained powders included three iron-oxygen mineral phases such as spinel ferrite (magnetite) (JCPDS file No 19-0629) and polymorphic ferric oxyhydroxides – lepidocrocite γ-FeOOH (JCPDS file No 08-0098) and goethite α-FeOOH (JCPDS file No 17-536). The trace peaks of the Green Rust I are seen on the XRD-patterns of both systems. In all cases the structures of the oxihydroxides and spinel ferrites coexist in the phase composition of the powders at T = 20 °C. But spinel ferrite phase got the predominant importance when the temperature was enhanced up to 50 °C, and under the following conditions both ferric oxyhydroxides were present in the patterns only as the admixtures. Thus, the temperature of the phase formation process strongly influenced not only the phase composition of the surface powders but their crystallinity degree as well. Whereas the powders obtained at T = 20 °C may be characterized as weak crystalline structures, the spinel ferrite particles formed in the mentioned systems at T = 50 °C were well crystallized.

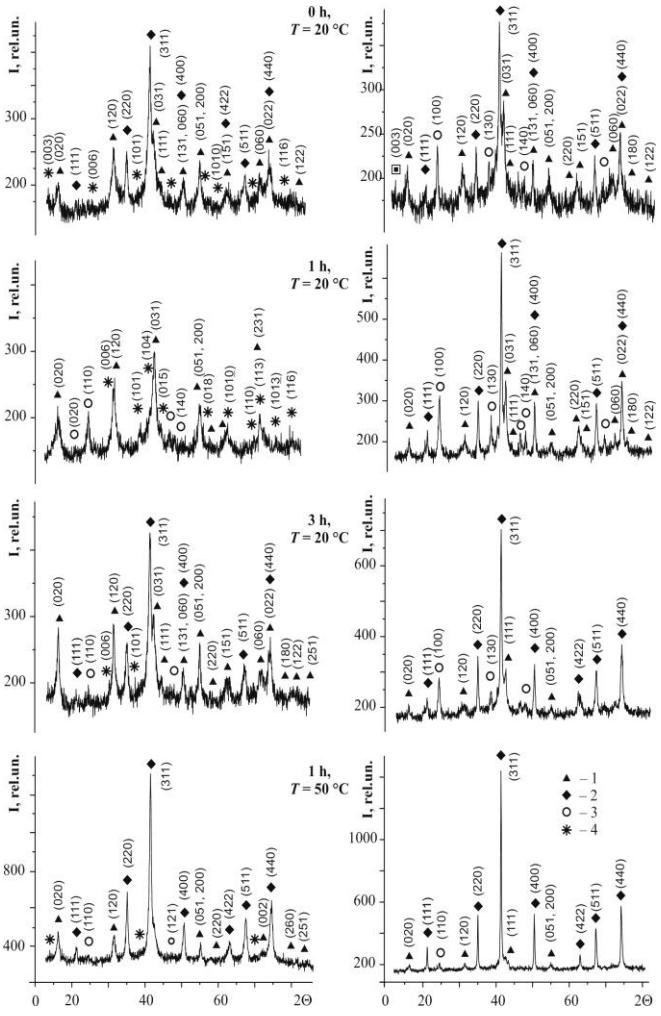

Figure 1. XRD-patterns of the powders formed on the steel surface contacting with the salt solutions: a – $ZnCl_2$; b – $NiCl_2$. Numbers correspond to the phases: 1 – lepidocrocite, 2 – spinel ferrite, 3 – goethite, 4 – Green Rust I.

When zinc and nickel sulfate solutions were chosen as the dispersion medium, the phase composition of the powders formed at T = 20 °C included mixed Zn(II)-Fe(II-III)-SO_4^{2-} and Ni(II)-Fe(II-III)-SO_4^{2-} layered double hydroxides (LDH) as a main mineral phase with an admixture of a relatively small amount of ferric oxihydroxides (Figure 2).

But when the *T* of the process was increased to 50 °C the mixed Ni(II)-Fe(II-III)-SO_4^{2-} LDH as well as spinel ferrite were determined as two main phases in the powders, but goethite and lepidocrocite played the role of mineral admixtures.

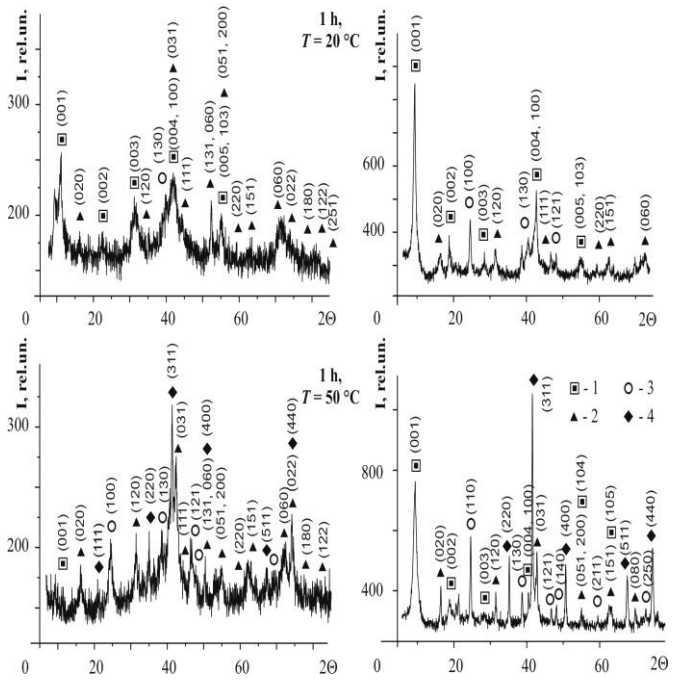

Figure 2. XRD-patterns of the powders formed on the steel surface contacting with the salt solutions: a – $ZnSO_4$; b – $NiSO_4$. Numbers correspond to the phases: 1 – Green Rust II, 2 – lepidocrocite, 3 – goethite, 4 – spinel ferrite.

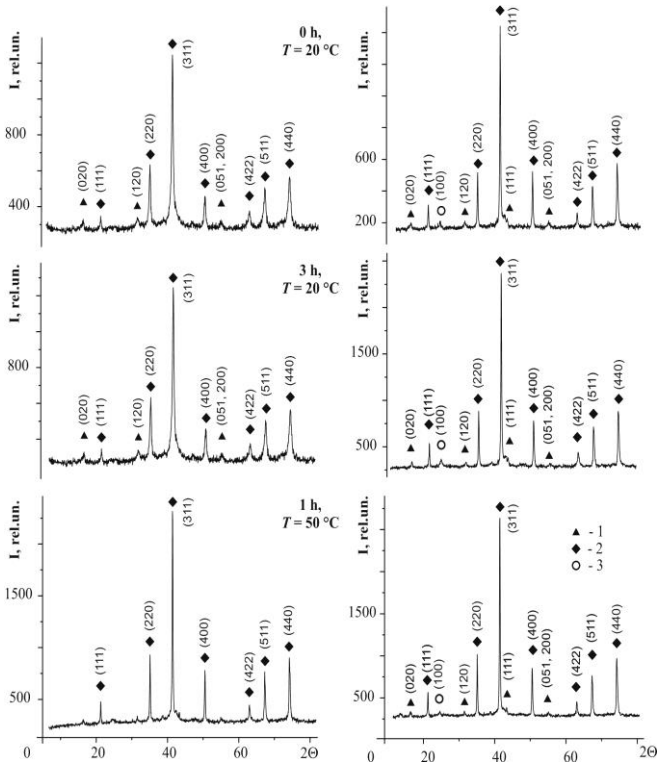

Figure 3. XRD-patterns of the powders formed on the steel surface contacting with the salt solutions: a – $Zn(NO_3)_2$; b – $Ni(NO_3)_2$. Numbers correspond to the phases: 1 – lepidocrocite, 2 – spinel ferrite, 3 – goethite.

But high-disperse weak crystalline phases of lepidocrocite and spinel ferrite phases coexist in zinc-bearing powders. According to the lattice parameters, the mixed LDH corresponds to hydrohonessite-like hydroxysulfate Green Rust II (JCPDS file No 41-0014). The usage of zinc and nickel nitrate solutions results in the formation of the homogeneous spinel ferrite phases at all temperature conditions (Figure 3). But the contact of high disperses spinel ferrites with air-oxygen results in the appearance of the small amount of ferric oxyhydroxides in the phase compositions of the powders. While the trace lepidocrocite peaks are clearly seen on the patterns of both systems, goethite is present only in the nickel-bearing powders.

Table 1. The lattice parameters (*a, b, c*) and primary particle size (*d*) of the powder components obtained on the steel surface

Salt solution	T, C°	The parameters of the mineral phases, nm		
		γ-FeOOH	α-FeOOH	Fe_3O_4
$NiCl_2$	20	*a*=0.3875	*a*=0.4649	*a*=0.8404
		b=1.2695	*b*=0.9946	*d*=21.9
		c=0.3022	*c*=0.3027	
		d=10.4	*d*=14.5	
	50	*a*=0.3875	*a*=0.4668	*a*=0.8419
		b=1.2630	*b*=0.9874	*d*=28.2
		c=0.2922	*c*=0.3007	
		d=13.3	*d*=21.0	
$NiSO_4$	20	*a*=0.3876	*a*=0.4630	*a*=0.8370
		b=1.2546	*b*=0.9969	*d*=24.8
		c=0.3059	*c*=0.3016	
		d=13.7	*d*=14.6	
	50	*a*=0.3889	*a*=0.4623	*a*=0.8389
		b=1.2608	*b*=0.9868	*d*=26,3
		c=0.3022	*c*=0.3001	
		d=20.0	*d*=18.9	
$Ni(NO_3)_2$	20	*a*=0.3872	*a*=0.4637	*a*=0.8386
		b=1.2599	*b*=0.9650	*d*=21.9
		c=0.3029	*c*=0.3022	
			d=23.2	
	50	–	–	*a*=0.8399
				d=26,3
$ZnCl_2$	20	*a*=0.3894	–	*a*=0.8399
		b=1.2527		*d*=9.9
		c=0.3079		
		d=8.9		
	50	*a*=0.3876	–	*a*=0.8395
		b=1.2638		*d*=10.4
		c=0.3067		
		d=13.3		
$ZnSO_4$	20	*a*=0.3858	*a*=0.4626	*a*=0.8404
		b=1.2692	*b*=1.0106	*d*=19.1
		c=0.3062	*c*=0.3013	
		d=21.7	*d*=16.2	
	50	*a*=0.3855	*a*=0.4636	*a*=0.8397
		b=1.2630	*b*=0.9950	*d*=27.4
		c=0.3044	*c*=0.3007	
		d=23.4	*d*=20.1	
$Zn(NO_3)_2$	20	–	–	*a*=0.8403
				d=15.8
	50	–	–	*a*=0.8398
				d=28.2

The crystal lattice parameters and the primary particle size (CSR) of the powder compounds are presented in table 1. As it is clearly seen, the CSR of lepidocrocite varies from ~10 to ~23 nm and the smallest particles correspond to chloride systems whereas the biggest particles relate to sulfate systems. The range of the goethite particle size is narrow in comparison with the previous case and it ranges from 14 to 23 nm. But variation of the magnetite CSR is more significant and we can see the smallest particles in zinc chloride systems (~10 nm). Generally, the average particle size of magnetite formed in nickel-containing systems is bigger than in zinc-containing systems and it is 22–28 nm in the first case and ~15–28 nm in the second case. The wt.% distribution of the metals in the powders formed in the presence of nickel- and zinc-containing water salt solutions is seen in table 2. Also, the weight ratio of iron to zinc is the most stable in zinc nitrate solutions and it gets 78 (82) : 22 (18) wt.%, but in the chloride-containing solution such parameter varies from 94 to 79 wt.%. (Fe) and from 6 to 21 wt.% (Zn), respectively.

Table 2. The wt.% distribution of iron and zinc or nickel in the powders depending on the period of the steel surface contacting with distilled water

***t*, h**	***T*, °C**	**Fe**	**Zn**	**Fe**	**Ni**
		$ZnCl_2$		**$NiCl_2$**	
0	20	94.2	5.8	88.4	11.6
1		82.8	17.2	93.9	6.1
3		81.3	18.7	94.6	5.3
1	50	79.4	20.6	92.4	7.6
		$ZnSO_4$		**$NiSO_4$**	
1	20	69.3	30.7	82.0	18.0
1	50	77.5	22.5	85.9	14.1
		$Zn(NO_3)_2$		**$Ni(NO_3)_2$**	
0	20	79.8	20.2	95.9	4.1
3		82.0	18.0	94.3	6.7
1	50	78.4	21.6	92.1	7.9

The weight ratio Fe : Ni in chloride and nitrate-containing solutions lies in the narrow range 88–96 wt.% for iron and 12–4 wt.% for nickel. But the relatively high concentrations of both zinc 22 (30) wt.% and nickel 14 (18) wt.% are fixed in sulfate-bearing systems. Thus the proportion of Zn and Ni in the powders obtained at 20 °C is higher in the comparison with powders formed at 50 °C.

Thermogravimetric and differential thermal properties of the powders

We have chosen four samples to study the thermal behaviour of the mineral powders formed on the steel surface in the presence of nickel and zinc-containing aqueous salt solutions (Figure 4). The in-depth analysis of nickel-bearing systems permitted us to determine the influence of anion composition on the phase transformation of the powder compounds. In addition, $ZnSO_4$ system was analyzed on account of the presence of mixed Zn(II)-Fe(II-III)-SO_4^{2-} LDH in the phase composition of the corresponding powder.

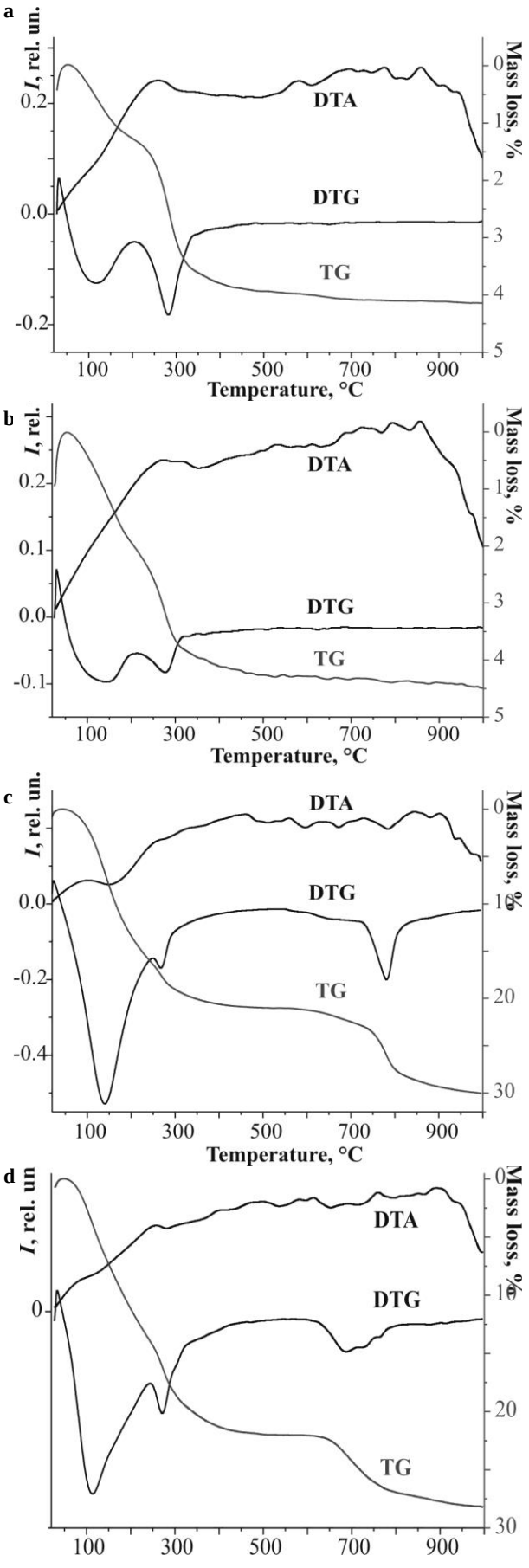

Figure 4. TG-DTA curves of the powders formed on the steel surface in contact with aqueous solutions: a – $NiCl_2$; b – $Ni(NO_3)_2$; c – $NiSO_4$; d – $ZnSO_4$.

According to the experimental data two endo effects are seen in all DTG curves. The first minimum is fixed in the temperature range of 110–137 °C. It corresponds to the loss of the adsorbed water. The second endothermic peak in the temperature range of 270–281 °C is related to the hydroxylation of oxyhydroxide lattice and formation of iron oxide phases. But both sulfate-containing samples show an additional endothermic peak in the temperature range of 622–784 °C ($NiSO_4$) and 725–822 °C ($ZnSO_4$). Those thermal effects are accompanied by the mass loss of the powders on the TG curves (28–30 %) probably because of the phase transformation (dehydroxilation) of mixed LDH and total destruction of SO_4^{2-} species. On the contrary, the mass loss of the nitrate- and chloride-containing samples amounts to 4.5 % only. Two exothermic peaks point to the oxidation of ferrous cations in the spinel ferrite lattice and phase transformation of Fe_3O_4 doped with Ni^{2+} or Zn^{2+} into maghemite γ-Fe_2O_3 at 200–245 °C and polymorphic transformation of γ-Fe_2O_3 into hematite α-Fe_2O_3 at 300–338 °C.

Morphology of the raw and heated powders

The SEM images of the mineral phases formed on the steel surface in contact with aqueous solution of $NiCl_2$ and $Ni(NO_3)_2$ are presented in Figure 5.

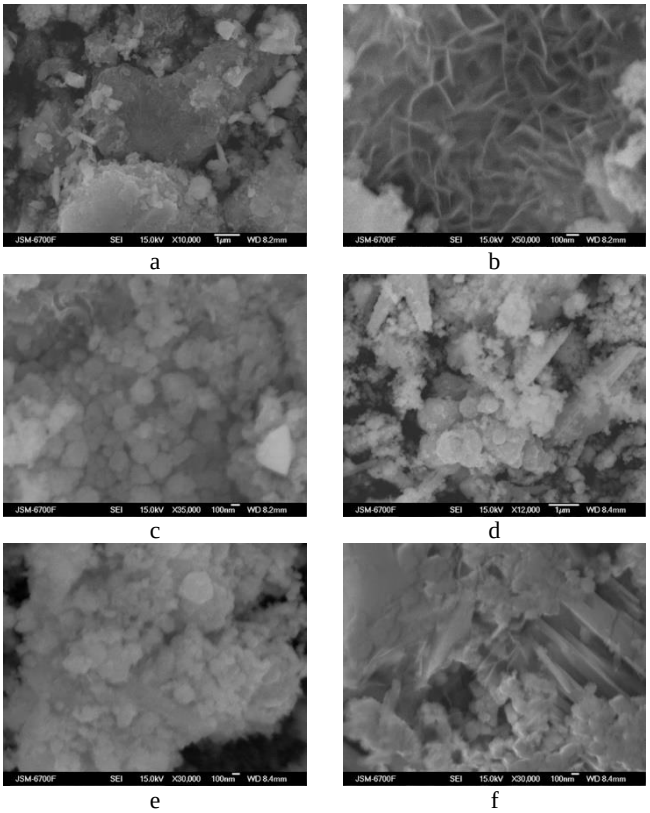

Figure 5. SEM-images of the surface structures formed on the steel surface in contact with aqueous solution of $NiCl_2$: a – the general view, b – mixed Ni(II)-Fe(II-III) LDH, c – spinel ferrite, and $Ni(NO_3)_2$: d – the general view, e – spinel ferrite; f lepidocrocite plates and spherical spinel ferrite particles

Generally, the morphology of the iron-oxygen surface structures is similar and it does not depend on the anion composition of the dispersion medium contacting with the steel surface. Whereas ferric oxyhydroxides are characterized by plate-like or lamellar shape of the particles (Figure 5 a, d, f), the spinel ferrites form spherical particles and aggregates (Figure 5 c, e). The relicts of the mixed Ni(II)-Fe(II-III) LDHs belonging to Green Rust I structure are seen in figure 5 b. Their morphology can be described as chaotic disordered plates and lamellas.

The EDS spectra of the mineral phases formed when the steel surface was in contact with $NiCl_2$ solution show that the average quantity of nickel associated with lepidocrocite phase is ~4.9 wt.%, its quantity in goethite is ~0.75 wt.%, and in spinel ferrite ~ 8.7 wt.%. The manganese and sulfur admixtures got into mineral phases, probably, from the material of the steel. The average content of Fe in all probes reaches ~72.78 wt.%, and content of oxygen equals ~22.23 wt.%.

Magnetic properties of the raw and heated powders

The magnetic study shows that all samples obtained in the presence of the zinc and nickel salt solution have not displayed the residual magnetization (M_r) and coercitivity (H_c). The saturation magnetization (M_s) of the nickel-bearing sample, formed on the steel surface at T = 50 °C within 24 h, equalled 55 $A \cdot m^2 \cdot kg^{-1}$ (Figure 6a). It is interested to note that the increase in temperature has led to reduction of the saturation magnetization of the powders formed in the presence of nickel chloride solutions to 40 $A \cdot m^2 \cdot kg^{-1}$ at 450 °C, and to 7 $A \cdot m^2 \cdot kg^{-1}$ at 750 °C. A powder formed in the presence of nickel sulphate solution showed M_s 32 $A \cdot m^2 \cdot kg^{-1}$ at 450 °C. When zinc chloride solution was used as the dispersion medium the samples formed on the steel surface at T = 50 °C displayed the saturation magnetization 40 $A \cdot m^2 \cdot kg^{-1}$ (Figure 6b). The increase in temperature to 450 °C caused the lowering of parameter M_s up to 5 $A \cdot m^2 \cdot kg^{-1}$ and a further increase of temperature to 750 °C resulted in the increase of M_s to 27 $A \cdot m^2 \cdot kg^{-1}$. Probably, such phenomenon is related to the phase transformation of magnetite into iron oxides doped with zinc cations. Also, the powders obtained at 50 °C in the zinc chloride and nickel sulfate and chloride system demonstrate superparamagnetic properties and, generally, they belong to highly permeable magnetic materials.

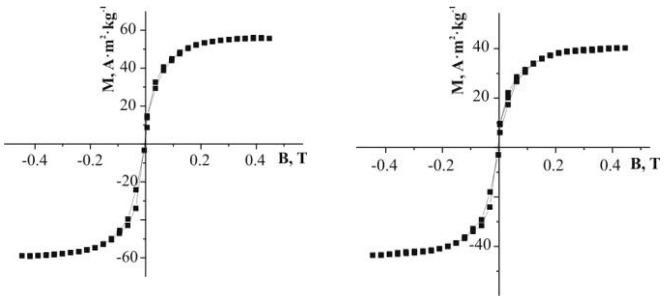

Figure 6. The magnetization curves of the iron-oxygen powders obtained at T = 50 °C on the steel surface when it was contacting with the solutions: a – $NiCl_2$, b – $ZnCl_2$.

Discussion

Depending on the geometrical shape of anions two types of Fe(II)-Fe(III) layered double hydroxides (Green Rusts) may be formed on the steel or iron surfaces. Planar and spherical anions (Cl^-, CO_3^{2-}) coordinate iron hydroxide layers as GR I and three dimension anions (SO_4^{2-}) take place in GR II structure.[16] According to literature data nickel as well as zinc can incorporate into a Green Rust lattice and form various LDH structures corresponding to the first [17, 18] and the second[19-21] lattice's type of Green Rust, respectively. Whereas Fe(II)-Fe(III) LDH under standard conditions do not keep stability against oxidation and solid state transformation into lepidocrocite[22] or its dissolution-re-precipitation into magnetite[23], the mixed LDH structures, due to Fe(II) exchange, lose the possibility for oxidation and, as a result, for phase transformation.

Hence, one of the mixed LDH applications is their thermal treatment to obtain chemically pure mixed oxides at T ~ 450–600 °C[24] or spinel ferrites in the T range from ~ 750 °C[25] to 1100 °C.[26] The formation of pure nickel spinel ferrites via calcination of tailored hydrotalcite-like hydroxysulfate LDH as a single molecular precursor has been mentioned.[27] In such case the precursor species was heated at 900 °C for 2 h to obtain the powder including two phases: α-Fe_2O_3 and NiO, afterwards the oxide mixture was sintered at 1100 °C for 10 h and then slowly cooled to the room temperature. This kind of the procedure is sensitive to metal molar ratios and certain stoichiometry has to be kept. But when the molar ratio of Me^{2+}/Fe^{3+} is broken the non-stoichiometric iron oxides or magnetite doped by 3*d*-metal cations are formed in the system.[28]

The investigation[29,30] of the products of thermal transformation of nickel-containing goethite gives the reason to think that ferric iron is substituted for nickel in the hematite structure. Thus the lattice parameters of hematite formed in the temperature range from 300 to 800 °C are determined by the composition of the precursor phase (ferrihydrite or goethite) containing nickel cations.[31] Moreover, the transformation of nickel-containing goethite into nickel-containing hematite on heating passes through the formation of an intermediate phase of nickel-containing maghemite. In such samples nickel diffuses to the hematite surface within the transformation row Fe_3O_4 – γ-Fe_2O_3 – α-Fe_2O_3[32]. However, in another work[32] it was shown that the heating of maghemite to T < 320 °C leads to the removal of more than 60 % of Co, Ni, Zn, and Cu cations from γ-Fe_2O_3 structure without their subsequent inclusion into hematite structure. But when the hematite obtained by heating maghemite at T = 650 °C for 3 h, it includes small amount of Co, Ni, Zn, Cu, Mn, V, Al, and Cr cations, however, the intensity of its X-ray diffraction peaks does not change.[33] It is possible that the presence of transition 3*d*-metal cations in the structure of maghemite increases the period of its transformation into hematite. This phenomenon has been explained[33] assuming that Co, Ni, Zn, and Cu cations give stability to a cubic lattice of maghemite and complicate its conversion into a hexagonal hematite lattice because some cations are not compatible with hematite structure.

In addition, the role of cations of the dispersion medium in the formation of polymorphic ferric oxyhydroxides has been widely discussed in the literature. The chemical studies[34-36] point out that small amounts of transition metals including Ni, Co, Cr, Mn, Cu, Zn, Cd, and Pb are usually associated with natural and synthetic goethite, whereas such metals as well as Al, Ti, and Mo may also be present in the structure of natural goethite, and hematite.[37,38] The mechanism of cation inclusion into the crystal lattice of goethite is determined via ferric iron substitution and ferric cations may be substituted in goethite lattice for cobalt[39] or nickel[40] cations.

In conformity with our observations, nickel may be included into a goethite lattice without destruction of its crystal structure.[41] Thus, zinc cations protect the lepidocrocite particles against dissolution in ferrous sulfate medium, but nickel ions do not affect the morphology and crystallinity of γ-FeOOH.[42] Ferrous cations are usually adsorbed on the lepidocrocite surface in aqeous medium and may be exchanged for nickel cations to form surface-modified iron oxides.[43] The analysis of our systems confirmed that only γ-FeOOH appeared on the steel surface in contact with all zinc-containing aqeous solutions, but both γ-FeOOH and α-FeOOH co-existed in the phase composition of the powders when the steel surface was in contact with nickel-containing solutions. Hence, the relative quantity of the goethite part was less in comparison with the lepidocrocite part.

The comparison of the powders formed on the steel surface in contact with aqueous solution of zinc and nickel salts with the products of the thermal transformation of mixed LDH precursors formed via co-precipitation of respective salts shows a few differences. Namely, the appearance of the spinel ferrites as a single phase on the steel surface is fixed in the systems where the mixed LDH structures are not formed, for example $Ni(NO_3)_2$ or $Zn(NO_3)_2$ (Figure 3). But when the relatively stable phase of mixed hydroxysulfate LDHs is formed the spinel ferrite is not obtained at T = 20 °C or it co-exists with LDHs and ferric oxyhydroxides at T = 50 °C (Figure 2). In our previous work[13] we have shown that the heating of the copper and cobalt-bearing powders formed under the RCD conditions at T = 740 °C led to the formation of a single hematite phase. No other oxide peaks were present in the XRD patterns. The XRFS study confirmed the association of iron and copper or cobalt cations in the chemical composition of the powders. Moreover, the relative quantity of the doped metal remained the same in the wide temperature range (50–740 °C). So, such powders may be used to obtain monomineralic polymorphic ferric oxides (γ-Fe_2O_3 and α-Fe_2O_3) doped by 3*d*-metal cations.

Conclusions

1. The usage of chloride solutions leads to obtaining of non-stoichiometric spinel ferrites and ferric oxyhydroxides, nitrate salts permit to form the single spinel ferrite phase. But the mixed LDHs appear among powder components in the presence of sulfate solution.

2. TG-DTA analysis of the powders shows four thermal effects corresponding to the loss of the adsorbed water (110–137 °C), hydroxylation (270–281 °C), transformation of Fe_3O_4 doped by Ni^{2+} or Zn^{2+} into maghemite γ-Fe_2O_3 (200–245 °C), and polymorphic transformation of γ-Fe_2O_3

into hematite α-Fe_2O_3 (300–338 °C). But both sulfate-containing samples show an additional endothermic peak accompanied by the mass loss (28–30 %) in the *T* range of 622–822 °C.

3. All mineral phases belong to nano objects and their primary particle size is 10–23 nm for lepidocrocite, 14–23 nm for goethite and ~15–28 nm for spinel ferrite. Depending on the chemical compositions of the water salt solutions the wt.% distribution of the metals in the powders (Fe : Me) varies from 96 : 4 to ~70 : 30.

4. The ferric oxyhydroxides and mixed Ni(II)-Fe(II-III) LDHs have a plate-like or lamellar morphology, and spinel ferrites form spherical particles.

5. All samples obtained in the presence of the zinc and nickel salt solution belong to superparamagnetics and they have not displayed the residual magnetization and coercitivity.

Acknowledgments

We gratefully acknowledge leading research scientist O.A. Vyshnevskyi of Mass-spectrometric centre of solid phase, for gas isotopic trace element analysis. We are thankful to M. P. Semenenko, Institute of Geochemistry, Mineralogy and Ore Formation of NAS of Ukraine, for the obtaining of the SEM images and EDS data. We acknowledge the support from leading research scientist M. V. Borisenko from O. O. Chuiko Institute of Surface Chemistry of NAS of Ukraine for the obtaining of TG-DTA data.

This paper has been presented at the 4th International Conference “Nanotechnologies”, October 24 – 27, 2016, Tbilisi, Georgia (Nano – 2016).

References

[1]Teja, A. S., Koh P.-Y., *Prog. Cryst. Growth Charact. Mater.*, **2009**, *55(1-2)*, 22.

[2]Levy, M., Wilhelm, C., Siaugue, J. M., Horner, O., Bacri, J. C., Gazeau, F., *J. Phys.: Condens. Matter*, **2008**, *20(20)*, 204133.

[3]Pankhurst, Q. A., Connolly, J., Jones, S. K., Dobson, J., *J. Phys. D: Appl. Phys.*, **2003**, *36*, R167.

[4]Chirita, M., Grozescu, I., *Chem. Bull. "Politehnica" Univ. (Timisoara)*, **2009**, *54(68)*, 1.

[5]Kang, Y. S., Risbud, S., Rabolt, J. F., Stroeve, P., *Chem. Mater.*, **1996**, *8(9)*, 2209.

[6]Zhao, N., Ma, W., Cui, Zh., Song, W., Xu, Ch., Gao, M.., *ASC Amer. Chem. Soc. NANO*, **2009,** *3(7)*, 1775.

[7]Fysh, S. A., Clark, P. E., *Phys. Chem. Miner.*, **1982,** *8*, 257.

[8]Shirane, G., Pickart, S. J., Nathans, R., Ishikawa, Y., *J. Phys. Chem. Solids*, **1959**, *10*, 35.

[9]Lei, Y., Cant, N. W., Trimm, D. L., *Catal. Lett.*, **2005**, *103*, 133.

[10]Suber, L., Imperatori, P., Ausanio, G., Fabbri, F., Hofmeister, H., *J. Phys. Chem.*, **2005**, *B 109(15)*, 7103.

[11]Hendy, S. C., Laycock, N. J., Ryan, M.P., *J. Electrochem. Soc.*, **2005**, *152*, B271.

[12]Laurent, S., Forge, D., Port, M., Roch, A., Robic, C., Vander Elst, L., Muller R. N., *Chem. Rev.*, **2008**, *108*, 2064.

[13]Lavrynenko, O. M., Dudchenko, N. O., Pavlenko, O. Yu., Brik, A. B., *Proc. Int. Conf.: NAP*-**2015**, *01001*.

[14]Lavrynenko, O. M., Pavlenko, O. Yu., Shchukin, Yu. S., *Nanoscale Res. Lett.*, **2016**, *11(67)*, 2

[15]Lavrynenko, O. M., Korol, Ya. D., Netreba, S. V., Prokopenko, V. A., *Chem. Phys. Tech. Surf.*, **2010**, *1(3)*, 338.

[16]Génin, J.-M. R, Ruby, C., *Solid State Sci.*, **2004**, *6*, 705

[17]Parida, K. M., Mohapatra, L., *Chem. Eng. J.*. **2012**, *179*, 131.

[18]Refait, Ph., Génin, J.-M. R., *Clay Miner.*, **1997**, *32*, 597.

[19]Ahmed, I. A. M., Shaw, S., Benning L. G., *Miner. Mag.*, **2008**, *72(1)*, 159.

[20]Garófalo Chaves, L. H, Curry, J. E, Stone, D. A, Carducci, M. D., Chorover, J., *Rev. Bras. Cienc. Solo*, **2009**, *33(5)*, 1115.

[21]Refait, Ph., Abdelmoula, M., Simon. L., Génin, J.-M. R., *J. Phys. Chem. Solids*, **2005**, *66*, 911.

[22]Schwertmann, U., Fechter, H., *Clay Miner.*, **1994**, *29*, 8.

[23]Sumoondur, A, Shaw, S., Ahmed, I., Benning, L. G., *Mineral. Mag.*, **2008**, *72(1)*, 201.

[24]Vaccari, A., *Catal. Today*, **1998**, *41*, 53.

[25]Fernández, J. M., Ulibarri, M. A., Labajos, F. M., Rives, V., *J. Mater. Chem.*, **1998**, *8*, 2507.

[26]Liu, J., Li, F., Evans, D. G., Duan, X., *Chem. Commun.*, **2003**, *21(4)*, 542.

[27]Li, F., Liu, J., Evans, D. G., Duan, X., *Chem. Mater.*, **2004**, *16*, 1597.

[28]Ishikawa, T., Nakazaki, H., Yasukawa, A., Kandori, K., Seto, M., *Mater. Res. Bull.*, **1998**, *33(11)*, 1609.

[29]Gerth, J., *Geochim. Cosmochim. Acta*, **1990**, *54(2)*, 363.

[30]Ruan, H. D., Gilkes, R. J., *Clay Miner.*, **1995**, *30*, 55.

[31]Lim-Nunez, R., *MSc Thesis*., Univ. of Western Australia, **1985**.

[32]Sidhu, P. S., Gilkes, R. J., Posner, A. M., *Soil Sci. Soc. Amer. J.*, **1980**, *44*, 135.

[33]Sidhu, P. S., *Clays Clay Miner.*, **1988**, *36(1)*, 31.

[34]Trolard, F., Bourrie, G., Jeanroy, E., Herbillon, A. J., Martin, H., *Geochim. Cosmochim. Acta*, **1995**, *59(7)*, 1285.

[35]Manceau, A., Schlegel, M. L., Musso, M., Sole, V. A., Gauthier, C., Petit, P. E., Trolard, F., *Geochim. Cosmochim. Acta*, **2000**, *64(21)*, 3643.

[36]Carvalho-de-Silva, M. L., Ramos, A. Y., Tolentino, H. C. N., Enweiler, J., Netto, S. M., Alves, M. C. M., *Am. Mineral.*, **2003**, *88*, 876.

[37]Wells, M. A., Fitzpatrick, R. W., Gilkes, R. J., *Clays Clay Miner.*, **2006**, *54(2)*, 176.

[38]Singh, B., Gilkes, R. J., *J. Soil Sci.*, **1992**, *43*, 77.

[39]Gasser, U. G., Jeanray, E., Mustin, C., Barres, O., Nuesch, R., Berthelin, J., Herbillon, A. J., *Clay Miner.*, **1996**, *31*, 465.

[40]Gerth, J., *Geochim. Cosmochim. Acta*, **1990**, *54(2)*, 363.

[41]Inouye, K., Ichimura, K., Kaneko, K., Ishikawa, T., *Corros. Sci.*, **1976**, *6*, 507.

[42]Ishikawa, T., Nagashima, A., Kandori, K., *J. Mater. Sci.*, **1991**, *26*, 6231.

[43]Taylor, R. M., McKenzie, R. M., *Clays Clay Miner.*, **1980**, *28*, 179.

Received: 22.12.2016.
Accepted: 04.02.2017.

METALLIC NICKEL NANOTUBES: INFLUENCE OF DEPOSITION PARAMETERS ON THEIRS STRUCTURE AND MAGNETIC PROPERTIES

A. Shumskaya,[a]* E. Kanyukov,[a] A. Kozlovskiy,[b,c] M. Zdorovets,[b,c] A. Tikhonov[d] and G. Kalkabay[d]

Keywords: Ion-track membrane, electrodeposition, Ni nanotubes, magnetic properties.

Arrays of Ni nanotubes have been synthesized in pores of polyethylene terephthalate membranes by electrochemical method. Morphological and structural characteristics were studied by scanning electron microscopy, gas permeability, energy-dispersive X-ray spectroscopy and X-ray diffraction analysis. It was shown that Ni nanotubes have lateral dimensions corresponding to the parameters of the membrane pores (length ~12 μm and pore diameters 400 nm) with the thickness of tube-walls in the range from 60 nm to 160 nm, depending on the deposition conditions. Ni nanotubes have the face-centered cubic lattice phase. The dependence of crystal structure parameters on temperature and voltage of synthesis has been established. Dependences of main magnetic parameters (coercivity value and magnetization of saturation and squatness) on deposition parameters have been studied. Significant magnetic anisotropy was found, but no evidence of influence of deposition parameters on magnetic properties was found.

*Corresponding Author:
E-Mail: lunka7@mail.ru
[a] Scientific-Practical Materials Research Center NAS of Belarus, Minsk, Belarus
[b] Institute of Nuclear Physics, Almaty, Kazakhstan
[c] L.N. Gumilyov Eurasian National University, Astana, Kazakhstan
[d] Nazarbayev University, Astana, Kazakhstan

Introduction

Nowadays a great attention is given to the nanostructures (NSs) due to their unique properties and application prospects as devices for chemical and biological practice[1,2] and catalysis,[3] objects for the biomedicine,[4,5] as well as sensitive elements of the magnetic field actuators.[6-9] There are many methods of NSs design like the spontaneous coalescence, hydrothermal synthesis, electrochemical deposition etc.[10-13]

In present work the electrochemical deposition method was used for a synthesis of magnetic NSs, which made it possible to control the structure, element and phase composition by means by varying the deposition parameters. The deposition process was carried out in the pores of polyethylene terephthalate (PET) membranes. The use of the pores with pre-determined geometry lead to synthesis of NSs with a desired form.

In this work the structural and magnetic properties of Ni nanotubes (NTs) and analysis of dependences of their properties on the deposition parameters i.e., temperature and potential were investigated.

Experimental

Ni NSs synthesis has been realized in the pores of the ion track polymer films on the base of the PET of the Hostaphan® type from the «Mitsubishi Polyester Film» (Germany) with thickness 12 μm, pores diameters 400 nm and density 4 $\times 10^7$ cm^{-2}. Before the synthesis a gold layer with thickness 10 nm was deposited by the magnetron sputtering in vacuum served as a cathode for the electrodeposition process. Electrochemical synthesis was carried out in the potentiostatic mode at cathode voltages in the range 1.25 to 2.0 V using the electrolyte $NiSO_4.6H_2O$ (100 g L^{-1}), H_3BO_3 (45 g L^{-1}), $C_6H_8O_6$ (1.5 g L^{-1}) at temperatures 25, 35 and 50 ^{0}C. The process was controlled chronoamperometrically by the multimeter Agilent 34410A.

Investigation of the structure and morphology of the synthesized NTs was carried out by the scanning electron microscopy (SEM) on the Hitachi TM3030 set up equipped with the Bruker XFlash MIN SVE the energy-dispersive

X-ray analysis (EDX) with the accelerating voltage 15 kV. X-ray diffraction (XRD) analysis was made on the D8 ADVANCE diffractometer with the use of X-ray tube with Cu anode and graphitic monochromator on the diffracted beam. The XRD patterns were recorded in the angles range $2\theta \sim 30–70^\circ$, with the step $2\theta \sim 0.02^\circ$.

Macromagnetic properties were investigated using the vibrational magnetometer (the Liquid Helium Free High Field Measurement System (Cryogenic Ltd.)). The measurements were implemented by the induction method, through a determination of the induced electromotive force of the induction in signal coils by a magnetized sample oscillating with a definite frequency at magnetic field B ± 3 T at temperature 300 K.

Results and Discussion

Synthesis

Synthesis of Ni NSs was carried out inside pores of the dielectric ion track membranes due to a gold cathode layer on the bottom part of membranes and the high degree of surface hydrophilicity (contact angle ~45°-47°). That allowed the electrolyte get inside pores. The gold cathode layer was thin (about 10 nm) and pores stood opened. This fact determined the hole structure of deposited NSs.[14] To investigate influence of electrodepositing parameters i.e., temperature and voltage, three sets of samples were made at different temperatures (25, 35 and 50 °C). In every set voltage was changed in a range from 1.25 to 2 V by step of 0.25 V. The upper level of temperatures was determined by temperature of dissolved gases releasing. The range of voltage was limited by deposition potential of Ni (the lower level) and by potential of water dissociation that led to the rapid evolution of hydrogen in the electrolyte (the upper level). The huge role of hydrogen evolution in forming nanotubes has been shown earlier.[15]

Aanalyzing of typical time dependence of current during deposition (figure 1) we found that process had four stages, which were determined by the size of cathode area at a moment, and amount of ions near it. The first stage, nucleation, was carried out on the interface insulator-cathode inside of pores and the nuclease of metal were formed on pores walls and on the cathode. This process led to exhaustion of electrolyte in pores and current dramatically decreased and stood almost constant during the next stage of the deposition, 1d structure growing. This second stage ended when the pores were completely filled with metal and the deposition proceeded on the upper part of membrane and, at first, the cups on the top of NSs grew (the third stage) and then the thin metallic layer was formed (the fourth stage).[16] During the two final stages, the cathode area became larger and the concentration of metal ions increased to the level of concentration above the membrane surface. The details of synthesis process and or the stages of growth process have already been reported.[17]

Structure characterization

By analysis of SEM images, it was determined that the obtained NSs had external dimensions corresponding to the original template parameters i.e., length of 12 mm and external diameters of 400 nm with a minor size deviation (within 5-8%). By permeability method, it was established that the NSs are hollow and have internal diameters, which increase with an increase in the voltage and/ or decrease in the deposition temperature. Thus, the wall thickness changes from 60 to 160 nm (figure 2a). This fact could be explained by the presence of two competing factors. A circular form of electrode induced the tubular growth due to the "tip effect" and could been seen mostly at higher voltage and/or temperature of a process. On the other side, due to a low voltage, the ions diffusion rate could overcome the "tip effect". This leads to a formation of NTs with thick walls and even rigid NSs in the form of wires. Influence of these two factors on the wall thicknesses (*h*) is shown on figure 2a. Dependences of a morphology of the deposited structure on the electrode form, temperature and voltage of a deposition process on was discussed in detail in an earlier report.[17]

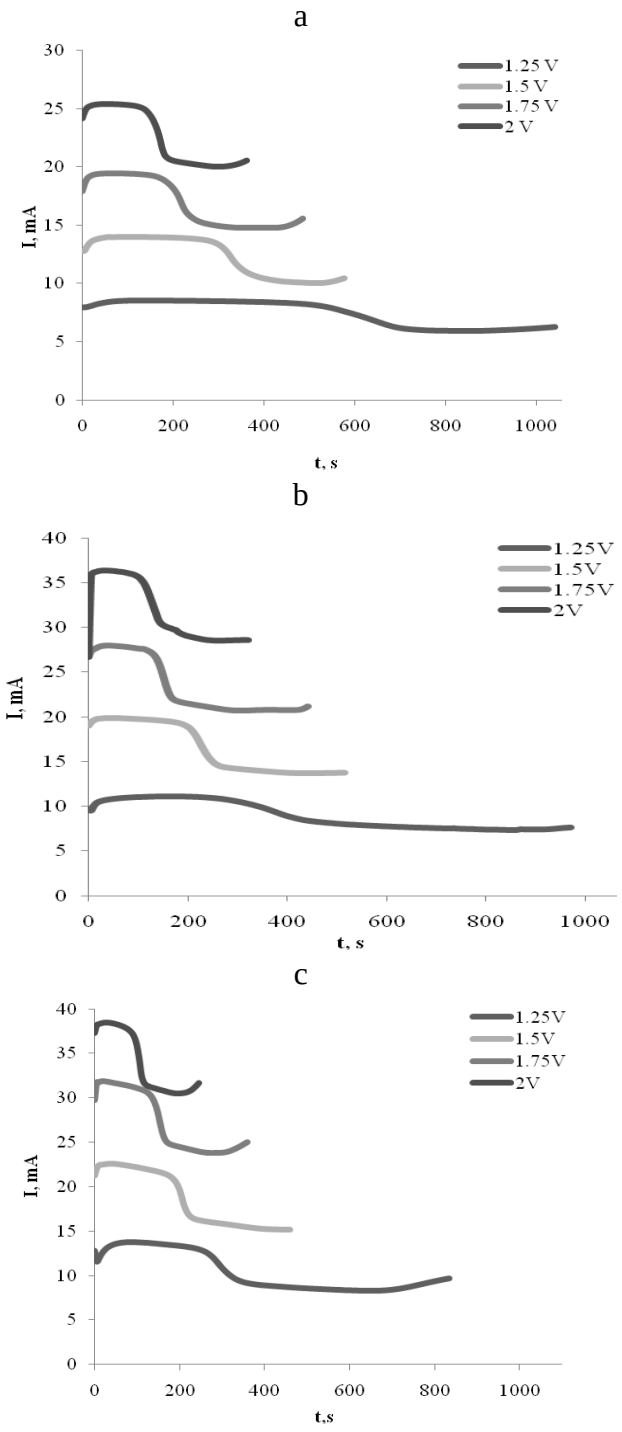

Figure 1. Time dependence of current of electrochemical deposition process: (a) t=25 °C, (b) t=35 °C, (c) t=50 °C.

XRD investigations of the samples prepared at different synthesis conditions were carried out to determine their influence on the crystal structure. A wide peak at the angle ranges 2θ = 20-35º and a small peak at the 2θ = 53-55º observed on the XRD spectra. These peaks are belonged to the PET membrane, where the studied NTs were during the analysis. All the XRD spectra have specific peaks for the diffraction on nanosized objects.

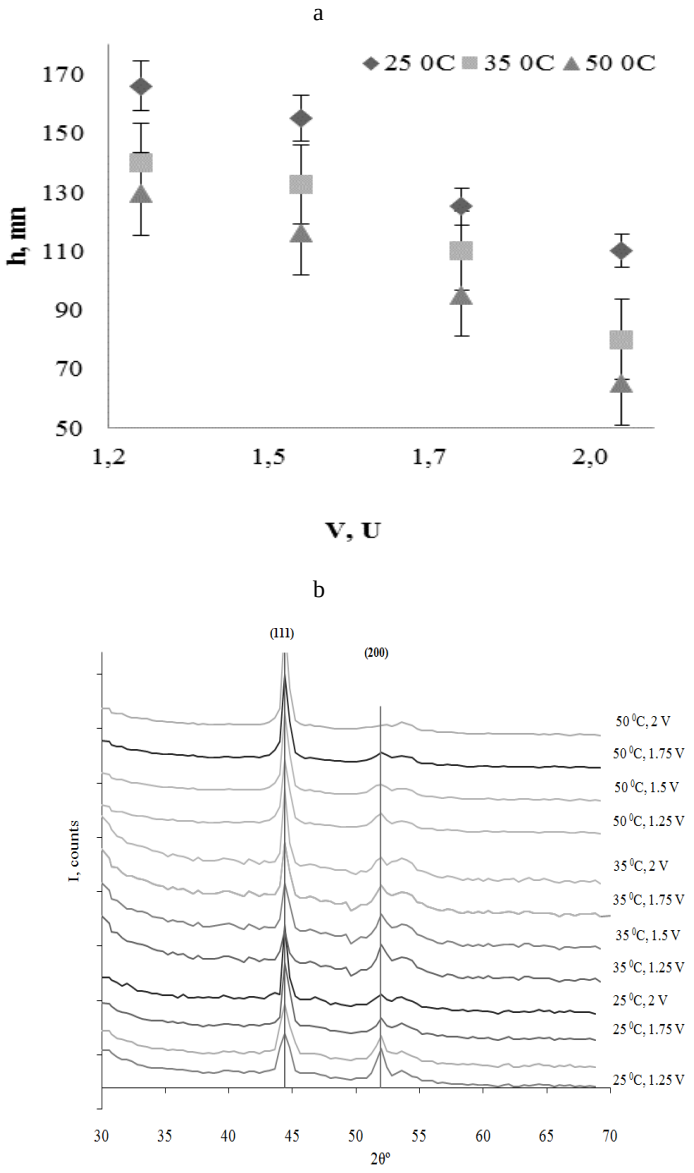

Figure 2. (a) Influence of deposition parameters on the wall thicknesses; (b) X-ray diffraction spectra of Ni NTs arrays.

Analysis of the XRD spectra shows that the Ni NTs possess the face-centered cubic (*fcc*) lattice phase with the crystal structure parameters being different from the reference values. On the XRD spectra one could observe ϕτ increase of the intensity of the peak with the Miller indexes (*hkl*) (111) with the increasing of voltage during the synthesis process and decrease of the intensity of the (200) peaks. This makes it evident the dominance of the [111] texture direction in the NTs crystal structure. The texture coefficients (TC(*hkl*)) have been calculated according to the Harris equation. Results of calculations are shown in table 1. The tendency of definition of priority texture direction along the NTs axis is explained by the intensification of the impact of hydrogen evolution in electrodeposition process.[15]

Lattice parameter (*a*) and crystals size (*L*) are shown in table 2. The parameters of crystalline structure change with deposition conditions. The most evident reason of these changes is inclusion of contaminants in the crystals structure such as hydrogen and salts, leading to the increase of lattice parameter and crystals size.

Magnetic properties

The investigation of macromagnetic properties has been carried out by the vibration magnetometry at temperature 300 K at magnetic field B = ±3 T for parallel and perpendicular directions of the field with respect to orientation of the NTs axis. The typical hysteresis loops obtained for the studied samples are presented in figure 3. Insets of images show enlarged detail of the hysteresis loops at fields up to 0.4 T. Using them, the main magnetic characteristics were determined (H_c = coercivity and M_r / M_s = squareness ratio of hysteresis loop). These characteristics are presented in table 3.

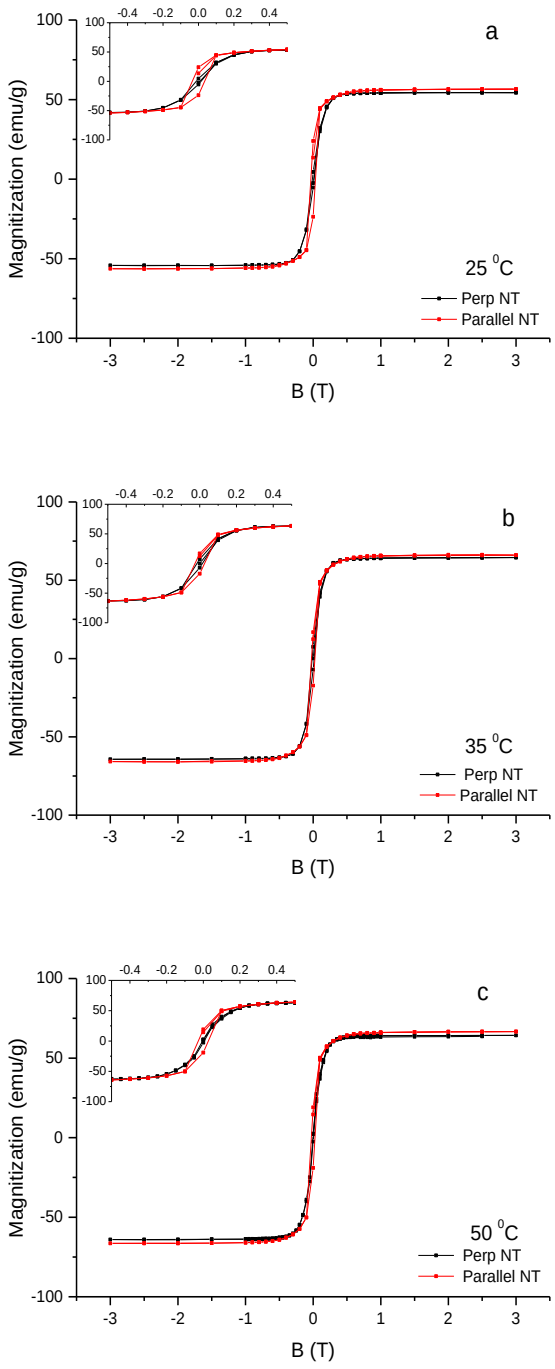

Figure 3. Hysteresis loops of Ni NTs synthesized at 1,75 V and temperatures: a) 25 °C, b) 35 °C, c) 50 °C.

 DOI: 10.17628/ecb.2016.5.531-535

Table 1. Crystalline parameters of nanotubes.

Temperature of synthesis, °C	2θ°	(hkl)	TC(hkl)			
			1.25 V	1.5 V	1.75 V	2.0 V
25	44.559	111	1.3415	1.4762	1.5741	1.7831
	51.930	200	0.9714	0.8224	0.6741	0.5421
35	44.559	111	1.3541	1.5413	1.6107	1.8741
	51.930	200	0.8702	0.7055	0.5467	0.4531
50	44.559	111	1.4531	1.5731	1.7762	1.9102
	51.930	200	0.5431	0.4211	0.3513	0.2365

Table 2. Crystalline parameters of Ni NTs.

Synthesis temp., °C	Para-meters	Voltage of synthesis, V			
		1.25	1.5	1.75	2.0
25	*a*, Å	3.517	3.5179	3.5192	3.5211
	L, nm	24.77	25.73	26.91	28.11
35	*a*, Å	3.5181	3.5194	3.5201	3.5232
	L, nm	25.15	26.11	27.21	29.34
50	*a*, Å	3.5195	3.5201	3.5216	3.5266
	L, nm	26.65	28.17	29.76	31.23

The experimental data show strong magnetic anisotropy of Ni NTs arrays in the entire range of the synthesis parameters coercivity and squatness value for parallel (∥) orientation of the field relative to the NTs axis is several times higher than the values for the perpendicular (PD) field direction. The anisotropy of the magnetic properties is caused by crystalline anisotropy, detected in the X-ray analysis, and shape anisotropy, caused by the fact that in an external magnetic field NTs with high aspect ratio (~100) need higher energy of demagnetization along their axis than in the perpendicular direction of the field.[18]

Table 3. Magnetic parameters of Ni NTs.

$T_{synthesis}$, °C	Voltage, V	H_C, Oe		M_r/M_s	
		PD	∥	PD	∥
25	1.25	160	240	0.14	0.25
	1.5	140	260	0.10	0.31
	1.75	130	330	0.09	0.39
	2	150	280	0.09	0.28
35	1.25	160	210	0.12	0.22
	1.5	150	280	0.12	0.25
	1.75	170	280	0.12	0.26
	2	130	250	0.11	0.24
50	1.25	50	330	0.07	0.30
	1.5	80	250	0.08	0.25
	1.75	70	270	0.04	0.29
	2	250	320	0.13	0.29

The values of the main magnetic characteristics of the Ni NTs are closely linked with their crystal structure. Considering the study of the structural features of NTs a strong correlation of the parameters of crystal structure of the samples with the temperature and the voltage of synthesis is established. An expected correlation of the main magnetic parameters with the synthesis conditions has not been proved, because, despite the variation of structural parameters, a dependence of the magnetic properties was not observed (see the data in table 3) in the considered range of deposition parameters.

Conclusions

Ni NTs have been obtained using ion-track PET membranes, by means of the electrochemical synthesis at various potentials and temperatures. Investigations of the morphological and structural characteristics of the NTs using SEM, EDX and XRD make it possible to determine that Ni NTs have lateral dimensions corresponding to the pores parameters (length ~12 μm and pores external diameters 400 nm) with the tubes walls thickness in the range from 60 nm to 160 nm, depending on the deposition conditions. The XRD analysis shows that the Ni NTs possess the *fcc* lattice phase with the crystal structure parameters being different from the reference values.

There is no evidence of the dependence of the changes of the magnetic parameters values on the experimental range of the voltage and temperature during the synthesis. Investigation of magnetic properties shows a significant magnetic anisotropy.

Acknowledgments

This paper has been presented at the 4th International Conference “Nanotechnologies”, October 24 – 27, 2016, Tbilisi, Georgia (Nano – 2016).

References

[1] Goldberger, J., He, R., Zhang, Y., *Nature*, **2003**, *422*, 599.

[2]Sanchez-Castillo, M.A., Couto, C., Kim, W.B., *Angew, Chem. Int. Ed.*, **2004**, *43*, 1140.

[3]Kros, A., Nolte, R.J.M., Sommerdijk, N.A.J.M., *Adv. Mater*., **2002**, *14*, 1779.

[4]Yu, S., Lee, S.B., Martin, C.R., *Anal. Chem*., **2003**, *75*, 1239.

[5]Dave, S.R., Gao, X., Wiley, Y., *Interdiscip. Rev. Nanomed. Nanobiotechnol*., **2009**, *1 (6)*, 583.

[6]Tans, S.J., Devoret, M.H., Dai, H., *Nature*, **1997**, *386*, 474.

[7]Dai, H., Hafner, J.H., Rinzler, A.G., *Nature*, **1996**, *384*, 147.

[8]Lieber, C.M., *Solid State Com*., **1998**, *107*, 607.

[9]Demyanov, S.E., Kaniukov, E.Yu., Petrov, A.V., Sivakov, V., A. *Phys.*, **2014**, *216*, 64.

[10]Sehayek, T., Lahav, M., Popovitz-Biro, R., *Chem. Mater*., **2005**, *17*, 3743.

[11]Li, Y., Wang, J., Deng, Z. *J. Am. Chem. Soc*., **2001**, *123*, 9904.

[12]Haehnel, V., Fähler, S., Schaaf, P., *Acta Mater*., **2010**, *58(7)*, 2330.

[13]Kaniukov, E., Kozlovsky, A., Shlimas, D., *IOP Conf. Ser. Mat. Sci. Eng.*, **2016**, 110.

[14]Tao, F., Guan, M., Jiang Y., Zhu J., Xu Zh., Xue Z., *Adv. Mater*., **2006**, *18*, 2161. DOI: 10.1002/adma.200600275

[15]Motoyama M., Fukunaka Ya., Ogata, Yu.H., Prinza, Fr. B., *J. Electrochem. Soc.*, **2010**, *157*(6), 357.

[16]Kozlovskiy, A., Zhanbotin, A., Zdorovets, M., Manakova, I., Ozernoy, A., Kiseleva, T., Kadyrzhanov, K., Rusakov, V., Kanyukov, E., *Nucl. Instrum. Methods Phys. Res. B*, **2016**, *381*, 103. 10.1016/j.nimb.2016.05.026

[17]Kozlovskiy, A.L., Shlimas, D.I., Shumskaya, E.E., Kaniukov, E.Yu., Zdorovets, M.V., Kadyrzhanov, K.K., *Phys. Metall Metallogr.*, **2017**, *2*.

[18]Shumskaya, E.E., Kaniukov, E. Yu., Kozlovskiy, A.L., Zdorovets, M.V., Rusakov, V.S., Kadyrzhanov, K.K., *Phys. Solid State*, **2017**, *4*, 766.

Received: 22.12.2016.
Accepted: 04.02.2017.

PHOTOSYNTHESIS STRUCTURAL INTERACTION

G. A. Korablev[a]*

Keywords: Spatial-energy parameter, free radicals, structural interactions, photosynthesis.

The application of methodology of spatial-energy interactions (P-parameter) to main stages of photosynthesis is given. Their energy characteristics are calculated. The values obtained correspond to the reference and experimental data.

* Corresponding Authors
E-Mail: korablevga@mail.ru
[a] Department of Physics, Izhevsk State Agricultural Academy

Introduction

Photosynthesis is the process of converting electromagnetic energy of the sun rays into the energy of chemical bonds of vital organic substances.[1]

It is the only natural process through which the organic world obtains the reserve of free energy and which provides all bio-organisms with chemical energy. From the moment photosynthesis was discovered by Priestly, the researches passed several important stages. Further development of bio-physicochemical aspects of synthesis till now resulted in its modern model and clarified the way of carbon during photosynthesis, concept of two photosystems, structure of reaction center etc.

The basis of photosynthesis, consecutive chain of redox reactions, during which electrons are transferred from donor-reducer to acceptor-oxidizer with the formation of reduced compounds (carbohydrates) and isolation of oxygen.

It is known that excitation energy for complex organic molecules of chlorophyll type lasts for 10^{-8}-10^{-9} sec and can be stored only for insignificant fractions of a second. But during photosynthesis the energy of absorbed light quantum is stored for a long period (from several minutes to millions of years). The energy is stored here in molecular as chemical bonds rich with energy in complex organic structures. Therefore, photosynthesis energy can be presented based on the analysis of changes in energies of chemical bonds of molecular structures in dynamics of all main types of photosynthesis. This is the aim to use the methodology of spatial-energy interactions (P-parameter) in this paper.

Spatial-energy parameter (P-parameter)

Structural and interatomic interactions are sure to have electronic nature. Thus the registration of the extent to which electrons fill the atom valence states is the basis of the method of valence bonds in chemistry and is numerically expressed through coulomb electrostatic interaction.

Also important are exchange-promotional structural interactions that determine isomorphism, solubility of components in solid, liquid and molecular media.[2]

During the interactions of oppositely charged heterogeneous systems, the volume energy of interacting structures is compensated to a certain extent thus leading to the decrease in the resultant volume energy.

The analysis of different physical and chemical processes allows assuming that in many cases the principle of adding reciprocals of volume energies or kinetic parameters of interacting structures is executed e.g., ambipolar diffusion, total rate of topochemical reaction, change in the light velocity when transiting from vacuum into the given medium, resultant constant of chemical reaction rate (initial product – intermediary activated complex – final product).

Lagrange equation for relative movement of isolated system of two interacting material points with masses m_1 and m_2 in coordinate x can be presented as eqn. (1) where ΔU_1 and ΔU_2 are the potential energies of material points in elementary section of interactions and ΔU is the resulting (mutual) potential energy of these interactions.

$$\frac{1}{\Delta U} \approx \frac{1}{\Delta U_1} + \frac{1}{\Delta U_2} \qquad (1)$$

The atom system is formed from oppositely charged masses of nucleus and electrons. In this system energy characteristics of subsystems are the orbital energy of electrons (W_i) and effective energy of nucleus that takes into consideration the screening effects.

Therefore, assuming that the resultant interaction energy of the system orbital-nucleus (responsible for interatomic interactions) can be calculated based on the principle of adding reciprocals of some initial energy components, we substantiate the introduction of P-parameter[2] as an averaged energy characteristic of valence orbitals in accordance with the following equations, where W_i is the bond energy of electrons,[3] r_i is the orbital radius of I orbital,[4] n_i is the number of electrons of the given orbital, Z* and n* are effective charge of nucleus and effective main quantum number[5] and R is the numerical characteristic of atom (bond).

$$\frac{1}{q^2/r_i} + \frac{1}{W_1 n_\mathrm{i}} = \frac{1}{P_\mathrm{E}} \qquad (2)$$

$$P_{\mathrm{E}} = \frac{P_0}{r_{\mathrm{i}}} \quad (3)$$

$$P_{\mathrm{E}} = \frac{P_0}{R} \quad (3a)$$

$$\frac{1}{P_0} = \frac{1}{q^2} + \frac{1}{(Wrn)_{\mathrm{i}}} \quad (4)$$

$$q = \frac{Z^*}{n^*} \quad (5)$$

The P_0 value will be called a spatial-energy parameter, and the P_{E} value is the effective P parameter. Effective P_{E} parameter has a physical sense of some averaged energy of valence electrons in atom and is measured in energy units, i.e. in electron-volts (eV).

The values of P_0- and P_{E}-parameters of some elements calculated based on eqns. (2-5) are given in Table 1.

Modifying the rules of adding reciprocals of energy characteristics of subsystems as applied to complex structures we can obtain[6] the equation for calculating P_{C}-parameters of complex structure where where N_1 and N_2 are the number of homogeneous atoms in subsystems.

$$\frac{1}{P_{\mathrm{C}}} = \left(\frac{1}{NP_{\mathrm{E}}}\right)_1 + \left(\frac{1}{NP_{\mathrm{E}}}\right)_2 + \cdots \quad (6)$$

The calculation results of some complex structures based on eqn. (6) are given in Table 2.

The calculations for 21 elements showed that the values of P_{E}-parameters are similar to corresponding values of total energy of valence electrons according to the statistic model of atom.

Simple dependence between P_{E}-parameter and electron density at the distance r_i can be obtained (according to the statistic model of atom) by eqn. (7), where A is a constant.

$$\beta_{\mathrm{i}}^{2/3} = A \times \frac{P_0}{r_{\mathrm{i}}} = AP_{\mathrm{E}} \quad (7)$$

When the solution is formed in the places of atom-components contact, the unified electron density has to be established. The dissolving process is accompanied by the redistribution of this density between valence areas of both particles and transition of some electrons from external spheres to the neighboring ones.

It is obvious that if electron densities in free atom-components of the solution at the distances of orbital radius r_{i} are similar, the transition processes between boundary atoms of particles are minimal thus favoring the solution formation. Thus the task of evaluating the solubility in many cases comes to comparative evaluation of electron density of valence electrons in free atoms (on averaged orbitals) participating in the solution formation.

In this regard the maximum total solubility evaluated through the coefficient of structural interaction and isomorphism α are determined by the state of minimal value that represent relative difference of effective energies of external orbital.

$$\alpha = \frac{P'0/r_{\mathrm{i}}' - P''0/r_{\mathrm{i}}''}{(P'0/r_{\mathrm{i}}' + P''0/r_{\mathrm{i}}'')/2} 100\ \% \quad (8)$$

$$\alpha = \frac{P'C - P''C}{P'C + P''C} 200\ \% \quad (9)$$

Multiple calculations and comparisons with the experiment allowed arranging the unified averaged figure-nomogram of degree of structural interaction and solubility (ρ) dependence upon coefficient α.[2]

The following spatial-energy principles defining the character of structural spatial-energy interactions were determined:

1. Complete (total-lot) isomorphic interaction takes place at relative difference of P-parameters of valence orbitals of interchanging atoms (within 4-6%).

2. P-parameter of the smallest value defines the orbital that is mainly responsible for isomorphism.

3. Qualitatively the isomorphism character is defined by geometrical similarity of orbital shapes responsible for isomorphism. At the same time, the more similar are the extensions, trajectories and inclination angles of such orbitals, the more perfect is isomorphism.

According to the degree of isomorphic similarity of interchanging structures they can be classified into three types (I, II, III) given for some cases in table 3.

Photosynthesis - Initial stage

Magnesium atom, four-coordinated with nitrogen atoms, is included into chlorophyll in the central cavity of the whole structure. The porphinated chlorophyll ring is located in aqueous medium. Each central Mg atom forming chelate compound has two bonds by donor-acceptor mechanism and two covalent bonds. Two molecules of bacterio-chlorophyll are located close to each other (about 3 Å) and form competent-structure – dimer chlorophyll. In the dynamics of structural permutations all four bonds of each Mg atom become equivalent.[7] All this allows assuming that total effective P_{E}-parameter of Mg will be approximately two times greater than from $2S^2$-orbital (5.4867 x 2 = 10.973 eV).

In the first stage of photosynthesis in the system of PS-2 dimensional characteristics of hydrogen atom can change in structured water molecules under the radiation with energy hν from boron radius (0.529 Å) to atomic ("metal") i.e.. 0.46 Å, this corresponds to the obtaining of P_E-parameter equal 10.432 eV by hydrogen that is similar to P_E-parameter of 2 Mg.

It should be pointed out that general change in the scale of photosynthesis potentials PS-2 approximately equals 1.5 eV, and the difference between the data of *P*-parameters of hydrogen atoms equals 1.37 eV. The rest of hydrogen atoms with "boron" P_E-parameter equal to 9.0624 eV have similar values with P_E-parameters of $2P^1$-orbitals of nitrogen atoms surrounding magnesium

.

Table 1. P-parameters of atoms calculated via the bond energy of electrons

Atom	Valence electrons	W (eV)	r_i (Å)	$q^2{}_0$ (eVÅ)	P_0 (eVÅ)	R (Å)	P_0/R (eV)
						0.5295	9.0624
H	$1S^1$	13.595	0.5295	14.394	4.7985	0.46	10.432
						0.28	17.137
						$R^-{}_I$=1.36	3.525
	$2P^1$	11.792	0.596	35.395	5.8680	0.77	7.6208
						0.69	8.5043
	$2P^2$	11.792	0.596	35.395	10.061	0.77	13.066
						0.69	14.581
	$2P^1{}_r$				4.4044		
C	$2P^3{}_r$				13.213		
	$2S^1$	19.201	0.620	37.240	9.0209	0.77	11.715
	$2S^2$				14.524	0.77	18.862
	$2S^1+2P^3{}_r$				22.234	0.77	28.875
	$2S^1+2P^1{}_r$				13.425	0.77	17.435
	$2S^2+2P^2$				24.585	0.77	31.929
	$2P^1$	15.445	0.4875	52.912	6.5916	0.70	9.4166
	$2P^2$				11.723	0.70	16.747
	$2P^3$				15.830	0.70	22.614
	$2P^4{}_r$				19.193	0.55	34.896
N	$2P^5{}_r$				21.966	0.55	39.938
	$2S^1$	25.724	0.521	53.283	10.709	0.70	15.299
	$2S^2$	25.724	0.521	53.283	17.833	0.70	25.476
	$2S^2+2P^3$				33.663	0.70	48.09
	$2P^1$	17.195	0.4135	71.383	4.663	0.66	9.7979
	$2P^1$					R_I=1.36	4.755
	$2P^1$					R_I=1.40	4.6188
	$2P^2$	17.195	0.4135	71.383	11.858	0.66	17.967
						0.59	20.048
						R_I=1.36	8.7191
O						R_I=1.40	8.470
	$2P^4$	17.195	0.4135	71.383	20.338	0.66	30.815
						0.59	34.471
	$2S^1$	33.859	0.450	72.620	12.594	0.66	19.082
	$2S^2$	33.859	0.450	72.620	21.466	0.66	32.524
	$2S^2+2P^4$				41.804	0.66	63.339
						0.59	70.854
	$4S^1$	5.3212	1.690	17.406	5.929	1.97	3.0096
Ca	$4S^2$				8.8456	1.97	4.4902
	$4S^2$					R^{2+}=1.00	8.8456
	$4S^2$					R^{2+}=1.26	7.0203
	3P1	11.901	0.808	48.108	6.0143	1.04	7.7061
	3P2	11.901	0.808	48.108	13.740	1.04	13.215
S	3P4	11.904	0.808	48.108	21.375	1.04	20.553
	3S1	23.933	0.723	64.852	13.659	1.04	13.134
	3S2	23.933	0.723	64.852	22.565		
	3S2+3P4				43.940	1.04	42.250
	4P1	10.963	0.909	61.803	8.5811	1.17	7.3343
Se	4P2				15.070	1.17	12.880
	4P2				15.070	1.6	9.4188

	4P2				15.070	1.14	13.219
	4P4				24.213	1.17	20.710
	4P4					1.6	15.133
	4S1	22.787	0.775	85.678	14.642	1.17	12.515
	4S2				25.010	1.17	21.376
	4S2+4P4				49.214	1.17	42.066
	4S2+4P4				49.214	1.6	30.759
	3P1	10.659	0.9175	38.199	7.7864	1.10	7.0785
	3P1					R3-=1.86	PƆ=4.1862
P	3P3	10.659	0.9175	38.199	16.594	1.10	15.085
	3P3					R3-=1.86	8.9215
	3S2	18.951	0.803	50.922	19.050	1.10	17.318
	3S2+3P3				35.644	1.10	32.403
	3S1	6.8859	1.279	17.501	5.8568	1.60	3.6618
Mg	3S2				8.7787	1.60	5.4867
						R2+=1.02	8.6066
	4S1	6.7451	1.278	25.118	6.4180	1.30	4.9369
	4S2				10.223	1.30	7.8638
	3d1	17.384	0.3885	177.33	6.5058	1.30	5.0043
Mn	4S1+3d1				12.924	1.30	9.9414
	4S2+3d2				22.774	1.30	17.518
	4S2+3d5				38.590	1.30	29.684
	3S1	4.9552	1.713	10.058	4.6034	1.89	2.4357
Na						R+I=1.18	3.901
						R+I=0.98	4.6973
	3P1	13.780	0.7235	59.849	8.5461	1.00	8.5461
Cl						R-I=1.81	4.7216
	4S1	7.0256	1.227	26.572	6.5089	1.26	4.8325
	3d1	17.603	0.364	199.95	6.2084		
Fe	4S1+3d1				12.717	1.26	10.093
	4S2+3d1				16.664	1.26	13.226
	4S1	4.0130	2.612	10.993	4.8490	2.36	2.0547
						R+I=1.45	3.344
K	4S2(*)				7.2115	2.36	3.0557
						R+I=1.45	4.9734

Other data are not less important. Initial value of P_E-parameter of $2S^2$-orbital of magnesium atom gives from P_E-parameter (Table 3) of radical (O-H) α = 8.24 % and $\rho \approx$ 77-82 %. This ρ value can increase to even 100 % under the light action due to minor changes in dimensional characteristics of atoms-components. Absolute difference of these *P*-parameters equals 0.43 eV, thus corresponding to the changes in the scale of potentials during the synthesis of ATP.

Total spatial-energy action upon the bond H-O-H of magnesium and nitrogen atoms (Table 3) results in the possibility of breaking this bond with the isolation of free hydrogen and oxygen atoms.

This initial process finishes with the participation of manganese-containing system connected with proteins of reaction center PS-2. Structural reconstruction can take place in manganese cluster (two-nucleus or four-nucleus) under the action of radiation[8,9] from univalent state (4.9369 eV, this is similar to initial values of Mg P_E-parameter) to bivalent (9.9414 eV) and further to quadrivalent state (17.518 eV).

All this provides enzymatic action of Mn upon the bond H-O-H, both upon oxygen and hydrogen atoms, and hydroxyl group in general. This is confirmed by the approximate equality of P_E-parameters of bi- and quadrivalent Mn with P_E-parameters of $2P^1$ and $2P^2$-orbitals of oxygen atom (Table 3). Thus, all the above interactions and structural re-groupings inducted with light result in the formation of oxidized chlorophyll based on the following reaction (eqn. 10),[10] with the isolation of two electrons and two protons. These electrons, broken off from the water, through the chain of "dark" reactions go further to PS-1 that utilizes them in the next photosynthesis stages to reduce $NADP^+$ to NADPN that is carried out also with the help of proton transfer system.

$$H_2O + 2h\nu \rightarrow 1/2\ O_2 + 2e^- + 2H^+ \qquad (10)$$

For double bond of $2P^1$-orbital the carbon atom has a P_E-parameter (8.5043 eV) similar to P_E-parameter of hydrogen atom (Table 1). Therefore, one of the freed hydrogen atoms join the double bond C=C available in NADPN with the formation of single bond with carbon atom.[9]

Phosphorylation

It is accepted[7,11] that directed transition of protons serves as energy source during phosphorylation. Between the numbers of transported protons and electrons certain stoichiometric relations are revealed. Thus, in the course of electron transfer

(along the whole transport system) ATP molecules are formed. Apparently, ATP phosphorylation energy can also be estimated through the system of electron transfer.

Table 2. Structural P_C-parameters calculated via the bond energy of electrons.

Radicals, fragments	$P_i^{'}$ (eV)	$P_i^{''}$ (eV)	P_C (eV)	Orbitals
OH	17.967	10.432	6.5999	O ($2P^2$)
	9.7979	9.0624	4.7080	O ($2P^1$)
	9.7979	10.432	5.0525	O ($2P^1$)
	17.967	17.138	8.7712	O ($2P^2$)
H_2O	2·9.0624	17.967	9.0226	O ($2P^2$)
	2·10.432	17.967	9.6537	O ($2P^2$)
	2·17.138	17.967	11.788	O ($2P^2$)
CH_2	28.875	2·17.138	15.674	C ($2S^12P^3{}_r$)
	31.929	2·17.138	16.531	C ($2S^22P^2$)
	28.875	2·9.0624	11.125	C ($2S^12P^3{}_r$)
CH_3	31.929	3·17.138	19.696	C ($2S^22P^2$)
	28.875	3·9.0624	14.003	C ($2S^12P^3{}_r$)
CH	28.875	17.138	10.755	C ($2S^12P^3{}_r$)
	31.929	9.0624	7.059	C ($2S^22P^2$)
	31.929	17.138	11.152	C ($2S^22P^2$)
H_3O	3·17.138	17.967	13.314	O ($2P^2$)
C_2H_5	2·31.929	5·17.138	36.590	C ($2S^22P^2$)
CH_2	31.929	2·9.0624	11.562	C ($2S^22P^2$)
CH_3	28.875	3·17.138	18.491	C ($2S^22P^3{}_r$)
CH_3	31.929	3·9.0624	14.684	C ($2S^22P^2$)
CH	28.875	10.432	7.6634	C ($2S^22P^3{}_r$)
CH	31.929	10.432	7.8630	C ($2S^22P^2$)
CO	31.929	20.048	12.315	C ($2S^22P^2$)
C=O	14.581	20.048	8.4416	C ($2P^2$)
C=O	17.435	20.048	9.3252	C ($2S^12P^1{}_r$)
C-O_2	28.875	2·20.048	16.786	C ($2S^12P^3{}_r$)
C-O_2	31.929	2·20.048	17.774	C ($2S^22P^2$)
CO-OH	12.315	8.7712	5.1226	C ($2S^22P^2$)
CH-OH	11.152	8.7712	4.9159	C ($2S^22P^2$)
CO-H	8.4416	9.0624	4.3705	C ($2P^2$)

In particular, electron transfer results in that phosphoric acid molecules present in ATP, NADP and NADPN contain oxygen atoms in the form of O^-. Spatial-energy interactions (including isomorphic) are objectively expressed both at similar and opposite electrostatic charge of atoms-components. Such interactions can also take place between two heterogeneous atoms, if only their P_E-parameters are roughly equal, and geometric shapes of orbitals are similar or alike.

The radiation energy hν in PS-1 promotes, apparently, the changes in dimensional characteristics of phosphorous and oxygen atoms from covalent to anion ones. Therefore, P_0-parameters of free phosphorus and oxygen atoms are distributed at the distance of their anion radii 1.86 Å and 1.40 Å, respectively. This similarity of values of their P_E-parameters, α = 5.19 % for $2P^3$-orbitals of phosphorous with $2P^2$-orbitals of oxygen (Table 3).

Such approximate equality of P_E-parameters and geometric similarity of shapes of orbitals of atoms-components shows that actual degree of their interaction ρ=100 %, thus providing the energy of formation of macroenergy bond P-O. Then bond energy of phosphorous and oxygen atoms from two different molecules of phosphoric acid necessary for structural formation during phosphorylation can be considered phosphorylation energy.

For double bond of $2P^1$-orbital the carbon atom has P_E-parameter – (8.5043 eV) – similar to P_E-parameter of hydrogen atom (Table 1). Therefore one of the freed hydrogen atoms join the double bond C=C available in NADPN with the formation of single bond with carbon atom .[9]

To calculate bond energies or energies of molecule reduction during photosynthesis (E) the technique previously tested[6] for 68 binary and more complicated compounds following the equation was applied, where N is the bond average repetition factor and K is the hybridization coefficient that usually equals the number of atom valence electrons registered.

$$\frac{1}{E} = \frac{1}{P_C} = \frac{1}{\left(P_E \frac{N}{K}\right)_1} + \frac{1}{\left(P_E \frac{N}{K}\right)_2} \quad (11)$$

The half of internuclear distance (for binary bond) of similar atoms or atomic, covalence or ionic radii (depending upon bond type) can be used as a dimensional characteristic of atoms.

The calculations involving anionic distances of atomic orbitals for P and O atoms were made, $3P^1$ (phosphorous)-$2P^1$ (oxygen) and for $3P^3$ (phosphorous)-$2P^2$ (oxygen). The values of E obtained appeared to be slightly greater than experimental and reference data (Table 4). But actual power physiological processes during photosynthesis have the efficiency below the theoretical, being in some cases about 83 %.[7]

 DOI: 10.17628/ecb.2016.5.536-544

Table 3. Photosynthesis structural interactions

SEI types		**I**	**II**	**II**	**II**	**II, III**	**II**	**I**	**II**	**I**
ρ (mol%)		100	100	100	100	100	77-82	100	100	55-60
α (%)		4.82	1.45	2.53	3.83	4.75	8.24	5.27	0.08	10.1
2 comp.	P_E. P_C, eV	10.432	9.7979	17.967	9.0624	4.7080	5.0575	3.525	13.215	3.525
	Orbitals	$1S^1$	$2P^1$	$2P^2$	$1S^1$	$2P^1$-$2S^1$	$2P^2$-$1S^1$	$1S^1$	$2P^2$	$1S^1$
1 comp.	P_E. P_C, eV	9.9414	9.9414	17.518	9.4166	4.3969	5.4867	3.344	13.226	3.901
	Orbitals	$4S^13d^1$	$4S^13d^1$	$4S^23d^2$	$2P^1$	$4S^1$	$2S^2$	$4S^1$	$4S^23d^1$	$3S^1$
Atoms, molecules, radicals		Mn-H	Mn-O	Mn-O	N-H	Mn-OH	Mg-(O-H)	K^+-H^-	Fe-S	Na^+-H^-

Table 3. contg.

SEI types		**I**	**I**	**I**	**II**	**I**	**II**	**II, III**	**III**	**I**
ρ (mol%)		100	60-65	100	100	100	90-95	100	100	100
α (%)		5.19	9.83	5.16	5.79	3.01	7.51	2.21	1.53	5.05
2 comp.	P_E. P_C, eV	8.9215*	4.1862*	9.0624	11.125	17.967	8.7712	9.0226	16.785	10.432
	Orbitals	$3P^3$	$3P^1$	$1S^1$	$2S^12P^3{}_r$-$1S^1$	$2P^2$	$2P^2$ -$1S^1$	$1S^1$-$2P^2$	$2S^12P^3{}_r$-$2P^2$	$1S^1$
1 comp.	P_E. P_C, eV	8.470*	4.6188*	8.6066	11.788	17.435	8.4416	9.3252	16.531	10.973
	Orbitals	$2P^2$	$2P^1$	$3S^2$	$1S^1$-$2P^2$	$2S^1$-$2P^1$	$2P^2$-$2P^2$	$2S^12P^1{}_r$-$2P^2$	$2S^22P^2$-$1S^1$	$3S^2$ ($3S^2$)*
Atoms. molecules. radicals		O-P	O-P	Mg^{2+}-H	H_2O-CH_2	C-O	CO-OH	CO-H_2O	CH_2-CO_2	2Mg-H

It is probable that electrostatic component of resulting interactions on anion-anion distances is registered in such a way. In fact, the calculated value 0.83*E* practically corresponds to the experimental bond energy values during phosphorylation (first line in Table 4) and free energy for ATP in chloroplasts (second line in Table 4).

The calculations of bond energy based on the same technique but on covalence distances of atoms for free molecule P…O (sesquialteral bond) and for molecule P=O in P_4O_{10} (double bond) are given in Table 4 for comparison. Sesquialteral bond was evaluated introducing the coefficient N=1.5 using the average value of oxygen P_E-parameter for single and double bonds.

It is interesting to that calculations of *E* based on covalence distances correspond to experimental data without introducing the coefficient 0.83.

Assimilation of CO_2

Binding of CO_2 takes place in aqueous medium by the carboxylation reaction of ribulose-diphosphate (RuDP) with the formation of 3-phospho-glycerine acid (PGA). Water molecule and radical C=O at the distances of molecular interaction have quite similar values of P_E-parameters for forming the general structural grouping of dimeric composite type. Total P_E-parameter of water molecule and radical C=O nearly equals P_E-parameter of CO_2 and therefore the molecules of CO_2 and H_2O join RuDP with the formation of two radicals COOHв PGA. In ferment RuDP-carboxylase, Mg atoms and O^- ions (5.4867 eV and 4.755 eV) play an active role, their P_E-parameters similar to P_E-parameter of radical COOH.

A great difference in the number of atoms of interacting structures proves that carboxylase can play only a fermentative role, "tuned" to obtain this final product (COOH).

The assimilations of CO_2 to form CH_2O flows through a series of intermediate compounds and reactions (Calvin cycle). Let us show some results of calculations of total spatial-energy assimilation processes of CO_2. When CO_2 is reduced to the level of its structural formation in CH_2O, the chemical bonds are reconstructed on all stages of the cycle. Therefore, the additional activation energy from ATP and NADPN is required.

It is also obvious that power consumption should be rationally calculated taking into account the reconstruction processes of chemical bonds, i.e. via the values of bond energy for binary structures, and reduction energy for more complex molecules and radicals (*E*).

Thus we calculated the value *E* based on equation (10) for several compounds and radicals during photosynthesis (Table 4). For radical – C=O the calculations were made in two possible variants of activity of valence orbitals of carbon atoms.

Table 4. Bond and reduction energies of molecules during photosynthesis (eV)

Notes		**11**	**Phospho-rylation**	**Δ*G* of ATP**	**Free PO molecule**	**In P_4O_{10} molecule**		**Decomp. of one molecule**		
E by[7,8,14]		10	0.34-0.35	0.67-0.59	6.14	6.504	3.772	2.476	5.11	5.11
Calcu-lation	0.83*E*	9	0.33 0.34	0.64	—	—	—	—	—	—
	E	8	0.400 0.405	0.77	6.277 6.024 <6.15>	6.697	3.797	2.570	4.90	5.012
3 comp.	*N*/*K*	7	— —	—	— —	—	—	—	—	—
	P_E, eV	6	— —	—	— —	—	—	—	—	—
2 comp.	*N*/*K*	5	1/6 1/6	1/6	1.5/6 1.5/6	2/2	1/1	1/6	1/1	2/4
	P_E (eV)	4	4.6188 4.755	8.470	70.854 63.339	20.042	9.0624	17.967	9.7979	20.048
1 comp.	*N*/*K*	3	1/5 1/5	1/5	1.5/5	2/3	1/2	1/1	1/1	2/4
	P_E (eV)	2	4.1862 4.1862	8.9215	32.403	15.085	13.066	2•9.0624	9.7979	20.048
Atoms, structures, orbitals		1	P-O 3P1-2P1	P-O 3P2-2P2	P…O 3S23P3- 2S22P4	P=O 3P3-2P2	C-H 2P2- 1S1	H2O 1S1-2S2	-O-O- 2P1- 2P1	O=O 2P2- 2P2

Table 4. contg.

Notes		**11**	**Reduc-tion**						**Free energy of the formation of one mole**
E by [7, 8, 14]		10	4.56		3.688	4.553	— 4.390	—	4.96-5.07
Calcu-lation	0.83E	9	—	—	—	—	— —	—	—
	E	8	4.717	8.8874	3.782	4.487	5.894 4.511	3.544	5.025
3 comp.	*N*/*K*	7	—	—	—	1/1	— —	—	2/2
	P_E, eV	6	—	—	—	9.0624	— —	—	20.048
2 comp.	*N*/*K*	5	2/6	2/2	1/2	2/2	1/1 1/1	1/1	1/1
	P_E, eV	4	2•20.04 8	20.048	17.967	20.048	17.137 9?062 4	5.894	2.90624
1 comp.	*N*/*K*	3	2/4	2/4	1/2	2/4	1/2 1/2	1/1	1.33/4
	P_E, eV	2	14.581	31.929	13.066	31.929	17.967 17.967	8.8874	31.929
Atoms, structures, orbitals		1	CO_2 $2P^2$-$2P^2$	=C=O $2S^22P^2$-$2P^2$	C-O $2P^2$-$2P^2$	(C=O)-H ($2S^22P^2$-$2P^2$)-$1S^1$	-O-H $2P^2$- $1S^1$	CO- OH($2S^22P^2$- $2P^2$)-($2P^2$- $1S^1$)	CH_2O $2S^22P^2$-$1S^1$-$2P^2$

 DOI: 10.17628/ecb.2016.5.536-544

The agreement of calculated E values with reference data[12,13] was in the range of 5 % for all bonds of covalence type without introducing the coefficient of 0.83.

The main part of light energy is stored by a plant on the reduction stage to PGA. At the same time, 4.56 eV (per molecule) are spent[12,13]. Our calculations give the reduction energy of radical COH equal to 4.487 eV. Free energy for the formation of one mole of CH_2O based on reference data[7,12] is 4.96-5.07 eV. The calculations following the method of P-parameter evaluate this energy as 5.025 eV.

In molecule O=C(H)–H the average repetition factor for carbon atom bond was taken as equal to (2+1+1)/3=1.33.

The values of bond energies (or the reduction energies) of structural subsystems for each stage, E_C, were calculated by using the accepted mode.It is known[7] that the cycle moving energy to PGA can be 1.06 eV due to three ATP molecules (per one CO_2 molecule), one ATP molecule is consumed in the cycle to PGA.

Following our data, the cycle moving energy (ΔE_C) equals the difference of E_C values for the corresponding stages:

1) stage CO_2 – FGAK: ΔE_C=1.770-1.401=0.369 eV

Phosphorylation energy of one ATP molecule = 0.34-0.35 eV

2) stage CO_2 – FGA: ΔE_C = 2.367-1.401 = 0.966 eV

Phosphorylation energy of three ATP molecules = 0.34 x 3 =1.02 eV

Thus P-parameter gives the satisfactory characteristics of energetics of the CO_2 assimilation cycle main stages. Photorespiration reaction is as if “competitive” to the CO_2 assimilation reaction. Also here it is possible to reveal similar values of P_E-parameters of interacting radicals C=O and HCOH with P_E-parameters of oxygen atoms. As in assimilation reaction the ferment RuDP-carboxylase “is tuned” for the formation of final product COOH. Other ferments can aslo participate in photosynthesis and photorespiration, for example, the substitution of Mg atoms for Fe atoms results in the formation of cytochromes, in which P_E-parameter of two-valence iron (P_E = 10.093 eV) is an active spatial-energy component of photosynthesis structural interactions. Therefore, iron-sulfur proteins – ferrdoxins executing various transport functions connected with ATP synthesis are initial and secondary acceptors of electrons in the system PSI.

Conclusion

In this approach, we have given the quantitative and semi-quantitative evaluation of spatial-energy interactions at main stages of complicated biophysical process of photosynthesis based on the utilization of initial atomic characteristics. The analysis of results after the application of P-parameter methodology shows that they correspond to reference data both in the direction and energetics of these processes.

Abbreviations

m_1 and m_2 – masses of material points (kg);

ΔU_1 and ΔU_2 – potential energies of material points (J);

ΔU – their resulting (mutual) potential energy of interaction (J);

Z^* – nucleus effective charge (Cl);

n^* – effective main quantum number;

Wi – bond energy of electrons on i-orbital (eV);

ri – orbital radius of i-orbital (Å);

ni – number of electrons on this orbital;

SEI – spatial-energy interactions;

P_0 – spatial-energy parameter (eVÅ);

P_E – effective P-parameter (eV);

R – dimensional characteristic of atom or chemical bond (Å);

$h\nu$ – light quantum energy (J, eV);

N_1, N_2, … – number of homogeneous atoms;

N – average repetition factor in the formula (10);

P_C – structural P-parameter of complex structure (eV);

α – coefficient of structural interactions, isomorphism (%);

ρ – degree of structural interaction (%);

PS – photosystem (PSI and PSII);

ATP – adenosine triphosphate;

RuDP – ribulose-diphosphate;

PGA – 3 phosphoglyceric acid;

NADP – nicotine-amide-adenine-dinucleotide-phosphate;

PGA – phosphor-glycerin aldehyde;

E – energy of bond or molecule reduction (eV);

E_C – resulting energy of bond or reduction for radical groups (eV).

References

[11]Edited by Petrovsky, B. V., *Big medical encyclopedia*, Soviet encyclopedia, Moscow, **1985**, *26*, 560.

[2]Korablev, G. A., *Spatial-Energy Principles of Complex Structures Formation*, Brill Academic Publishers and VSP, Netherlands, **2005**, 426.

[3]Fischer, C. F., *Hartree-Fock Results for the Atoms Helium to Radon, Atomic Data*, **1972,** 301-399.

[4]Waber, J. T., Cromer. D. T., *J. Chem. Phys*.,**1965**, *42(12)*, 4116-4123.

[5]Clementi, E., Raimondi, D. L., *J. Chem. Phys*., **1963**, *38(11)*, 2686-2689.

[6]Korablev, G. A., Zaikov, G. E, *J. Appl. Polym. Sci.*, **2006**, *101*, 2101-2107.

[7]Govingi, M., *Photosynthesis*, Mir, Moscow, **1987**, *728*, 460.

[8]Clayton, P., *Photosynthesis: Physical mechanisms and chemical models*, Mir, Moscow, **1984**, 350.

[9]Schukarev, S. A., *Inorg. Chem.*, **1974**, *2*, 382.

[10]Hall, D., Rao, K., *Photosynthesis*, **1983,** 6th ed.; Cambridge University Press, Cambridge, UK

[11]Edwards, J., D., Walker, D., *Photosynthesis of C_3 and C_4-plants: Mechanisms and regulation*, **1986**, Boston, Blackwell Scientific Publication.

[12]Vvedensky, B. A., Encyclopedia in physics, Soviet encyclopedia, Moscow, **1966**, *5*, 576.

[13]Kamen, M. D., *San Pietro, A.*, Primary processes in photosynthesis, ISBN: 978-1-4832-2959-1 **1963**. Elsevier, 1963. https://doi.org/10.1016/c2013-0-12206-4

[14]Edited by V.I. Kondratjev, *Break-off energy of chemical bonds. Potentials of ionization and affinity to electron*, Science Moscow, **1974**, 351.

Received: 14.12.2016.
Accepted: 08.02.2017.

REMOVAL OF COPPER (II) AND IRON (III) MIXTURE BY PILOT NANOFILTRATION

Aoufi Boutheyna[a] and Mohamed Amine Didi[a]*

Keywords: extraction; nanofiltration; copper(II); iron(III); mixture; synergism.

In the current study, the effect of operating conditions such as pH value, feed flow, concentration of the solution and the applied pressure for the removal of copper(II), iron(III) and their mixtures for the production of drinking water by nanofiltration membrane was investigated. The results show that it is possible to extract all of the iron (III) and copper (II) at the same time to a salt mixture of Fe 50% - salt Cu 50% for concentration 4 ppm, pH = 4.5 and pressure = 6 bars. The best results for the copper(II) were obtained for the various mixtures at the pressure of 6 bars at varying pH.

*Corresponding Author
madidi13@yahoo.fr (M.A. Didi),
Tel. +213 552639237,
Fax: +213 43213198
[a] Authors Address: Laboratory of Separation and Purification Technologies, Department of Chemistry — Faculty of Sciences, Box 119, Tlemcen University — 13000, Algeria.

Introduction

Heavy metals exist in the natural state in the sea water, the minerals or the volcanic compounds. A large number of techniques such as waste water treatment, adsorption, the electrolysis, the flotation, the exchanges of ions, the liquid – liquid extraction, the membrane processes etc. have been used to obtained these metals in metallic form.

Advances over the last 10 years have shown a significant growth of papers published on nanofiltration (NF) membranes in many different areas. NF membranes in contact with aqueous solution are slightly charged due to the dissociation of surface functional groups or adsorption of charge solute. These properties have allowed NF to be used in niche applications in several areas especially for water and wastewater treatment, pharmaceutical and biotechnology, and food engineering.[1] In recent years, the use of nanofiltration membranes (NF) has increased rapidly in the chemical, petrochemical, biotech and desalination industries, since the NF technology over comes operational problems that are associated with conventional techniques. Several studies have been reported in which NF membranes have been used as tools for heavy metal removal.[2]

Heavy metals of the greatest concern in the treatment of waste waters are copper and iron, as they are highly toxic, non-biodegradable and have the tendency to accumulate in living organisms.[3] Nanofiltration has some advantages over other membrane techniques, for example it has higher rejection of divalent ions and lower rejection of monovalent ions, lower operating pressure, higher flux and lower energy consumption compared with RO. These features recommend NF as a promising and innovative technology which can be widely applied in drinking water and the treatment of industrial effluent.[4] The aim of this work was to study the efficiency of copper(II), iron(III) and their mixture retention by using the SNTE NF270-2540. The effects of pressure and initial feed concentration on the membrane performance were studied.

Experimental

Apparatus

All chemicals used in this research were of analytical grade. All metal salt solutions were prepared by dissolving the appropriate weight of the salt of each metal in distilled water and made to a total volume of 50 L. The pH of solutions was measured using a pH-meter (Adwa), provided with a glass combine electrode. The conductivity measurements were carried by using MC126 Conductivity meter provided with an electrode.

The metal ion concentrations were determined by atomic absorption spectrophotometer (PINA cle 900 H - Perkin Elmer), using an air acetylene flame, two wavelengths were used 327.40 nm (linearity: 0.17 - 8 ppm) for copper and 302.06 nm (linearity: 0.4-20 ppm) for iron a range of standards solutions for various concentrations were prepared from a standard solution of 10 ppm for iron and 8 ppm for copper (board 1).

Pilot equipment

Filtration was performed with a tangential filtration, capacity100 L (Figure 1). All the experiments were carried out in a closed system, where the permeate does not return to the tank whereas the retained liquid returns to the tank.

Membrane description

The module membrane spiral used was 1016 mm long and has a width of 61 mm. The nanofiltration membrane is a thin film composite membrane. All is established by three layers: A layer support in polyester (120 µm); a micro porous intercalary layer Polysulfone (40 µm) and a layer barrier (active layer) ultrathin of polyamide on the superior surface (0.2 µm).

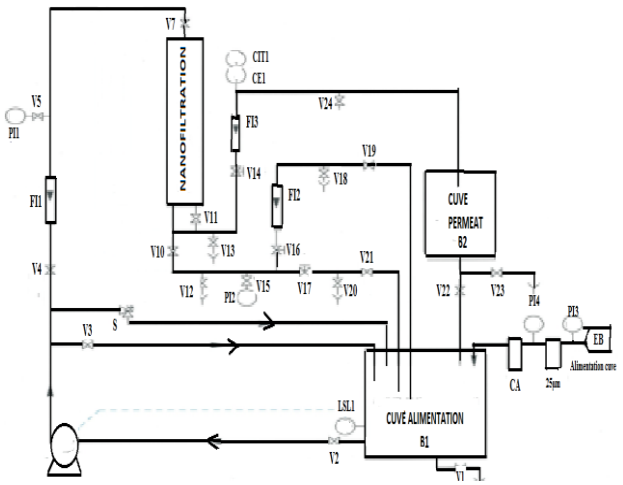

Figure 1. Schematic diagram of nanofiltration pilot.

V1: drain valve ,V2: valve for alignment of the tank,V3: valve for putting in recycling,V4: valve for alignment of the circuit in entrance of membranes,V5: valve for alignment of the manometer PI1,V7: valve for alignment of nanofiltration membrane(entry), V10: valve for alignment of the membrane of nano-filtration (taking out retention),V11: valve for alignment of the membrane of nano-filtration (taking out permeate),V12: drain valve of the retentate circuit after module, V13: drain valve for the circuit of permeate after module (side sounds of conductivity), V14: valve for isolation of the circuit of permeate after module (probe conductivity), V15: valve for alignment of the manometer PI2 (taken out of module) ,V16: Valve for regulation of the flow of retained towards tank B1 or got out of it ,V17: valve for return of the retained towards tank B1 or got out of it, V18: valve of racking of the retained,V19: valve for isolation of the circuit of return of the retained towards the tank B1,V20: valve for racking of the retained ,V21: valve for isolation of the circuit for return of the retained towards the tank B1,V22: valve for return of the tank of permeate B2 towards the tank B1,V23: drain valve of the tank of permeate B2,V24: valve for taking of sample of permeate, P: high-pressure multicellular centrifugal pump, B1: tank of 100 L in PVC, B2: tank of collection of permeate of 20 L in PVC, C1: membrane of reverse osmosis (SNTE company ref XLE-2540), C2: Membrane of nano-filtration (SNTE company ref NF270-2540)THAT Filters with cartridge in the activated charcoal (SNTE company ref 25554) 25 um filter with wound cartridge 25um (SNTE company ref 25552), S: the safety valve of the circuit PVC, FI1: ratemeter with block 100-1000 L/h - measure of the debit of entry, FI2: ratmeter with block 100-1000 L/h - measurement of the retentate output flow, FI3: ratemeter with block 10-100 L h^{-1} - measure of the debit of exit of permeate, PI1, PI2 manometers 0-16 bars in entrance (entry) and taken (brought) out of the module, PI3, PI4 manometers 0-2.5 bars for follow-up of the state of filters, LSL1: sounds of low level (safety (security) pumps), CE1: probe of measure of conductivity.

Extraction procedure

The experiments were carried out at the Laboratory of Separation and Purification Technologies. After each experiment the membrane is cleaned by a hydrochloric acid solution for 10 min, and then it is rinsed with distilled water.

Analytical methods

The volumetric flux was determined by measuring the permeate volume collected in given times interval. Owing to electro neutrality conditions, it was observed that both cation and anion rejection rates were the same, that is to say $R_{cation} = R_{anion} = R$. Consequently, the rejection rate can be calculated by Eq. (1):

$$R = 100\left(1 - \frac{C_p}{C_0}\right) \quad (1)$$

where:

C_p concentration of salt in the permeate (ppm),
C_0 concentration of salt in the feed solution (ppm).

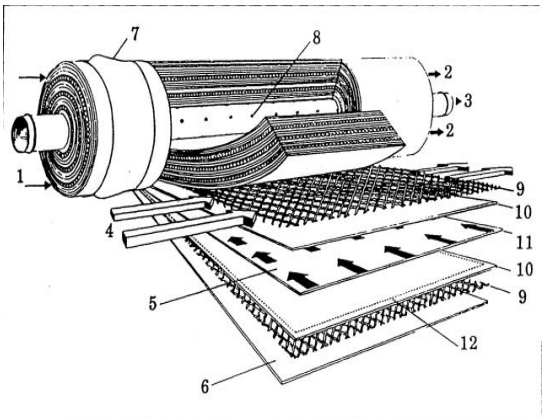

Figure 2. Membrane description.[6]

1-water inlet; 2-taken out of water; 3-taken out of permeate; 4-Smell of selling of the raw gross water; 5- Direction of permeate flow; 6- Materiel of protection; 7- Seal enters module and envelope; 8- Perforations collecting the permeate; 9-spacer; 10-membrane; 11-collector of permeate; 12- Line of weld of both membranes.

RESULTS AND DISCUSSION

Determination of the hydraulic membrane permeation

The permeability of the membrane is given by the slope of the Figure 3 which is equal with L_P= 3.95 m s^{-1} bar^{-1} and the resistance, R_m = 0.253 bar m^{-1} s, Eqn. (2).

$$R_m = \frac{1}{A} = \frac{S\Delta P_m}{Q_p} \quad (2)$$

where :

A permeability of the membrane
S membrane area
ΔP_m the effective transmembrane pressure
Q_P permeation volume flow rate.

The value of the L_p obtained on the used membrane (SNTE NF270-2540) was proved to be 1.457; 106 times as large as that obtained on the membrane Nanomax-50 (Millipore USA)[5] and on the Duramem MWCO 900, where L_P is 0.028 x 10^{-6} m s^{-1} bar^{6} what shows that our membrane is very successful, and can be used in the industrial scale.

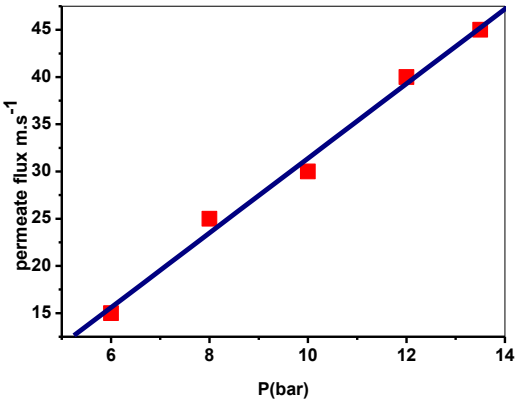

Figure 3. Permeate flux variation as a function of pressure for distilled water.

Effect of pressure and concentration for iron ion

In view of the Figure 4, we note that in the solutions containing 100 ppm and 300 ppm, the yield is 100 % for pressures varying between 6 – 13.5 bars. These results are similar to those given in the literature.[7, 10-12] For an initial concentration of 4 ppm, the pressure has an influence; indeed for a variation of pressure of 6 - 12 bars, the yield passes from 82 % to 94 %. The pressure of 12 bars corresponds to an optimum, because beyond this pressure the retention decreases.

These results differ from the works on the nano-filtration.[10] Here, the screen phenomenon was neglected because the weak concentration of the studied solution was insufficient to create this phenomenon.[10,13] This phenomenon can be also explained differently. In the solution of concentration equal to 4 ppm, the iron ions are present in 11.4 % under the form of Fe^{3+} and 65.01 % for $Fe(OH)^{2+}$ in pH 3.85 (Cheaqs Pro (Release P 2013, 1: a program for calculating of the chemical equilibria in aquatic systems, Wikovermeij, on 1999-2013). These ions characterized by small ionic ray (0.055 nm for Fe^{3+} and 0.3958 nm for Fe $(OH)^{2+}$) can enter into the pores of the membrane (diameter of pores = 1 nm) where they are partially retained by the membrane surface forces (electrostatics and friction forces).[8, 9, 13] When the pressure increases the surface forces remain constant, whereas the sweeping forces increase due to flux in the pores.

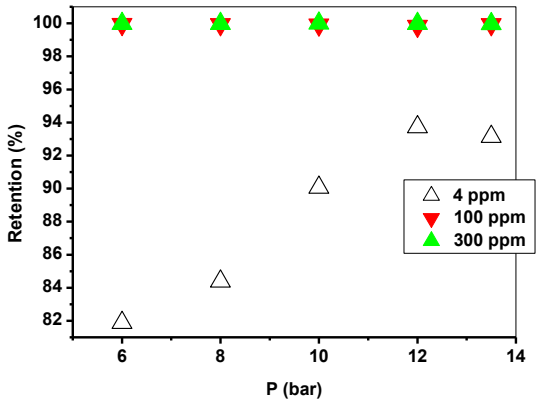

Figure 4. Variation of iron retention as a function of the pressure for different concentrations.

In view of the Figure 5, no gap was observed between the results regarding water and those corresponding to the solution of 4 ppm for pressures varying of 6 bars to 13.5 bars. This shows that the iron cations are not rejected of the surface of the membrane. For the solutions to 100 ppm and 300 ppm, the gaps regard to the water become important; about or admitted pressure the iron ions are rejected farther from the surface of the membrane. This effect makes the concentration gradient weak for 4 ppm, and consequently it results by a weak difference in osmotic pressure with having a consequence of maintaining of effective pressure.10, 12 At concentrations higher (100 ppm and 300 ppm), the gap increases on concentration in iron because of the polarization.7,10

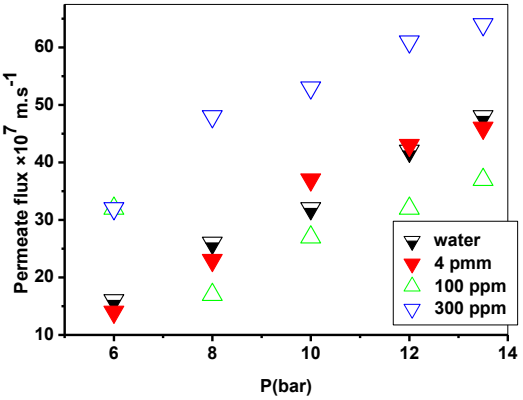

Figure 5. Variation of flux of permeate and the flux of water according to the pressure for different iron concentration.

Effect of pressure and concentration for copper ion

In view of the Figure 6, we note that for an initial concentration of 4 ppm, the pressure influence is not neglected on the yield of extraction, because for a variation of pressure from 6 - 10 bars, the yield passes from 92 % to 94 %. The pressure of 10 bars corresponds to an optimum, because beyond this pressure the retention decreases. We notice that for the solution containing 100 ppm, the yield varies from 80 % - 82 %, for pressures which vary between 6 - 13.5 bars. For the solution containing 300 ppm, the yield passes from 82 % - 84 %. The pressure of 12 bars corresponds to an optimum, because beyond this pressure the retention decreases. These results are not similar to those obtained in other works.7,10-12 Here, the screen phenomenon was neglected because the weak concentration of the studied solution was insufficient to create this phenomenon.10,13 This phenomenon can be also explained differently. In the solution of concentration equal to 4 ppm, the copper ions are present in 70.57 % under the form Cu2+ and 22.02 % for a pH=7.4 (Cheaqs Pro (Release P 2013, 1: a program of calculation of the chemical equilibria in aquatic systems, Wikovermeij, on 1999-2013). These ions characterized by a small ionic ray (0.073nm for Cu2+) can penetrate in the pores of the membrane (diameter of pores = 1 nm), where they are partially retained by the membrane surface forces (electrostatic and friction forces). 8,9,13 When the pressure increases, the surface forces remain constant whereas the sweeping forces due to flux in pores increases.

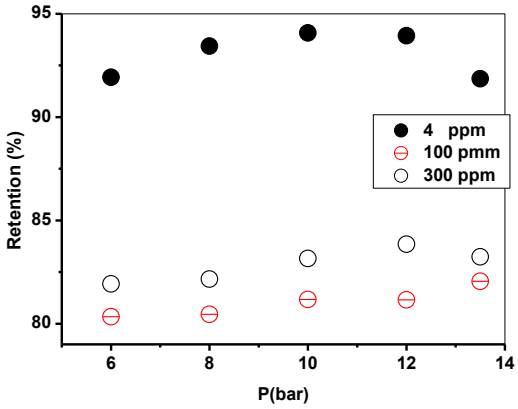

Figure 6. Variation of copper retention as a function of the pressure for different concentrations

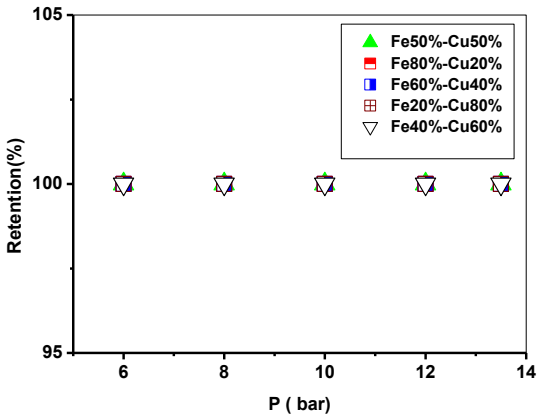

Figure 8. Variation of iron retention as a function of the pressure for different mixtures

In view of the Figure 7, contrary to the iron, a small gap was observed between the results regarding water and those corresponding to the solutions of 4 ppm. This could be explained by a weak rejection of the copper ions farther from the membrane surface. This effect makes the concentration gradient weak, and consequently it results in a weak difference in osmotic pressure and to have consequently the effective preservation of the pressure.10,12 Between 8-12 bars and in higher concentrations (100 ppm and 300 ppm), there is no gap between flows, but the gradient of concentration increases because of the of the polarization.7,10

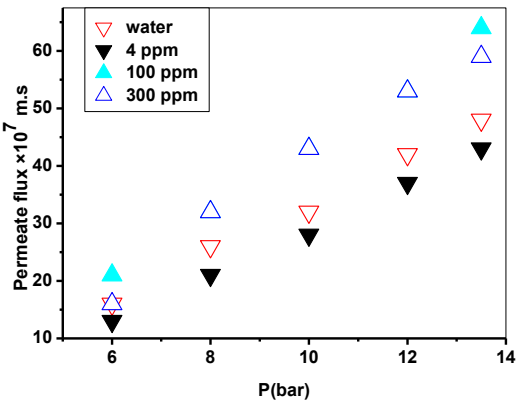

Figure 7. Variation of flux of permeate and the flux of water according to the pressure for different copper concentration.

Effect of pressure and concentration for mixtures

Effect of pressure and concentration for iron

Figure 8 shows that, for variations of pressure from 6 - 13.5 bars, the retention is quantitative (100 %) for iron and copper at different proportions, while maintaining a total concentration of 4 ppm for the mixture. A pressure of 6 bars is enough for a full purification of iron. The difference between the iron and the copper is not observable, because the presence of the copper in the mixture does not influence the retention of the iron.

Effect of pressure and concentration for copper

The presence of iron influences the retention of the copper as seen from the results presented in Figure 9. The best retentions were obtained for the mixture Fe 60 % + Cu 40 % about pressure from 12 bars. For the mixture Fe 80 % + Cu 20 %, pressure up to 10 bars, the retention is constant (around 74 %) then increases exponentially until 97 % beyond this pressure. The effect of pressure was important on the retention, whatever the proportions of the mixture; the total concentration being always maintained at 4 ppm.

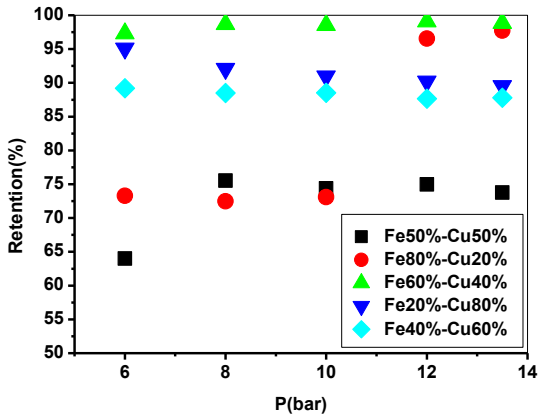

Figure 9. Variation of copper retention as a function of the pressure for different mixtures.

Effect of pH for the retention of iron and copper in the mixture iron salt 50% - copper salt 50%

In view of the Figure 10 (A), the obtained results show that the accepted pressure is about (6 - 13.5 bars) and the pH =6.8; the retention of the iron is total (100 %). With pressure 6 bars, the retention of the iron is also total, in pH = 4.5. The difference at pH=6.8 and pH=3.7 then 5.5 becomes important. The best conditions of extraction of the iron correspond to pH = 4.5 and the pressure of 6 bars, with the addition of some mL of HCl. Without the addition of HCl, the best conditions are pH = 6.8 and the pressure of 6 bars

For pH 3.7, 4.5 and 5.5, the retention of the iron at the pressure of 13.5 bars is almost the same (78 %) We can conclude that there is an interaction between these two parameters. A study of plan of experience would allow quantifying this interaction. The purification is total for the mixture in the pressure of 6 bars and in pH = 4.5. Whereas the best selectivity is obtained for a pH = 6.8 (without addition of HCl) and the accepted pressure of 6 bars.

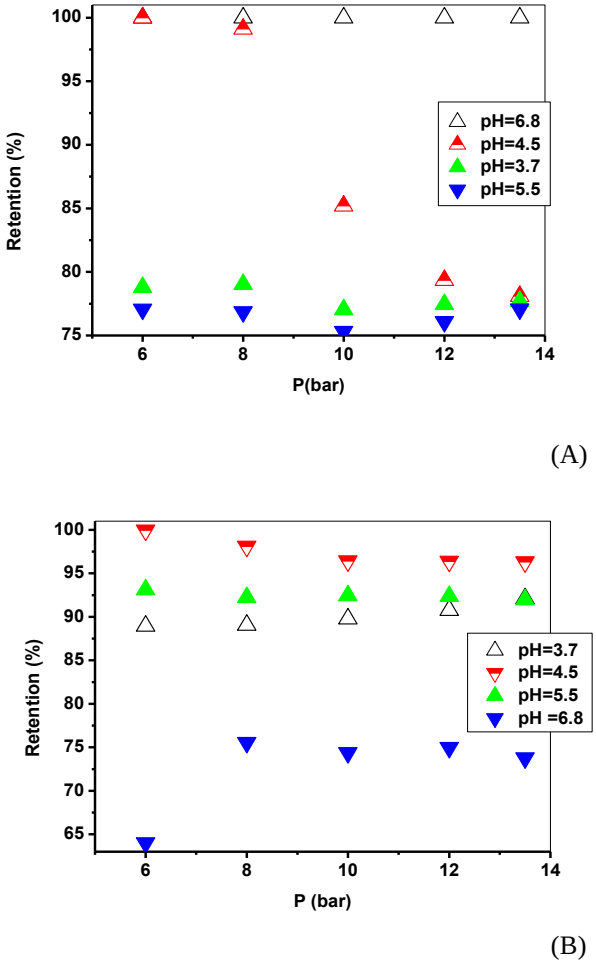

Figure 10. Variation of iron (A) and copper (B) retention as a function of the pressure for mixture salt iron 50%-salt copper 50%

Effect of pH for the retention of iron and copper in the mixture iron salt 80%-copper salt 20%

In view of the figure 11 (A), the obtained results show that the retention of iron is total (100 %) at pressure 6 - 13.5 bars and pH 3.3 - 7.5. In view of the figure 11 (B), for pH 3.3; 4.5 and 5.5 (with the addition of some mL of HCl) and a pressure from 6 - 13.5 bars the retention of copper is total (100 %).

The membrane extracts the mixture without distinction between the iron and the copper, although these two metals have different physical-chemical properties; the iron Macke left some ferromagnetic metals. The best selectivity is obtained for a pH = 7.5 (without addition of HCl) and the accepted pressure of 8 bars.

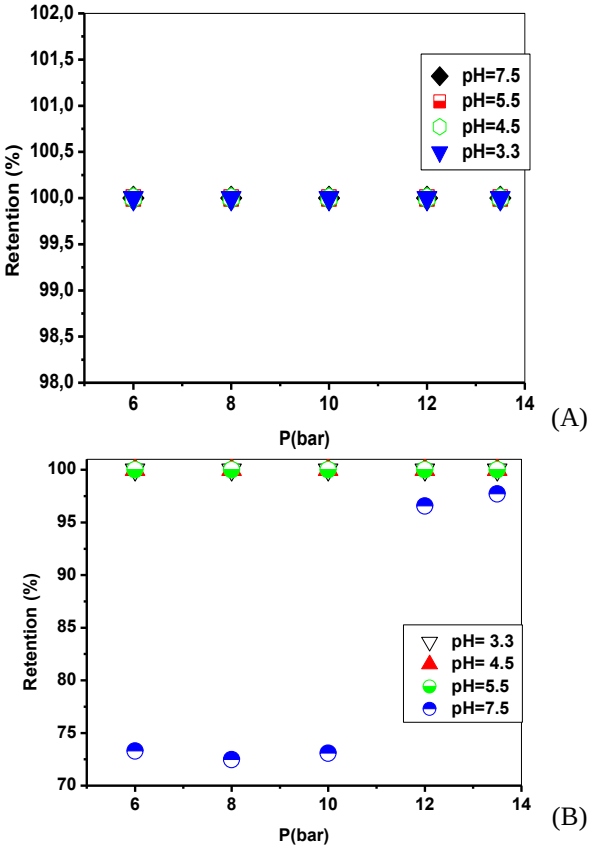

Figure 11. Variation of iron (A) and copper (B) retention as a function of the pressure for mixture salt iron 80%-salt copper 20%

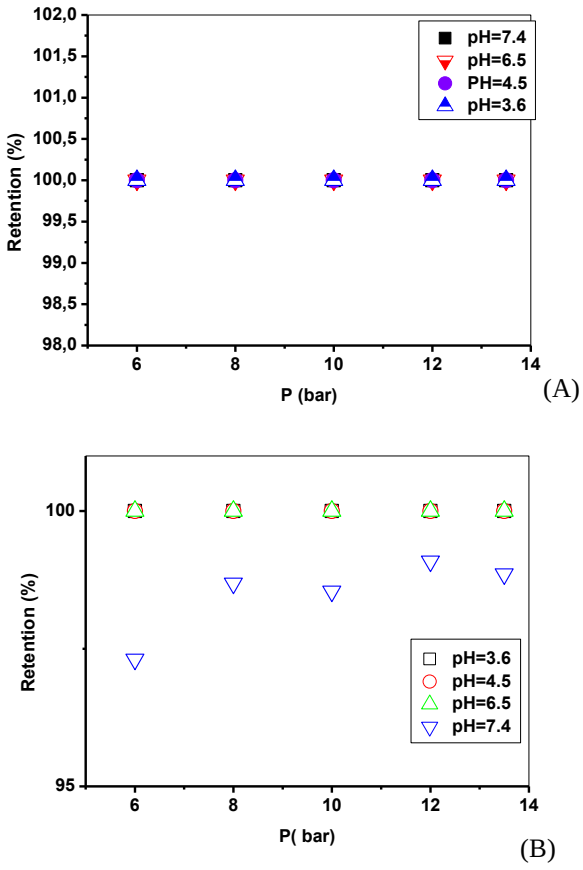

Figure 12. Variation of iron (A) and copper (B) retention as a function of the pressure for mixture salt iron 60% - salt copper 40%.

Effect of pH for the retention of iron and copper in the mixture iron salt 60%-copper salt 40%

In view of the Figure 12 (A), the obtained results show that the retention of the iron is total (100%) at pressures from 6 to 13.5 bars, and pH from 3.6 to 7.4. In view of the Figure 14 (B), pH 3.6, 4.5, and 6.5 (with the addition of some mL of HCl) and a pressure from 6 to 13.5 bars the retention of the copper is total (100%). The separation takes place at P = 6 bars and pH = 7.4 which is a neutral pH. On these conditions of separation the speeds of diffusion through the membrane have different values.

Effect of pH for the retention of iron and copper in the mixture iron salt 20%-copper salt 80%.

In view of the Figure 13(A), the results show that at pressures from 6 to 13.5 bars and pH from 3.7 to 6.4, the retention of the iron is total (100%). In view of the figure 13(B), for pH 3.7, 4.9, and 5.4 (with the addition of some ml of HCl) and at pressures from 6 to 13.5 bars the retention of the copper is total (100 %). In these pH, the process does not make a difference between the iron and the copper. In pH = 6.4 and at P =13.5 bars, the separation between both metals is the most important. The retention decreases at pH = 6.4 with the increase of the pressure.

Effect of pH for the retention of iron and copper in the mixture iron salt 40%-copper salt 60%

In view of the Figure 14(A), the results show that the retention of the iron is total (100%) at pressure from 6 to 13.5 bars and at pH from 3.7 to 6.8.

In view of the Figure 14(B), the retention of the copper is total (100 %) for pH 3.7, 4.5, (with the addition of some ml of HCl) and 6.8 (with the addition of some ml of NaOH) at pressures from 6 to 13.5 bars. The difference of retention is obtained at pH = 5.8. In this pH, the effect of increase in pressure on the retention was weak.

Effect of pH for the retention of copper

The retention is minimal at pH 6.7 and at pressure from 8 bars. In pH = 6.7 the charge loss is important. It makes an effect of the screen on the membrane surface, so preventing it from making cross the copper.

Na^+ added, can enter it competitions with the copper (II). For three other pH, the influence of the pressure is small. However the retention contrary to the iron does not affect the 100 %.

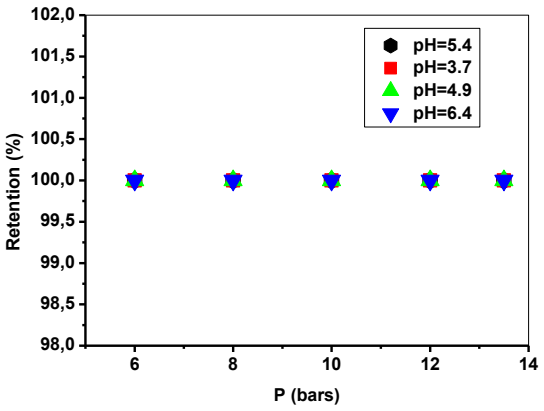

(A)

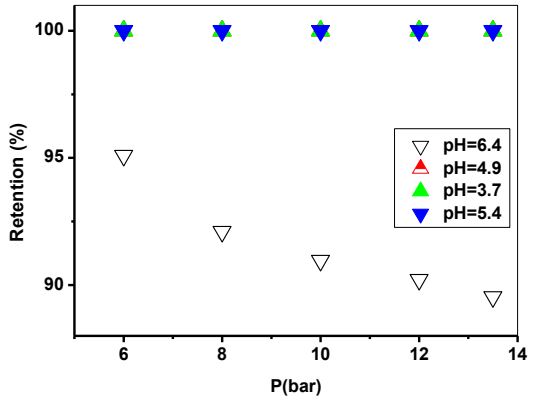

(B)

Figure 13. Variation of iron (A) and copper (B) retention as a function of the pressure for mixture salt iron 20%-salt copper 80%.

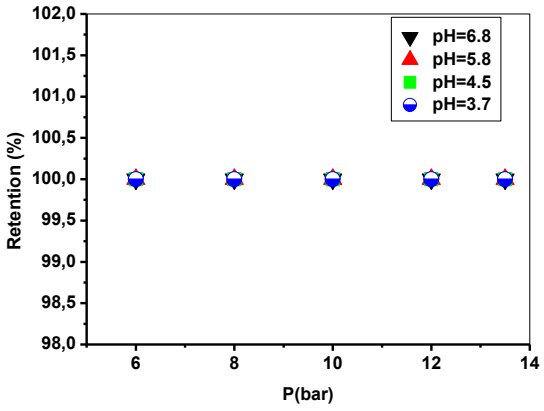

(A)

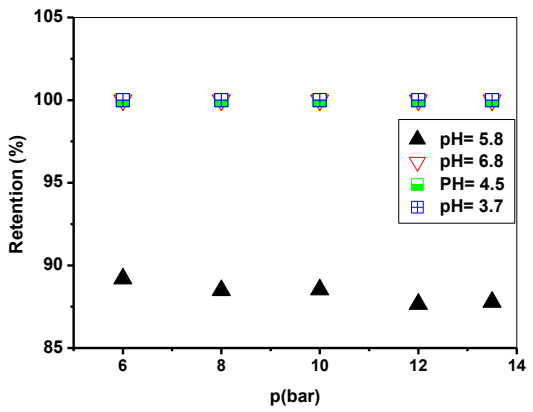

(B)

Figure 14. Variation of iron (A) and copper (B) retention as a function of the pressure for mixture salt iron 40%-salt copper 60%.

Table 1. Effect of copper in the mixture (C_{Ps} = 0.22 ppm**)**

Mixture	$C_{P,m}$	$C_{P,m}/C_{P,s}$	Effect
Salt of Fe 50%-salt of Cu 50%	0.95	4.32	synergism
Salt of Fe 80%-salt of Cu 20%	0.07	0.32	antagonism
Salt of Fe 60%-salt of Cu 40%	0.03	0.14	antagonism
Salt of Fe 20%-salt of Cu 80%	0.19	0.86	antagonism
Salt of Fe 40%-salt of Cu 60%	0.40	1.82	synergism

Table 2: Effect of iron in the mixture (C_{Ps} = 0.21 ppm)

Mixture	$C_{P,m}$	$C_{P,m}/C_{P,s}$	Effect
Ssalt of Fe 50%- salt of Cu 50%	0.00	0.00	antagonism
Salt of Fe 80%- salt of Cu 20%	0.00	0.00	antagonism
Salt of Fe 60%- salt of Cu 40%	0.00	0.00	antagonism
Salt of Fe 20%- salt of Cu 80%	0.00	0.00	antagonism
Salt of Fe 40%- salt of Cu 60%	0.00	0.00	antagonism

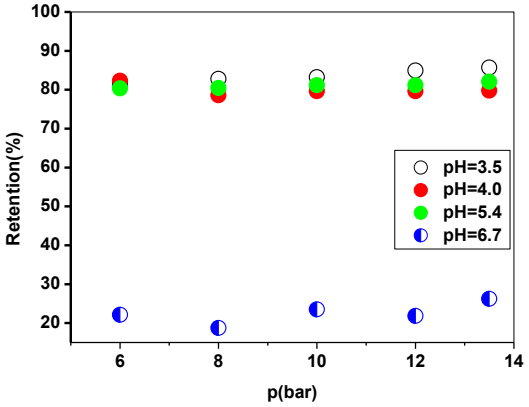

Figure 15. Variation for the retention of copper as a function of the pressure.

Effect of pH for the retention of iron

Within 1%; Independently of the pH, the retention was total; whatever the admissible pressure is total. Nanofiltration is better suited for iron than copper.

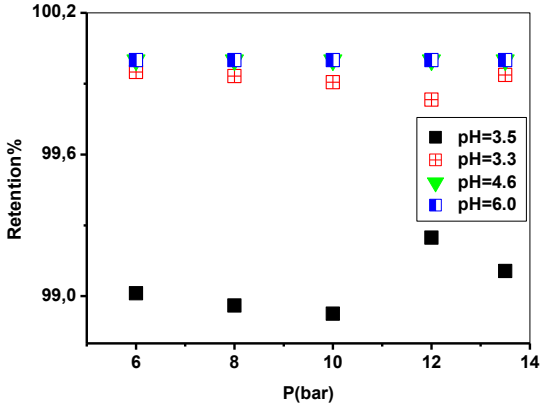

Figure 16. Variation for the retention of iron as a function of the pressure.

Effect of synergism.

The numerical value of $C_{P,m}/C_{P,s}$ ratio gives information about presence/absence of synergism or antagonism. If $C_{P,m}/C_{P,s}>1$, synergism takes place (the effect of the mixture is greater each of the ion in the mixture). If $C_{P,m}/C_{P,s}<1$, ant**agonism is occurred** (the effect of the mixture is less than that each of the ion in the mixture). If $C_{P,m}/C_{P,s}=1$, there is no **interaction** (interaction the mixture has no effect on the adsorption of each of the adsorbates in the mixture).[14,15]

Several factors are considered to correlate metal ion uptake and metal ion properties. Factors like electronagetivity of the metal ion, electrostatic attrition due to charge to radius ratio, ability to form metal hydroxide complex and suitable site for adsorption on adsorbent are responsible for competitive adsorption of one metal ion over another.[10,11]

Conclusion

The retention of a species in nanofiltration is done as a function of the ionic and steric exclusion which it undergoes. The charge of ions (sign and valence), compared with the sign of the active groups of the membrane (polyamide), is an element prevailing in the retention of the ion. The bivalent co-ion (Cu^{2+}) or trivalent (Fe^{3+}) is strongly retained and against monovalent ion (NO_3^-) , by its presence to the membrane, may do a screen effect partially by the residual ionized groups of the membrane until invert the sign of its potential. The monovalent co-ions (Na^+) cross all the better the membrane than their Ionic mobility is stronger and than the number of groups ionized by the membrane is low. The strong retention of a co-ion Bivalent or trivalent inferred also a superior transmission in co-ions and against monovalent ions, so as to compensate for the led (inferred) imbalance of load (responsibility).

During the term of this study, the consideration of the difference (pH_r - pH_n), the retention of H^+ or of OH^- according to its sign, establishes a good descriptor of the imbalance of Ionic partitions realized between the solution and the pores of the membrane.

The mechanisms of transfer of ions to be proposed in this study should allow a better understanding the selectivity observed during the nanofiltration.

Symbols

pH_r pH of permeate

pH_n pH of retentate.

C_{Pm}: concentration of an ion in the mixture (Fe^{3+}, Cu^{2+}).

C_{PS}: concentration of a single ion in solution.

Acknowledgements

We gratefully acknowledge the ATRST-Algeria (ex. ANDRU) for their financial support.

Conflict of Interest

The authors declare that they have no conflict of interest.

References

[1]Mohammad, A. W., Teow, Y. H., Ang, W. L., Chung, Y. T., Oatley-Radcliffe, D.L., Hilal, N., *Desalination*, **2015**, *356*, 226.

[2]Al-Rashdi, B., Somerfield, C., Hilal, N., *Sep. Purif. Rev.*, **2011**, *40*, 209.

[3]Gherasim, C. V., Mikulášek, P., *Desalination*, **2015**, *343*, 67.

[4]Mulder, M., *Basic Principles of Membrane Technology*, Kluwer Academic Publisher, Dordrecht, **1996**.

[5]Belkhouche, N., Didi, M. A., Taha, S., Benfarés, N., *Desalination*, **2009**, *239*, 58.

[6]Tsibranska, I., Saykova, I., *J. Chem. Technol. Met.*, **2013**, *48*, 333.

[7]González-Muñoz, M.J., Rodríguez, M.A., Luque, S., Álvarez, J.R., *Desalination*, **2006,** *200*,742.

[8]Artu, G., Hapke, J., *Desalination*, **2006**, *200*, 178.

[9]Fatin-Rouge, N., Szymczyk, A., Ozdemir, E., Vidonne, A., Fievet, P., *Desalination*, **2006**, *200*, 133.

[10]Ben Frarès, N., Taha, S., Dorange, G., *Desalination*, **2005**, *185*, 245.

[11]Pontié, M., Lhassani, A., Diawara, C.K., Elana, A., Innocent, C., Aureaua, D., Rumeau, M., Croue, J.P., Buisson, H., Hemery, P., *Desalination*, **2004**, *167*, 347.

[12]Paugam, L., Taha, S., Carbon, J., Gondrexon, N., Dorange G., *Rev. Sci. Eau.*, **2001**, *14*, 511.

[13]Szymczyk, A., Fievet, P., Ramseyer, C., *Desalination*, **2006**, *200*, 125.

[14]Roy, A., Bhattacharya, J., *Sep. Purif. Technol.*, **2013**, *115*, 172.

[15]Mahamadi, C., Nharingo, T., *Bioresour. Technol.*. **2010**, *101*, 859.

[16]*Bulletin technique, Pilote d'osmose inverse et de nanofiltration*, MP72 / N°24.

Received: 08.01.2017.
Accepted: 12.02.2017.

ON INVESTIGATION OF HUMAN BRAIN USING WATER DIFFUSION METHOD

T. Khechiashvili[a]* and K. Kotetishvili[a]

Keywords: DWI, MRI, diffusion, DTI, experiments with Phantom.

Using the method of water diffusion, the DWI (Diffusion Weighted Imaging), is one of the advances in clinical research of human brain. It can help neurosurgery to avoid the different kind of risks, for instance, disability of walking, talking, moving the arms, and so on. Human brain research in this direction makes possible to make tumour surgery using the DTI (Diffusion Tensor Imaging) mapping. The experiments done with phantom give us the histograms which shows the results in form of homogeneous signals in different areas of the phantom which means that human resources can be replaced with phantom and experiments done with it. This advantage gives us reason to develop this approach further.

* Corresponding Author: Tamar Khechiashvili
E-Mail: tamo.xechiashvili@gmail.com
[a] Department of Engineering Physics
Georgian Technical University, Tbilisi, Georgia

Introduction

Research in the structure and activities of brain involves experiments. We have carried out experiments involving measurements in phantom cylindricals. Phantom experiments are important for many reasons, for example, brain scan is not always possible and therefore various forms of phantom (cylindrical, transversal, parallel etc.), which are almost exactly what is in brain fibers adhesion, can be used instead. Using a phantom in turn leads to various challenges. But these will be considered in details later.

Experimental

Presented work was conducted in the direction of brain research using diffusion magnetic resonance imaging (MRI).[1,2] For the experiments a cylindrical phantom has been used.

The design constitutes a cylindrical form made of plastic materials. Plastic tube was wrapped around 10 mm filamentary fibers which in our case constitutes analogue of regional connectivities in brain. The main part of the experiments conducted in the condition of homogeneity of the signal since for the cylindrical phantom signal from fibers directed along the magnetic field is stronger than that from fibers which are positioned perpendicularly to the magnetic field. It also depends on the magnetic field susceptibility.

In this case, there is a signal from fibers directed along the magnetic field, but from the perpendicular fibers there is a noise and accordingly obtained results seem to be wrong.

The experiments in a cylindrical phantom were conducted during approximately 40 min with different number of parameters.

The most important safety issue in the process of the experiment is that it is necessary to keep the safety rolls and to enter the scanner room without any metal thing. Otherwise in many cases the situation can be dangerous for both the patient as well as for the responsible person.

Results and Discussion

The main idea was that, we wanted to get homogeneous signal for different areas of the phantom placed in the magnetic field. For this task first experiment was conducted with only water at different time points: 7.4 and 120 ms.

Second experiment was performed by fibers and with 10 different time points. It is necessary to explain the use of different time points. In some time-interval we can see how water molecules are distributed so that water diffusion can be visualized (Figure 1). In these histograms we can see some conditions affecting direction of movement of water molecules but we cannot see how really signal looks. So we need to make maps from this signal (Figures 2 and 3).

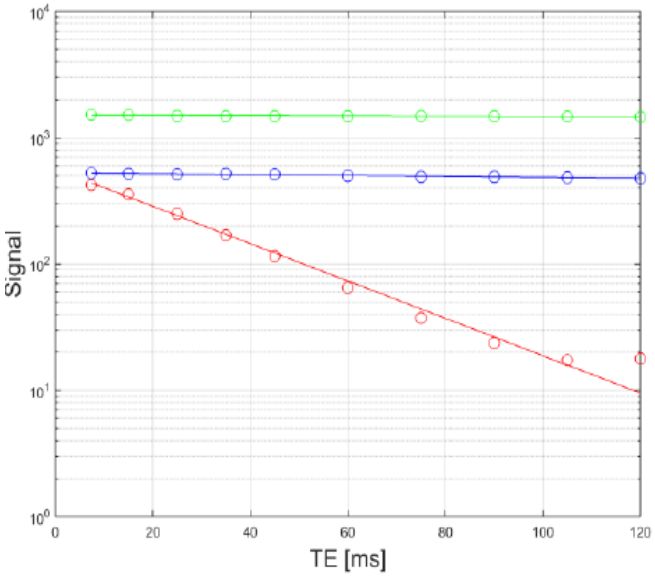

Figure 1. Histogram with 3 different areas and 10 time points.

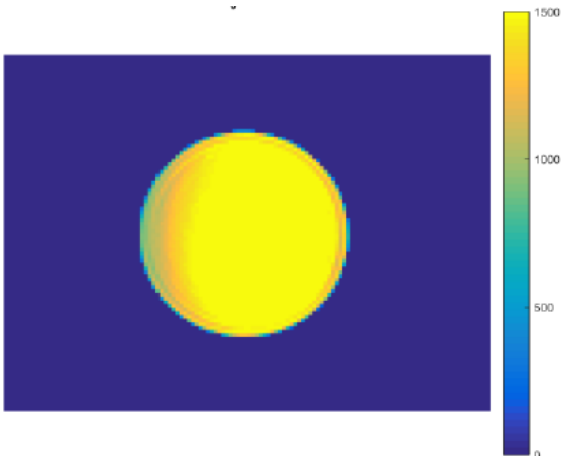

Figure 2. S_0 map giving signal visualization.

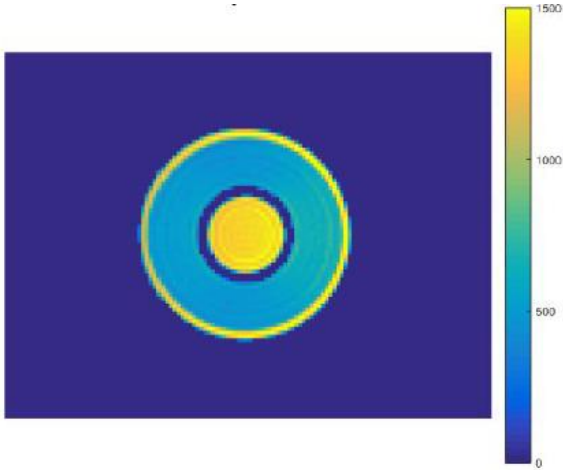

Figure 3. S_0 map with fibers and NaCl.

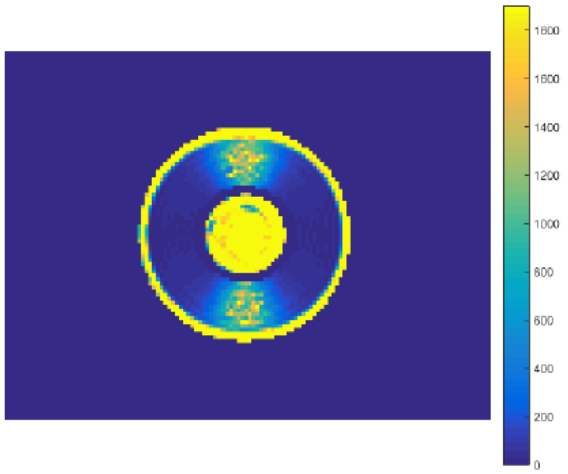

Figure 4. T^2 map for case with fibers. Yellow dots represent noise.

There was clear that during next experiments in T^2 maps we have not exactly homogenous signal – in some regions there was a noise (Figure 4). That's why we tried to add in the water a chemical mixture which is sensitive to diffusion and makes pathological areas looking differently. We used NaCl in condition: 0.6 L of water + 300 g NaCl. We performed two more experiments with chemicals added in water but, third one has to be scraped as during the experiment the phantom was counted wrongly in scanner. The next experiment gave us the expected results (Figure 5).

As it was mentioned, third experiment was not successful but fourth experiment gave us the good results.

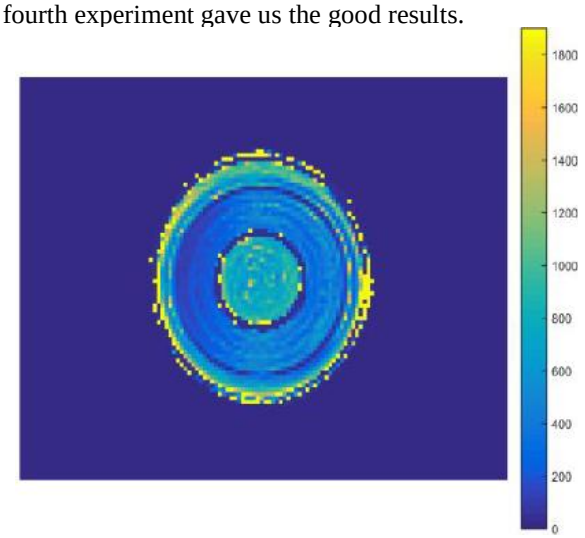

Figure 5. T^2 map for water and chemical mixture (NaCl) and with no noise.

Conclusion

The fundamental result of this work is that the studies of human brain experiments can be performed with phantom structures. It is apparent that the present research is not conclusive. However, the preliminary results can be termed as successful as the data gives us general view about what was anticipated and the result obtained is line of assumption. The major task, undertaken in the present work was to obtain homogeneity of the signal, which was achieved in the last experiment.

It is established that diffusion studies are a step forward for the neurosurgical operations for treatment of tumours.

Acknowledgments

This paper has been presented at the 4th International Conference "Nanotechnologies", October 24 – 27, 2016, Tbilisi, Georgia (Nano – 2016).

References

[1]Grinberg, F., Farrher, E., Maximov, I. I., Shah, N. J., *Micropor. Mesopor. Mater.*, **2013**, *178*, 44. https://doi.org/10.1016/j.micromeso.2013.02.046

[2]Grinberg, F., Farrher, E., Ciobanu, L., Geffroy, F., Le Bihan, D., Shah, N. J., *Plos One*, **2014**, *9*, e89225. https://doi.org/10.1371/journal.pone.0089225

Received: 17.12.2016.
Accepted: 12.02.2017.